COMPARISON OF FINITE ELEMENT BUCKLING SOLUTIONS FOR FLAT PLATES UNDER COMPLEX COMBINED LOADING TO ANALYTICAL METHODS

Aerospace engineering Bachelor thesis,
Universidad Carlos III de Madrid, July 2015

Author: Guillermo Jacobo Huguet Rodríguez

Tutor: Jesús Jimeno Martínez

Table of contents

1. Introduction

Since mid 30s (Theory of Elastic Stability, Timoshenko, 1936) up to now, buckling of plates subjected to in plane combined loadings has been a matter of concern for many investigators in structural engineering. When buckling occurs, there is a sudden change in deformation state, which occurs at the critical load.

Being able to determine the critical stress for a given loading condition is of remarkable importance in aeronautical industry. There are some areas at which it is of paramount importance to know under which load the structure buckles, to design it appropriately. In some other areas, like the skins of aerodynamic surfaces, buckling needs to be avoided so as not to change the geometry of the aerodynamic surface.

This phenomena occurs, among other structures, in plates, such as fuselage or wing skin panels. Those panels or sheets in the wing, fuselage or other parts are subjected to combination of complex loadings. For instance, the upper surface of an aircraft wing in flight may be subjected to combined shear and compressive stress. Wing panels are delimited by spanwise stiffeners and chordwise ribs.

Note that the panels in the wing are not flat but slightly curved. The buckling load of those panels can be computed assuming they are flat, because it is a conservative estimate (curved panels have greater buckling loads).

To solve flat plates buckling problems for different loadings and boundary conditions, currently two different methods are used; the analytical method and the Finite Element Method.

This work will compare the flat plates combined loadings buckling results obtained analytically with those obtained from Finite Element Method.

1.2 Project summary

This project compares Finite Element Method and theoretical buckling solutions for flat plates under combined loadings. Comparisons are carried out for combined axial compression and bending, shear and bending, transverse compression and bending, and axial compression and shear. Flat pates with all edges simply supported and all clamped are studied. Theoretical results have been based in available results, and FEM results have been obtained using Femap and Nastran tools

Theoretical solutions, based on the references available, are based on Rayleigh-Ritz energy method. This method is based on the fact that when a structure buckles at the critical buckling load, the strain energy of the deformed plate equals the energy stored in the plate by the critical load. The energy method initially estimates the deflection function of the buckled structure using a function that satisfies the boundary conditions of the problem. Then, with the assumed deflection function, the energy stored on the plate and the work performed by the critical load are computed. Equating them, the critical load is obtained in terms of the structure geometry and two coefficients, n and m, which are related to the energy state of the structure. The buckling load corresponds to the lowest energy state satisfying the energy equilibrium, so those coefficients are selected to give the lowest critical load. The buckling load is often expressed in terms of the buckling coefficient, which depends on the geometry of the structure, n and m. These methods

model the structure as a finite system (with limited degrees of freedom), while actual structures are continuous systems with infinite degrees of freedom. This makes the modeled structure stiffer than the actual one, estimating a higher critical load than the actual one. The key to approach reality is to initially estimate accurately the deflection function. The closer the estimated deflection function is to the actual deformation, the better (and less optimistic) will be the predicted critical load.

Based on this procedure, references present single and combined loading solutions for flat plates. For single loadings, shear, axial compression, transverse compression and bending loads have been studied. The critical buckling load is computed using the buckling coefficients k from plots in the references, which have been constructed using the energy method. Critical loads decrease as the aspect ratio, a/b, increases. For a certain a/b, buckling load does not decrease any more, and plates are considered *infinitely long*. Combined loadings buckling is based on ${R_1}^p + {R_2}^q + {R_3}^r + \ldots = 1$ shaped interaction equations and curves. For each of the combined loading cases, the available curves and equations will be compared with FEM results.

Finite Element Method is based on discretizing the structure in finite elements (smaller units) which are defined by their stiffness matrix $[K]$, which relate the applied load to the structure with its displacement $[X]$ by $\{F\} = [K][X]$. The FEM method assembles the global stiffness matrix $[K]$ from the individual element stiffness matrices and solves the boundary value problem obtaining the corresponding displacements $[X]$. Then, the strains and the stresses can be obtained. To solve buckling problems (which apparently would require a FEM non-linear solution) FEM uses the differential stiffness matrix, which modifies the linear stiffness matrix. This allows solving the problem linearly, and buckling becomes an eigenvalue problem.

FEM has been used with Femap (pre and post processor) and Nastran (solver) tools. Part of the work was based on familiarizing with the tools. Then, problem of interest has been modeled involving selecting the material and property, elements, mesh size, combination of loads and boundary conditions, and analysis type. A mesh sensitivity analysis has been performed to determine the mesh size adequately. For combination of loads and boundary conditions, several approaches have been studied and finally one selected for consistent use in all FEM models. Nastran offers various methods for solving the eigenvalue problem. Each method was studied and the most appropriate one selected.

Results obtained from FEM have been carefully validated checking the static loads distributions, reactions, displacements and mode shapes, error messages and comparing with expected theoretical results. For single loadings the critical buckling loads have been obtained, and the buckling mode shapes for different boundary conditions and geometries have been studied. For combined loadings, a data fit has been successfully performed onto the obtained FEM results in order to obtain interaction equations. ${R_1}^p + {R_2}^q + {R_3}^r + \ldots = 1$ type equations have been obtained with small errors for all load combinations except for combined transverse compression and bending. For this combination, the results have been partially fitted using linear functions. The variation of the mode shapes along the interaction curves has also been studied.

The obtained FEM results and available analytical results based on the energy method have been compared. For single loading, small differences have been found except for transverse compression. It has been found that some energy method results were conservative, which does not agree with the theory. Consequently, an analysis has been carried out to find the root of the disagreement. The inaccuracies coming from FEM modeling and from the digitalizing process of

the theoretical solution plots have been studied. This has partially explained the disagreement. As for combined loading cases, FEM results and theoretical results have been compared. The comparisons focus on determining the validity, for engineering purposes, of theoretical curves and equations based on the differences with respect to FEM results.

In conclusion, it has been found that most of the theoretical equations and curves are reasonably accurate for engineering purposes, with almost all of theoretical equations and curves studied providing slightly optimistic buckling loads. The scope of validity of several equations and curves has been extended, recommending its use for other aspect ratios or boundary conditions in addition to those stated in some references.

1.3 Project planning

To organize the Project, it has been divided in several phases which are to be explained below.

First of all, a research of the graphs and equations that exist nowadays to predict plate buckling for different load combinations has been carried out. This task is based in looking for the currently industry employed graphs and equations, and analyzing and understanding how those are produced, their assumptions and limitations. Once all the meaningful information has been extracted, it has been processed ready for comparison with Finite Element Method results. This phase, together with the launch of the project has taken 4 weeks.

Secondly, theory behind Finite Element Method has been studied during 1-2 weeks, trying to understand the theory behind this computational method. Once this task was done, the first contact with Femap and Nastran software has been done, involving understanding how the tool works with static problems, and then with buckling problems in particular.

Then, once being familiar with the software, the project has focused on the modeling of the buckling problems to be analyzed. This implies designing a proper FEM model reliable enough to be later compared with existing results from graphs and equations. A large part of the time invested in the project has been concentrated in this stage.

After the modeling of the different problems, they have been analyzed with Femap and Nastran, obtaining Finite Element Method results. When analyzing the problem, many times the results were not validated and therefore, the model had to be redesigned. In other cases the model was redesigned to optimize it using the knowledge acquired with the practice. Therefore, the last two phases have been carried out concurrently and iteratively, until a proper model with reliable results is generated. These last two phases had a combined duration of around 6 weeks. Obtaining FEM results accurately was a vital task, to later be able to carry out a meaningful comparison.

Finally, during 1 month, Finite Element Method results have been compared to the critical buckling loads determined theoretically. From this comparison, several conclusions have been reached and the differences where determined and quantified. This part is the core of the work, in which once the theory and FEM results are understood, the author is able to carry out a reasonable comparison and satisfying the main goal of this work.

One additional week has been devoted to the revision and correction of this final report.

2 Goals

In order to estimate flat plates critical buckling load, aeronautical industry uses Finite Element Method software, as well as some equations and graphs for quick calculations. The main goal of this project is to compare both methods, determining and quantifying the difference between them.

For that purpose, previously the following goals need to be achieved through the process.

- Understand the theoretical solutions available and the theory behind them.
- Understand Finite Element method.
- Model plates accurately in FEM for different loadings and boundary conditions.
- Validate FEM results.
- Compare FEM and theoretical results for different loadings and boundary conditions.

The achievement of the main and secondary goals is shown and proven along the work.

3 Theoretical analysis

There are some different theoretical approaches to solve combined loading buckling problems. However, there is no general theory developed applicable to all cases of loading and boundary conditions.

This section will present the analytical results for plate buckling problems and the theory behind it. Additionally, the state of the art of plate buckling phenomena and its solutions will be presented along the section.

Most of the investigations have focused in Rayleigh-Ritz energy method. This section will focus in this method. It is worth mentioning that there is an exact solution that is obtained solving the differential equations, but it is out of the scope of this work to go in detail of the derivation of the equations. This works aims to present the theoretical solutions of buckling problems, to later compare it with Finite Element Method solution.

The procedure to get plates buckling loads is as follow. Firstly, using the energy method solution, k coefficients plots are obtained in terms of the geometry and the boundary conditions. These coefficients are directly related to the single buckling load. Consequently, with the corresponding k, the structure geometry and the material properties, the buckling load can be obtained. Then, for combined loadings, interaction equations and graphs are used, which are also obtained from energy method. These equations and graphs provide the buckling load of a structure in terms of non-dimensional ratios (there is one for each load in the combined loading), which are the ratio of the actually applied load and the buckling load of the structure if that load was applied alone.

3.1 Analytical methods

Energy method is the simplest and most direct method to solve elastic stability problems with different boundary conditions. This section is devoted to explain the most important aspects of the method. However, the reader may also read reference 1 for further understanding of the method.

The idea behind the Rayleigh-Ritz energy method is introduced in the reference as follows. When a structure buckles, it changes from a planar to a new slightly bent state, and just at the critical buckling load, both the planar and slightly bent shapes exist at once. Therefore, at the critical buckling load the strain energy of the plate (sum of the work done by bending and twisting moments) equals the energy stored in the plate by the critical load.

Based on that, energy obtains the critical buckling load by equating the energy stored on the plate (eq.3.1) to the work performed by the critical buckling load (eq.3.2).

$$U = \frac{1}{2} D \int_0^a \int_0^b \left\{ \left(\frac{\partial^2 w}{\partial x^2} + \frac{\partial^2 w}{\partial y^2} \right)^2 - 2(1-\nu) \left[\frac{\partial^2 w}{\partial x^2} \frac{\partial^2 w}{\partial y^2} - \left(\frac{\partial^2 w}{\partial x \partial y} \right)^2 \right] \right\} dxdy \tag{3.1}$$

$$T = \frac{1}{2} \int_0^a \int_0^b \left[N_x \left(\frac{\partial w}{\partial x} \right)^2 + N_y \left(\frac{\partial w}{\partial y} \right)^2 + 2N_y \frac{\partial w}{\partial x} \frac{\partial w}{\partial y} \right] dxdy \tag{3.2}$$

$$U = T \tag{3.3}$$

As the energy stored on the plate and the work performed by the critical load depend on the plate deflection, it is required to estimate a deflection function. This function will need to satisfy the boundary conditions (clamped, simply supported edges…) of the plate.

To achieve a good estimation of the buckling load, the key of the energy method is to select properly the approximated deflection function at the beginning. This implies that the accuracy of this method with respect to the exact solution can vary greatly from one problem to another, since the approximation of deflected functions for some problems may be more complicated. The approximated deflection function should approximate as much as possible to the exact deflection, which in turn satisfies all geometric and natural boundary conditions, and the differential equations governing the particular problem.

In order to approximate the deflection, a complete set of functions is used, with a finite number of equations. This does not match reality, because the structure is a continuous system, with infinite degrees of freedom, which implies that it will have a deflection function of infinite set of functions. Therefore, the more degrees of freedom are considered in the approximation, the closer to reality it will be.

The effect a finite number of equation to estimate the deformed function is that the estimated system is more constrained and with higher energy than in reality. Then, since the buckling load is obtained from the lowest energy state, the estimated load will be higher than the exact one. As the buckling load is obtained from the lower energy state, the resulting energy method estimated buckling load is greater than the actual one.

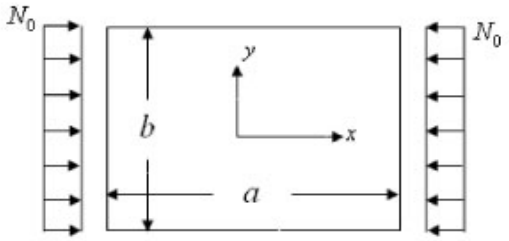

Figure 3.1. Simply supported plate in uniaxial compression

As an example of the application of the energy method, for the case of a simply supported plate under uniaxial compression (Fig.3.1) the deflection function, w, can be defined by eq.3.4. This equation can be seen to satisfy the boundary conditions of the problem, in this case eq. 3.5, 3.6, 3.7 and 3.8.

$$w = A_{mn} \sin\frac{m\pi x}{a} \sin\frac{n\pi y}{b} \tag{3.4}$$

$$w = 0 \quad at\ x = 0\ , y = 0 \tag{3.5}$$

$$w = 0 \quad at\ x = a, y = b \tag{3.6}$$

$$\frac{\partial^2 w}{\partial x^2} = 0 \quad at\ x = 0, x = a \tag{3.7}$$

$$\frac{\partial^2 w}{\partial y^2} = 0 \quad at\ y = 0, y = b \tag{3.8}$$

Then, substituting the deflection function in eq.3.1 and 3.2, after some derivations the following expressions are obtained for the energy stored on the plate (eq.3.9) and the work performed by the critical buckling load (eq.3.10).

$$U = \frac{ab}{8} D {A_{mn}}^2 \left[\frac{m^2\pi^2}{a^2} - \frac{n^2\pi^2}{b^2}\right]^2 \tag{3.9}$$

$$T = N_x {A_{mn}}^2 \frac{b\, m^2\pi^2}{8a} \tag{3.10}$$

Using the energy method approach, from conservation of energy the energy stored in the plate just at buckling is equal to the work done by the critical buckling load. Therefore we can equate eq.3.9 and 3.10, and isolate the buckling load N_x (eq.3.11).

$$N_x = \frac{\pi^2}{a^2} D \left[m + \frac{n^2}{m}\frac{a^2}{b^2}\right]^2 \tag{3.11}$$

The terms m and n represent the number of deformed plate semi-waves in longitudinal and transverse directions respectively. And these depend on the energy state of the plate. Since there are multiple combinations of m and n, they are multiple energy states. Remember that the buckling load is obtained from the lowest energy state. Then, observing eq.3.11 one notes that the buckling load for a given geometry (for given a and b) is obtained by choosing m and n to make N_x minimum. It is appreciable in the same equation that for all geometries minimum N_x is achieved with $= 1$. So imposing this and rearranging eq.3.11, one can obtain eq.3.12.

$$N_x = \frac{\pi^2}{b^2} D \left[\frac{m}{a/b} - \frac{a/b}{m}\right]^2 \tag{3.12}$$

The term depending on the plate geometry and m coefficient is denoted as coefficient k (eq.3.13), which is seen to be directly related to the buckling load. This term can be expressed in graphs showing its evolution with the plate aspect ratio a/b .

$$k = \left[\frac{m}{a/b} - \frac{a/b}{m}\right]^2 \tag{3.13}$$

If the obtained eq.3.13 is plotted in a graph (Fig.3.2) it can be observed that depending on the m chosen, one different curve will appear. Each curve represents one different energy state. Note

that among the different energy states illustrated, none has the lowest energy state for all a/b . In other words, which energy state is the minimum depends on each a/b. Observe that for instance, while for a/b=1, m=1 curve gives the lowest energy state, for the case of a/b=2, m=2 gives the lowest one). Therefore, in order to get the buckling load, m shall be selected in eq.3.12 to give the minimum energy state for the plate (because actual buckling load is obtained with minimum energy).

It is also worth mentioning that the peaks represent the moment in which the plate energy state shifts to another energy state. This is clearly seen in the buckled plates deformed shape, in which the number of half-waves (recall that it is determined by m) changes when there is a change in the energy state. For example, in the plate of Fig.3.2, when the aspect ratio is increased above $a/b = \sqrt{2}$ modal shape will change from having one single half wave in longitudinal direction, to have two. Finally, note that as m increases, the corresponding curves slopes decrease, which in turn makes the intersections (the peaks) between the curves to take place at a lower buckling load: the peaks are lower, and the final curve (in red) becomes flatter.

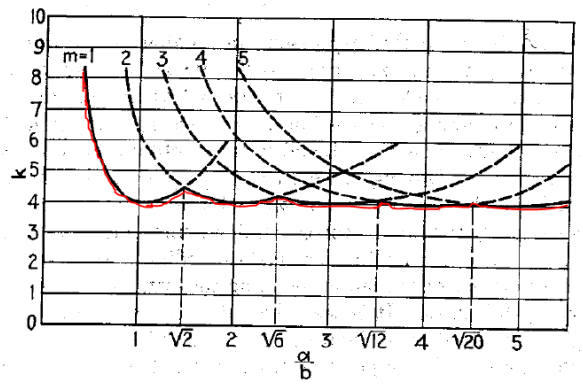

Figure 3.2. Buckling of simply supported rectangular plate under uniaxial compression. Source: Ref.1

Note that the detailed derivations of the buckling load by energy method can be found on reference 1 for the cases of simply supported rectangular plates under biaxial compression (Section 9.3), axially compressed rectangular plates with unloaded edges simply supported and loaded edges with different rotational restraints (Section 9.4), buckling of a rectangular plate simply supported along two opposite sides and uniformly compressed in the direction parallel to those sides (Section 9.5), rectangular plates under shearing (Section 9.7), and eventually buckling for rectangular plates for some cases with all edges clamped (Section 9.8).

3.2 Analytical results

Based on currently available investigations, theoretical solutions for single loading cases and for most important combined loading cases have been reached. Those results are presented in following sections.

3.2.1 Single loading

Theoretically calculated critical buckling single loads are computed using eq.3.14 and charts to obtain the factor k or K. It is appreciated that buckling load depends on the plate geometry, material, boundary conditions and loading case (recall that k depends on the type of loading, the boundary conditions at the loaded and unloaded edges and the plate geometry).

$$\sigma_{cr} = k\frac{\pi^2}{12(1-\nu^2)}E\left(\frac{t}{b}\right)^2 = K \cdot E\left(\frac{t}{b}\right)^2 \tag{3.14}$$

These charts (Fig. 3.3, 3.4 and 3.5) that provide k factor, come in their vast majority from the energy method. They are considered to be exact, because the approximated deflection function is equal or extremely close to the real one.

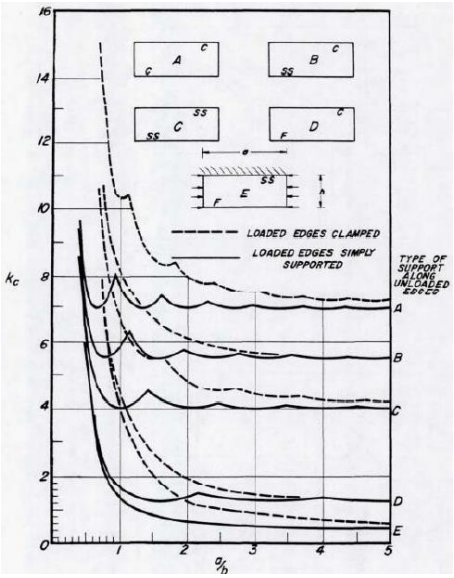

Figure 3.3. Compressive buckling coefficients for flat rectangular plates with different boundary conditions. Source: Ref.2

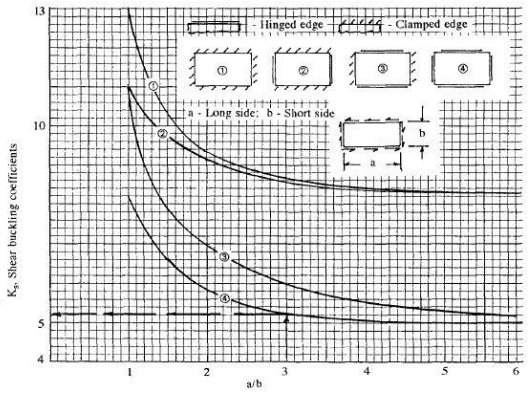

Figure 3.4. Shear buckling coefficients for flat rectangular plates with different boundary conditions. Source: Ref.4

It is observed that for all loadings except for shear, some peaks are present on the curves. The peaks become progressively shallower as the aspect ratio increases, and the curve becomes flat. Those peaks are related to the energy state of the plate. However, only the one which produces the lowest energy state of the plate (and correspondingly the lowest buckling load) is of interest.

Additionally, it is observed in all the charts that the critical buckling load increases as the elastic restraint increases. This seems reasonable, since the more constrained is the plate, the more load that will be needed to make it unstable.

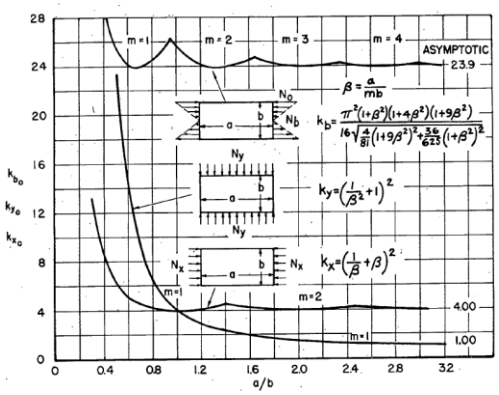

Figure 3.5. Pure bending, transverse compression and axial compression buckling coefficients for simply supported edges flat rectangular plates. Source: Ref.5

As for Fig.3.3, some interesting features can be appreciated. First of all, the boundary condition on the lateral edges is more determinant in the buckling load than those of the loaded edges. Secondly, for high aspect ratios plate buckling is no longer dependent on loaded edges boundary conditions. Finally, above certain aspect ratios, the buckling load no longer depends on the aspect ratio. This value can vary; around 3 for uniaxial compression (Fig.3.3), above 23.9 for pure bending (Fig.3.5) and around 6 for shear (Fig.3.4).

Finally, it is worth exploring the difference in the buckling loads between the different load cases. It can be observed that for a given aspect ratio, bending buckling coefficient (Fig.3.5) is the highest, meaning that a plate can withstand before buckling a much higher bending load than an axial compression load. Shear buckling load is also significantly higher than axial compression critical load, for a given aspect ratio.

Note that no references have been found providing analytical results for clamped plates under bending and transverse compression. It is also worth mentioning that Fig.3.4 gives K buckling factor (instead of k used in other plots). This factor depends on ν, which is particular for each material. Since Ref.4 does not specify the material for which this graph is constructed, $\nu = 0.3$ has been assumed because it is the most common one in graphs with K. However, note that it is not certain that is assumption is correct and therefore, this could be a source of errors.

3.2.2 Combined loading

Single loading cases establish the base for the study of combined loading cases. Based on the obtained results with the energy and alternative methods for single loading cases, eq.3.15 can be used to determine combined loading buckling, where R_1, R_2 and R_3 are stress ratios (eq.3.16) and p, q and r are exponents that need to be determined to fit the results. Observe that interaction equations for combined loadings are based in non-dimensional load ratios, which represent each of the individual loadings (compression, shear, bending...). Note that σ_{cr} in a stress ratio (eq.3.16) is the critical buckling load of the structure as if it was subjected to a single loading. So conceptually speaking, in a case of combined compression and shear (for example), R_C indicates how much compression the structure is withstanding, with respect to the compressive buckling load of the structure as if the structure was subjected only to compression (without shear).

$$R_1{}^p + R_2{}^q + R_3{}^r + \ldots = 1 \tag{3.15}$$

$$R = \frac{\sigma_{applied}}{\sigma_{cr}} \tag{3.16}$$

Based on eq.3.15, the interaction equations formulas currently available from the references are presented in Table 3.1.

Interaction equation	$\boldsymbol{R_S{}^2 + R_C = 1}$		$\boldsymbol{R_S{}^2 + R_B{}^2 = 1}$	$\boldsymbol{R_B{}^{1.75} + R_X = 1}$	$\boldsymbol{R_B{}^{1.75} + R_Y = 1}$
Combined loading	Axial compression Shear		Shear Bending	Axial compression Bending	Transverse compression Bending
a/b	All	Infinite	Infinite	All	All
Edges rotational restraints	Simply Supported	Clamped	Simply Supported	All	All

Table 3.1. Interaction equation formulas published, June 2015. Source: Ref.3, 5, 6, 7, 8, 9, 10

- ***Combined shear and axial compression***

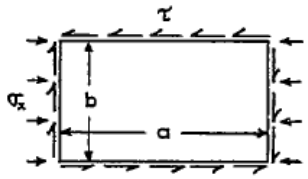

Figure 3.6. Combined shear and axial compression

According to Elbridge Z. Stowell and Edward B. Schwartz (November 1943), eq.3.17 provides with reasonable accuracy (and valid for engineering purposes) the values of combined shear and direct stress (Fig.3.6) at which infinitely long plates with equal restraints against rotation in all edges, at which a flat plate will become unstable. The equation is derived from energy method in Appendix B of reference 5.

$$R_S{}^2 + R_C = 1 \qquad (3.17)$$

This reference determines that eq.3.17 is valid if "*the restraint supplied to the sheet by the stiffeners is independent of the wave length of the buckles*". Then, his author follows that "*In an actual structure, however, the restraint is usually dependent upon the wave length of the buckles*". In order to see to what extent this relation affects the validity of eq.3.17, his author tests the equation comparing exact results to the interaction equation curve (Fig.3.7). That is why this reference provides the Appendix A deriving the exact solution for this particular combined loading, for infinitely long plates, for the cases of all edges with $\varepsilon = 0$ (simply support), $\varepsilon = 10$ and $\varepsilon = \infty$ (clamped).

This reference finally concludes that the difference between exact solution and eq.3.17 is small, proving the validity of the equation for the case of infinitely long plates, with same equal restraints against rotation in all edges (independently of the degree of restraint).

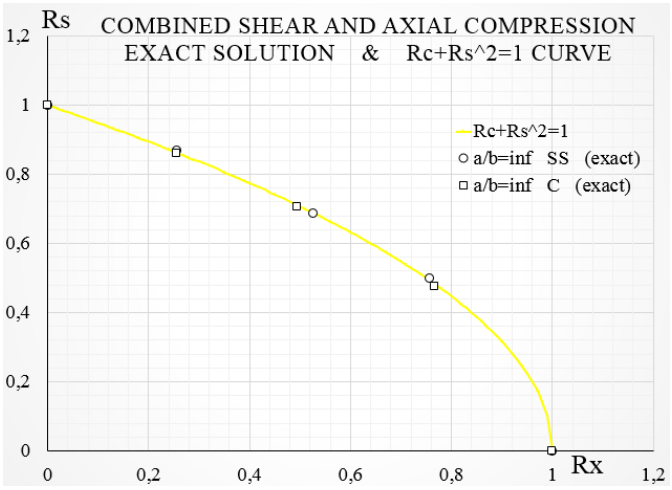

Figure 3.7. Comparison of interaction curve and exact solution results in infinitely long plates. Source: Ref.5

As for the case of small aspect rations, reference 10 shows that the equation is also considerably accurate for square plates with simply supported edges

Additionally to the case of square plates, reference 6 proves that eq.3.17 is also valid for the aspect ratios 1, 2 and 4. This author shows that results obtained with the energy method for this loading combination (and with all edges simply supported), follow reasonable degree of accuracy the parabola defined by eq. 3.17 (Fig.3.8). It is concluded then, that this equation is valid for all geometries if all edges are simply supported.

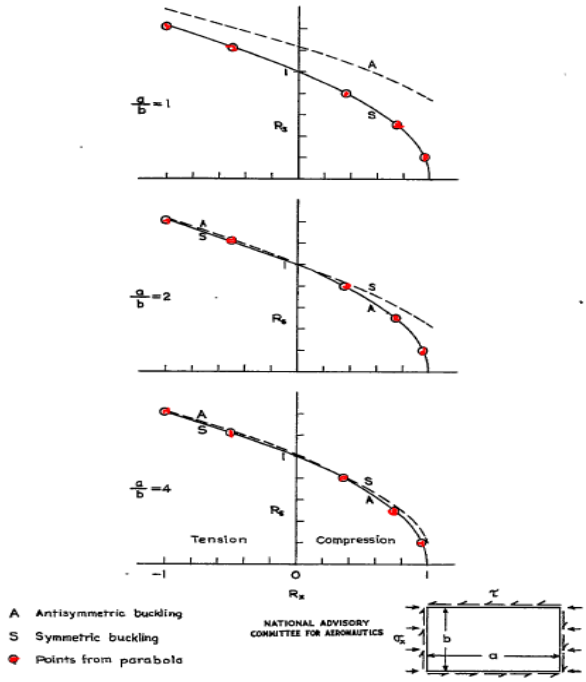

Figure 3.8. Comparison of interaction curve and energy method solution with all edges simply supported, for a/b=1, 2 and 4. Source: Ref.6

It is worth mentioning that apart from eq. 3.17, for the combined loading of axial compression and shear, references 9 and 10 recommend eq.3.18. Reference 10 recommends it for clamped edges flat plates with any aspect ratio. Reference 9 recommends it for any flat plate independently of the aspect ratio and the edges rotational restraint. This curve is conservative for all those cases, but does not approach as accurately the exact results as eq. 3.17 does.

$$R_S{}^{1.75} + R_C = 1 \qquad (3.18)$$

- ***Combined shear and bending***

For combined shear and bending (Fig.3.9), references 3, 11 and 12 present different interaction curves.

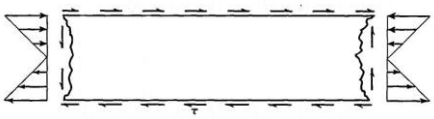

Figure 3.9. Combined shear and bending

Regarding reference 12, it presents an interaction curve (curve in blue in Fig.3.10) which is constructed based on an average of. This curve is presented for the case of infinitely long flat plates with all edges simply supported

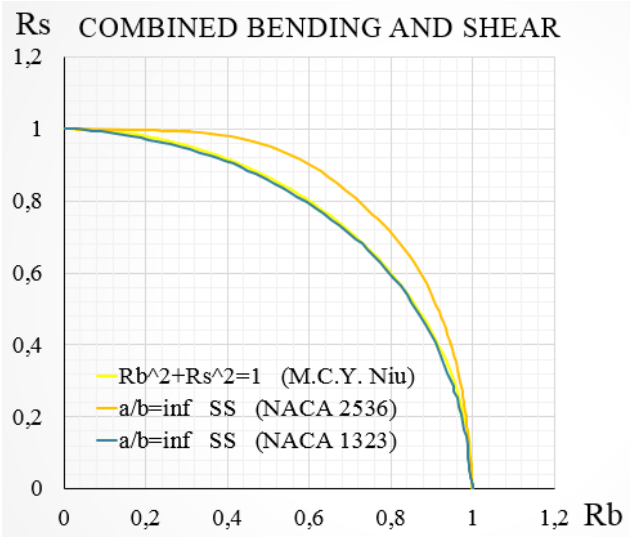

Figure 3.10 Comparison of interaction curves from different sources: NACA 1323 (Ref.12), from Rb^2+Rs^2 of M.C.Y.Niu (Ref.3) and NACA 2536 (Ref.11).

Then, reference 3 presents eq.3.19 (curve in yellow in Fig.3.10), without specifying its field of validity as far as the aspect ratios and the edges rotational restraints are concerned.

$$R_B{}^2 + R_S{}^2 = 1 \qquad (3.19)$$

Thirdly, the interaction curve in orange (Fig.3.10) is presented in reference 11, which is obtained by the energy method, which is carefully explained in Appendix A of this reference. This curve is presented for the case of infinitely long plates and all edges simply supported.

Finally, it is interesting to appreciate in Fig.3.10 that the curve provided by NACA 1323 (in blue), is in good agreement with curve from eq.3.19 (in yellow). These two lay notoriously below the curve provided by NACA 2536 (in orange).

- ***Combined axial compression and longitudinal bending***

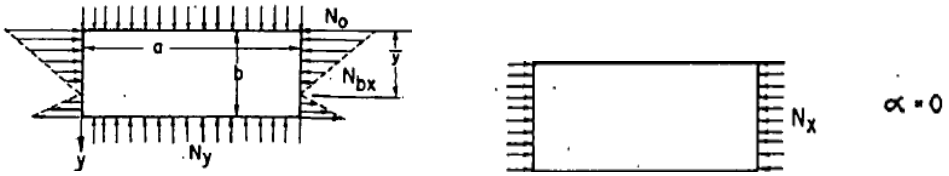

Figure 3.11. Longitudinal bending for a non-zero $\propto$ value (left) and longitudinal bending for $\propto = 0$ case (right).

When combining bending with axial compression, it should be noted that compression is a particular case of longitudinal bending. That is, being the bending load defined by eq.3.20, see that for the case of $\propto = 0$ (where $\propto$ represents the ratio N_{BX}/N_0) the loading becomes a pure axial compression.

$$N_{BX} = N_0\left(1-\propto \frac{y}{b}\right) \tag{3.20}$$

When there is a combined loading of pure bending and compression, the system can be illustrated as Fig.3.12.

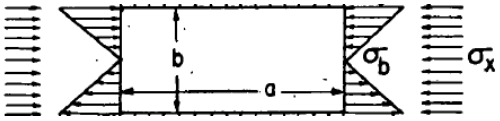

Figure 3.12. Combined axial compression and longitudinal bending in a rectangular flat plate.

For this combined loading case, reference 4 presented several interaction curves (Fig.3.13) for plates with simply supported edges and different aspect ratios. Note that since the reference only provides 11 points of the curve (it does not provide the curve itself), only the actual points can be considered a reliable data source, being the line joining the points only a tool to define the general trend.

Overall, it is appreciated that the change of the curves as the aspect ratio increases from 1 to 4 does not follow a predictable trend. That is, curves for a/b=2 and 3 are not an intermediate transition between square plate curve and the one for a/b=4. That is why, it is probable that the curve, for example, of a/b=1.5 will not lay between curves for a/b=1 and 2.

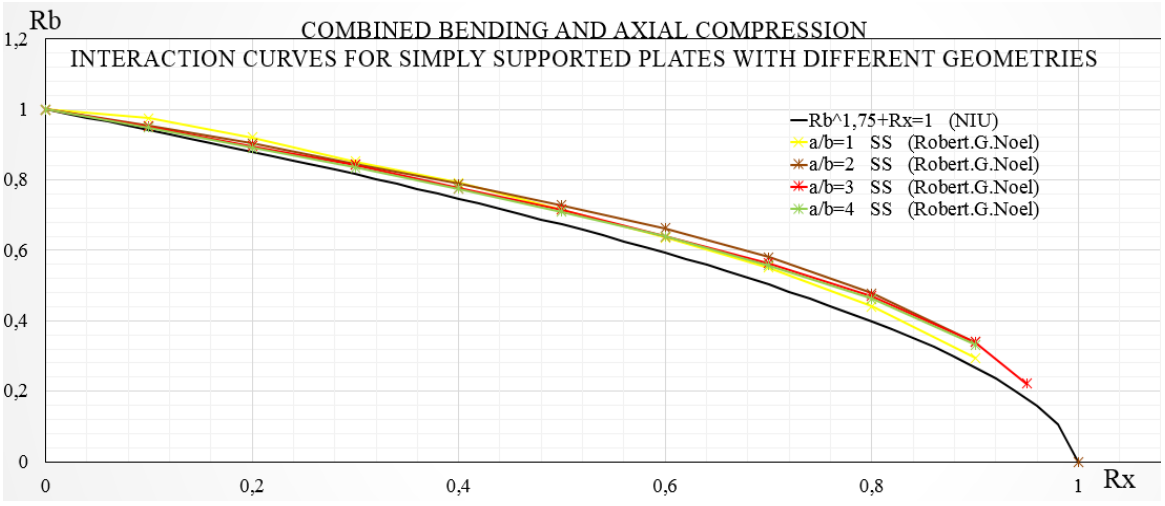

Figure 3.13. Interaction curves all edges simply supported rectangular plates with a/b=1, 2, 3 and 4.

The results provided by reference 4 are attained by using the energy method (derived in Theoretical Analysis of the reference). The different results observed according to the plate geometry, makes Robert. G. Noel to conclude that no general interaction equation is available for the combination of bending and axial compression. Nevertheless, this statement is in disagreement with reference 3, which proposes equation ${R_B}^{1.75} + R_X = 1$. Both approaches will be evaluated in a later section when comparing theoretical and Finite Element Method results.

- ***Combined transverse compression and longitudinal bending***

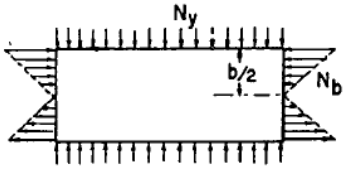

Figure 3.14. Combined transverse compression and longitudinal bending in a rectangular flat plate.

Regarding combination of transverse compression and bending, Norman Grossman published in 1948 (Ref.13), the resulting interaction curves produced by this combination for different aspect ratios (solid curves in Fig.3.15). These results are obtained with the Rayleigh-Ritz energy method (detailed derivation in the reference 13), whose accuracy is increased in this case by performing a matrix iteration procedure (see Mathematical Analysis in the reference), which iterates until convergence is achieved and results are satisfactorily accurate. This allows high accurate in the results and therefore, it can be expected little difference between these results and the exact solution.

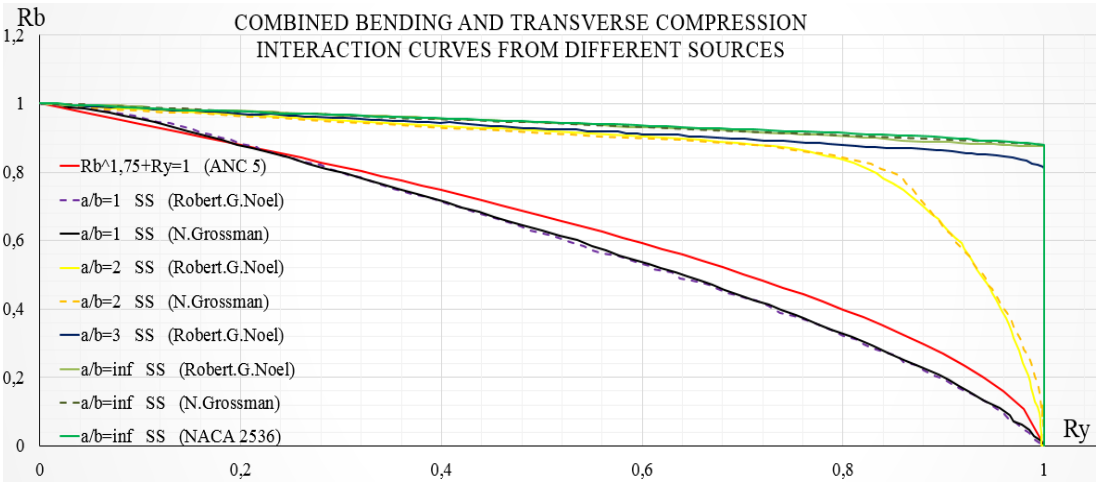

Figure 3.15. Comparison of interaction curve for several aspect ratios and edges rotational restraints, from different sources. References 4, 9, 11 and 13

This reference concludes proving that being the interaction curves for this loading combination dependent on the geometry, no general interaction curve is valid for all cases, as it was presented in ANC 5 (Ref.9), which presented equation $R_B{}^{1.75} + R_Y = 1$. The disagreement between the equation curve (red curve in Fig.3.15) and the results provided by N.Grossman in reference 13 illustrates this fact.

Additionally, reference 13 also relates graphically (Fig.3.16) the plate buckling half waves with the aspect ratio.

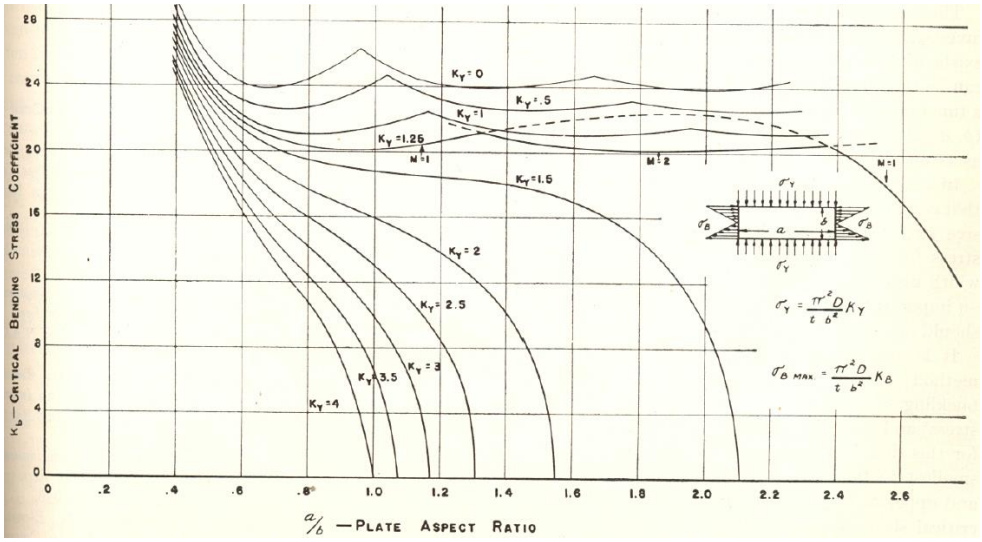

Figure 3.16. Instability coefficients for flat plates in combined bending and compression with simply supported edges. Source: Ref.13

Later, in 1951, interaction curves for this loading combination were published (Ref.11). Similarly to that happened with N. Grossman results, these curves (Fig.3.15) were also computed by the energy method (Appendix A in reference 11). The curves were tested and validated comparing them with the interaction curves published by N. Grossman. Observation of both set of curves (Fig.3.15) show that the results are quite the same, having only small difference due to the digitalization process from the original source to this work. Some negligible differences are also due the number of roots used when applying the energy method.

NACA 2536 also includes additional features with respect to the previous work of N. Grossman. Among others, it is worth to mention the relation it stablishes between the changes in slope of the interaction curves, and the buckle wave lengths transitions. This work states that when sharp changes in the slope occur, the plate wave changes from finite to infinite length. In the case the slope change rather than sharp is gradual, a gradual transition to infinitely long buckle wave length takes place.

Finally, reference 4 also presents several interaction curves (Fig.3.15) that are seen to be consistent with the other references, and in fact, his author used some of the findings in reference 13 for his publication. These results are also obtained with the energy method, whose detailed theoretical analysis can be found in reference 4. As it can be appreciated in the figure, the curves provided by this reference match the results of previous references presented curve sets.

4 FEM analysis

Once having analyzed the problem with theoretical methods, the problem is to be analyzed with Finite Element Method. This section is devoted to explaining how FEM works theoretically when solving the static and buckling problems. Additionally, in this section the description of the most relevant Nastran used in the project will be described. Finally, the particulars of the FEM models used will be explained in detail.

4.1 Finite Element Method approach

Finite Element Method is a computational technique used to solve a great variety of problems in engineering, like those related to structures. It is used in complex problems where analytical solutions are difficult to obtain, or where the simplifications required to obtain one are such that the solution is heavily restricted and loses practical application.

FEM models a structure by discretizing it into an equivalent set of smaller units (finite elements) which are interconnected by points called nodes.

The most important characteristic that defines a finite element is its stiffness matrix$[K]$. This matrix contains information of the geometric and material behavior of the element, which determines the resistance of the element to deformation when subjected to loading. In other words, it relates the element deformation $\{X\}$ to the load applied to the element (eq.4.1)

$$\{F\} = [K]\{X\} \tag{4.1}$$

FEM computes the approximate solution of boundary value problems, where the values of the dependent variables (which are governed by the differential equations) are calculated. On the boundaries of the dependent variables field, the boundary conditions are the specified values of the dependent variables. If the loads $\{F\}$ applied to the structure are known, and the displacements$\{X\}$ are to be determined (they are the dependent variables), the problem is solved as shown in eq.4.2. In this case, the boundary conditions determine the value of the displacements at certain nodes.

$$\{X\} = [K]^{-1}\{F\} \tag{4.2}$$

Once known the displacements, strains and stresses are easily obtained following strain and stress equations (eq. IA and IS).

$$\varepsilon = \frac{\Delta u}{L} \tag{4.3}$$

$$\sigma = E\,\varepsilon \tag{4.4}$$

The dependent variables are calculated at the nodes. The values of the dependent variables at the elements can be calculated by means of interpolation functions from the grid point data. The number of degrees of freedom associated with a finite element is the product of element nodes and the amount of the field variables to be computed at each node. In a linear static model, this implies a total of 6 degrees of freedom at each node (the three translations and three rotations about the coordinate system axes).

When the geometric deformations due to the applied loads are small and the strain levels remain within the elastic region of the material, the stiffness matrix [K] can be assumed to remain constant through the problem and eq.4.2 can be solved directly by performing a matrix inversion. This is method of solution of a static linear elastic FEM model. When [K] changes significantly due to large displacements or strains past the elastic limit of the material, the linear elastic FEM will not provide an accurate solution to the problem. In those circumstances, a more complex geometric and/or material non-linear FEM model can be built.

The phenomenon of buckling consists in an abrupt change in deformation that would lend itself to the use of non-linear FEM solutions. However, a much simpler solution method exists that provides excellent accuracy for most applications, which is rooted in the principle of the differential stiffness matrix.

The role of the differential stiffness matrix $[k_d]_i$ is to reduce (soften) or increase (stiffen) the linear stiffness matrix $[k_a]_i$ depending on if the applied load is compressive or tensile respectively. Note that the differential stiffness matrix depends on the geometry, element type, and applied loads to the structure. Mathematically, this is represented by eq.4.5, 4.6 and 4.7, representing the whole system linear stiffness matrix, differential stiffness matrix and overall system stiffness matrix respectively, where *i* stands for each of the model elements.

$$[K_a] = \sum_i^n k_{a_i} \tag{4.5}$$

$$[K_d] = \sum_i^n k_{d_i} \tag{4.6}$$

$$[K] = [K_a] + [K_d] \tag{4.7}$$

If eq.4.8 defines the total potential energy, for the static equilibrium of the system, total potential should be constant, satisfying eq.4.9.

$$[U] = 0{,}5\{u\}^T[K_a]\{u\} + 0{,}5\{u\}^T[K_d]\{u\} \tag{4.8}$$

$$\frac{\partial[U]}{\partial u_i} = [K_a]\{u\} + [K_d]\{u\} = 0 \tag{4.9}$$

Since $[K_d]$ can be expressed in terms of P_a (the applied load) and $[\overline{K_d}]$ (material stiffness) as shown in eq.4.10, then eq.4.9 can be rewritten as eq.4.11, where it is appreciated that static equilibrium of the system is only satisfied for certain loads P_a.

$$[K_d] = P_a[\overline{K_d}] \tag{4.10}$$

$$\left[[K_a] + P_a[\overline{K_d}]\right]\{u\} = 0 \tag{4.11}$$

By solving eq.4.11 forP_a , the critical buckling load is obtained. Note that while in reality a continuous system has infinite degrees of freedom, the Finite Element Method is based on an approximation, in which the number of degrees of freedom is finite. The structure will have as many buckling loads as the number of degrees of freedoms in the model. This can be defined by eq.4.12, which introduced in eq.4.11, produces eq.4.13 which has the form of an eigenvalue problem, where λ_i are the eigenvalues and P_a is the applied load.

$$P_{cr_i} = \lambda_i P_a \tag{4.12}$$

$$\left[[K_a] + \lambda_i[\overline{K_d}]\right] = 0 \tag{4.13}$$

Buckling loads will be obtained using eq.4.12.

Some Finite Element Method limitations and assumptions exist for the linear buckling problem. Deflections shall be small, element stresses shall be elastic and the distribution of the internal element forces due to applied loads remains constant.

4.2 Femap and Nastran elements

In order to perform FEM analysis, the tools employed are Femap (pre and post-processor) and Nastran (solver), which have been selected among other tools (such as ABAQUS) because in addition to being widely used in aeronautical industry, it is currently used at Airbus. Furthermore, while ABAQUS was used for some degree courses, and therefore its use would not be new for the author, Femap and Nastran have not been used by the author before. Consequently, academically speaking, performing the project with Nastran and Femap would be more profitable and challenging.

The following sections focus on the description of most important elements used in the project.

- ***CQUAD4 element***

Plates are characterized geometrically by having one dimension (thickness) small compared to other two dimensions. Therefore, it is reasonable to use Two-Dimensional elements (also called surface elements) in Nastran to model plates. Within this element category, CQUAD4 plate-shell element was used.

It is worth mentioning that Nastran plate elements follow classical assumptions of thin plate behavior, which therefore proves the validity of the election of these elements. The thin plate behavior assumptions that apply to the project are:

- Thickness is much smaller than the next larger dimension.
- Plate´s midsurface deflection is small compared to its thickness.
- The normal to the midsurface remains normal during bending.

The membrane (in-plane) stiffness of a surface element is calculated assuming plane stress theory. This theory (as opposed to plane strain) has been used because most of thin structural elements made of aluminum (usual material in wing panels) are modeled successfully in this way. As for the elastic stiffness out of plane, CQUAD4 elements do not provide any stiffness for the rotational degrees of freedom perpendicular to the element surface

CQUAD4 has been the specific surface element employed. It is an isoparametric quadrilateral shape element with optional coupling of bending and membrane stress systems. It is worth noting that the coupling of membrane and bending is a high order effect that is not necessary to consider in this project, because this effect only applies to plates with not symmetric section or plates whose neutral axis is displaced with respect to the points of support. The previous are not the case of the problem studied.

- ***Coordinate systems***

Basically, two coordinate system types appear in Nastran: basic (defined by default) and local (defined by the user) reference systems. Both, the local coordinate systems and the basic one are related (Fig.4.1). In this project only basic reference system has been used.

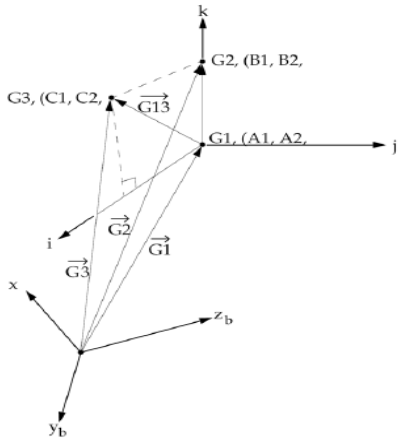

Figure 6-2. Coordinate System Definition

(i, j, k) = local (user defined) coordinate system (x, y, z) or (r, θ, z) or (r, θ, ϕ)
(x_b, y_y, z_y) = basic coordinate system

Figure 4.1. Basic and local coordinate systems (Source: Nastran User Guide, Figure 6-2)

The basic coordinate system is, as said, defined by default and it is used to locate the model in the space, locate grids points, elements, applied forces, to define the degrees of freedom (in single point constraints) and it provides the nodal displacements and forces.

For the particular case of this project, the basic coordinate system has been located in the center of the plate, with x axis parallel to plate long edge, y axis parallel to plate short edge and z axis defined by right hand rule. This convention has been used following that used in the theory.

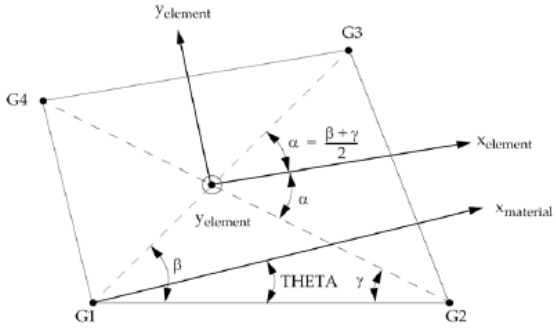

Figure 18-12. CQUAD4 Element Geometry and Coordinate Systems

Figure 4.2. CQUAD4 Coordinate System Definition (Source: Nastran Quick Reference Guide)

Independently of basic and local reference system, each element has its own element reference system. For the CQUAD4 elements used in this project, the element coordinate system is defined shown in Fig.4.2. The x axis is defined by the bisector formed by the center with nodes G2 and G3. The y axis is defined to be perpendicular to x axis in the plane of the. Finally, z axis is perpendicular to the xy-plane in accordance to the right hand rule.

Element output provided by Nastran (stresses, forces and strains) is given in the local coordinate system of each element. The sign convention employed by the program is shown in Fig.4.3.

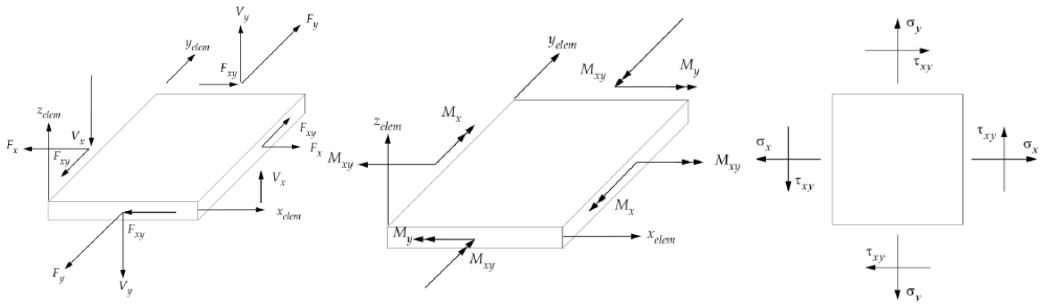

Figure 4.3. Sign criteria in shell elements for forces (left), moments (center) and stresses (right). Source: Nastran Element Library Reference, fig.4-11, 4-12, 4-13

- ***RBE3 element***

RBE3 establishes a connection between one node (*dependent* node) and several nodes (*independent* nodes, which can be one or several nodes), such that the loads applied in the dependent node are translated and distributed to all the independent nodes. That is, if a compression force of 100 N is applied to the dependent node, and this is connected to 100 independent nodes, each dependent node will be subjected to a compression force of 1N.

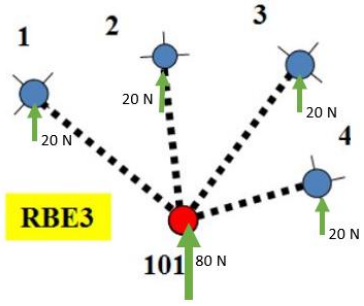

Figure 4.4. Nastran RBE3 element. Source: www.stressebook.com

As for its application for the present project, this element revealed to be extremely useful. This project involved the design of multiple loading conditions distributed along the plate edges. In the absence of RBE3, each loading would have to be distributed manually along all the nodes of the edge. Thanks to RBE3, it was possible to apply the load at a single node and letting the software properly distribute the loads among all the nodes.

It is worth to clarify that RBE3 facilitates the work (as explained before), but it does not perform the work better (than distributing the load manually). The RBE3 only distributes the load along all edge nodes, in the same manner as if the user constructed one nodal load at each of the nodes of the edge.

4.3 FEM modelling phase

Once a proper theoretical FEM background is acquired, the next critical step is to model in FEM the plates that will be analyzed for future comparison with theoretical results.

The goal of the models is to be able to simulate accurate enough plates buckling under the combinations of loads and boundary conditions analyzed. Since we want to perform a proper comparison of the buckling predicted by FEM and charts and equations, the difference shall never be due to incorrect modeling in FEM. This could lead to wrong conclusions. Therefore, this stage is vital for the project, and a severe validation of the models has been followed to validate each model.

4.3.1 Material and property

For the material, an aluminum alloy with elastic Young modulus of $E = 70\ GPa$ and Poisson ratio of $\nu = 0.3$ has been used. These properties do not correspond to a common aluminum alloy. Initially, Aluminum 6061-T6 was used ($E = 70\ GPa$, $\nu = 0.33$), but theoretical results for shear (Fig.3.4), coefficient K is given for a Poisson ratio of $\nu = 0.33$. Although K could be converted into k (independent of the material), for simplicity a material with $E = 70\ GPa$ and $\nu = 0.3$ was selected. Note that if the same material is used in FEM and theory, the comparison will not be affected by using different materials.

The property has been defined with the selected material and a thickness of $0.5\ mm$. This value was selected to be small enough in comparison to plate dimensions and satisfy thin plate theory.

4.3.2 Transverse shear considerations

When modeling the plates in FEM, an important point to consider is the convenience of accounting for transverse shear. Buckling problems in rectangular plates solved by the energy equation (resulting in the graphs and the equations) ignore transverse shear capability (reference 14). In order to perform a comparison with FEM results as reliable as possible, and with the aim of reducing the potential sources of divergences in the results, transverse shear has been neglected in FEM modeled problems.

It is worth to mention that assuming negligible transverse shear effect is quite reasonable for the problems analyzed in this project. Note that plate edges dimensions (from 100 to 2000 mm) are much higher than plate thickness (0,5mm). However, it has been found interesting to quantify with FEM the effect of the transverse shear on the critical buckling load for the case of axial compression for different thickness. These differences can be appreciated in Table 4.1, for the case of axial compression in a rectangular plate of a/b=2 (a=200mm, b=100mm) simply supported.

σ_{cr}	t=0,25mm	t=0,5	t=0,75mm	t=1mm
With TS (MPa)	1,5861	6,3375	14,2399	25,2751
Without TS (MPa)	1,5871	6,3482	14,2835	25,3930
Difference(%)	**0,06**	**0,17**	**0,31**	**0,47**

Table 4.1. Differences between critical load with and without the effect of transverse shear.

This analysis proves that as expected, the effect of transverse shear in the obtained results is negligible. However, if the thickness was increased, it would reach a point in which accounting for transverse shear would be desirable. It is appreciated that not accounting for transverse shear is not conservative, which reinforces the importance of considering it for larger thicknesses.

4.3.3 Elements

Since CQUAD4 elements used in this work do not have stiffness in the rotational degree of freedom out of plane (remember previous CQUAD4 element definition), stiffness was added manually to this degree of freedom. This was done by adding K6ROT parameter card, which ads the desired stiffness by the user to the degrees of freedom associated to a CQUAD4 element. A card with value 100 has been used as it is the suitable one for static and buckling analysis.

4.3.4 Mesh

The choice of the mesh to be employed is an important decision when a model is designed. While the reality could not be properly simulated if the mesh is not fine enough, working with an extremely fine mesh could lead to longer analysis times.

An important consideration when deciding the mesh to be used has been the need defined by Nastran User Guide of having at least five grid points per half sine wave, which has set the lower limit requirement.

Apart from that, the mesh has been designed so that the elements (all of the CQUAD4) are square shaped, because as this elements tend to be more rectangular shaped, their accuracy in the results is reduced.

Once considered the previous points, a study has been carried out analyzing the effect of different mesh densities in the buckling load (Table 4.2).

MESH SENSITIVITY ANALYSIS, a/b=1 (single loadings)			
Axial compression, Simply Supported			
Element size	Model nº elements	σ_{cr} (MPa)	Difference with analytical, %
$2x2\ mm^2$	2500	6.3585	-0.07
$1x1\ mm^2$	10000	6.3499	-0.21
$0.8\ x\ 0.8\ mm^2$	15625	6.3453	-0.28
Axial compression, Clamped			
$2x2\ mm^2$	2500	16.0306	0.40
$1x1\ mm^2$	10000	15.9878	0.13
$0.8\ x\ 0.8\ mm^2$	15625	15.9772	0.06
Bending, Simply Supported			
$2x2\ mm^2$	2500	41.1370	1.07
$1x1\ mm^2$	10000	40.8202	0.58
$0.8\ x\ 0.8\ mm^2$	15625	40.7329	0.36
Shear, Simply Supported			
$2x2\ mm^2$	2500	14.7557	1.17
$1x1\ mm^2$	10000	14.7638	1.23
$0.8\ x\ 0.8\ mm^2$	15625	14.7601	1.20
Shear, Clamped			
$2x2\ mm^2$	2500	23.1014	0.50
$1x1\ mm^2$	10000	23.1362	0.65
$0.8\ x\ 0.8\ mm^2$	15625	23.1396	0.67

Table 4.2. Mesh sensitivity analysis for aspect ratio 1 with different single load cases.

MESH EFFECT ON ANALYSIS TIME		
a/b=1		
Element size	Model nº elements	NASTRAN analysis time (min)*
$2x2\ mm^2$	2500	3.2
$1x1\ mm^2$	10000	16.5
$0.8\ x\ 0.8\ mm^2$	15625	27.1

*Times corresponding to a computer with a AMD Quad-Core Processor, and the analysis being performed providing the same range of eigenvalues, and asking for the same results (all single loading cases) for all meshes.

Table 4.3. Analysis of the effect of the mesh on the analysis time.

Mesh sensitivity analysis for single loading (Table.4.2) has shown that the difference between FEM and analytical results is already very low for any of the mesh densities studied. Note that the change in σ_{cr} is very low (of the order of 0.01-0.03 MPa) as the mesh is refined, except in the case of simply supported longitudinal bending, for which the change is of the order of 0.3 MPa (still low). Therefore, as far as the accuracy is concerned, any of the three options would provide valid results.

In order to decide among the options discussed, the time required to perform a reference analysis was studied for each of the meshes (Table. 4.3). Note that the times shown are not important (though the order of magnitude can provide an idea of the times required for single loading buckling analysis), but the relation between the times for different meshes. Since one of the characteristics of Lanczos analysis (method employed in the analysis for eigenvalue extraction) is that the analysis time of the buckling problem is proportional to the amount of eigenvalues extracted, it is reasonable to think that for complex loading cases (where more eigenvalues are extracted to build up the curves) the times will increase, but the relation between times for different meshes will be similar. Finally, note that when solving the buckling problem Nastran also performs a static analysis, whose analysis time is much shorter than that of the buckling analysis.

The results of the study of the analysis times reveals that notorious difference in time happen for different meshes. Note that from the fastest (3.2 min with 2500 elements) and slowest analysis (27.1) there is a great difference (8.47 times).

In conclusion, it has been decided to use a mesh with 2 mm square elements because the results are reasonably accurate, and although these results could be slightly improved (in the order of 0.01-0.03 MPa, for general cases, it is not worth the increase in time, which is notorious (up to 8.47 times). On the other hand, for particular cases in which a given loading case requires higher accuracy, a finer mesh will be employed.

Finally, note that this was a preliminary mesh analysis to know a suitable mesh to work with, and that is why only single loading cases have been analyzed. Nevertheless, in the later section in which FEM and analytical results are compares, several mesh sensitivity analysis in combined loading cases will be performed.

4.3.5 Loads and boundary conditions

Although the proper modelling of the boundary conditions and loads might look an easy task, designing the boundary conditions of a plate such that it represents exactly the reality can become a challenging activity. This is mainly, among other causes, because of the reactions that appear

each time something is constrained, which is very detrimental specially when trying to combine various loadings. Note that boundary conditions and loads will be explained in the same section because their modeling is very much interrelated as it will be observed along the section.

First of all, it is worth explaining how boundary conditions work in Nastran. Each grid in the plate will have six degrees of freedom (three in translation and three in rotation), which can be either restricted or constrained or left free.

If a degree of freedom is constrained in one direction (for example in x) and the model is subjected to a resultant load in this direction, the constrained grid will react this load, creating a reaction force in the opposite direction. For this project, note that in reality plates do not present reactions (resultant forces are in equilibrium in all cases) so either they are avoided in FEM, or they are used as applied loads.

On the other hand, if no degree of freedom is constrained in one direction in which a resulting load is acting, Nastran will raise an error because it cannot compute this mathematically (and it will therefore raise a fatal error). In other words, it can be said that Nastran will understand that not being any restriction in the given direction, the plate will "jump" in this direction when the load is applied.

The boundary conditions of simply supported and clamped edges seen in the references (and presented in the theoretical analysis) are defined in FEM restricting translation degrees of freedom in the case of simply supported edges, and restricting all degrees of freedom (translations and rotations) in the case of clamped edges. However, it is not always necessary to restrict all the degrees of freedom, because sometimes some degrees of freedom might be already restricted due to the geometry of the problem. For the particular case of the plates in this project, when modeling clamped edges, the edges parallel to y direction (short edges) do not have rotations in x and z constrained. This is because the grid points of the edge are joined in y direction, which implies that the only possible rotation there is the one for which the axis of rotation is the edge itself; rotation parallel to y axis. That is also why long edges (parallel to x axes) do not have rotations in y and z restrained.

At the first stages of the modeling phase, the approach taken ("Approach 1" to model loads and boundary conditions was based on using the reactions as applied loads. For example, in the case of simple axial compression, if one edge is loaded in negative y direction at 100N and the opposite edge is restrained in y direction, a reaction load of 100N will appear along the opposite edge in positive y direction. Additionally, the perimeter was restrained as explained before for simply supported and clamped edges. Apart from those restrains, in one of the corners of the constrained edge, all the degrees of freedom was restrained, which as explained before, is to avoid mathematical error of FEM when not all the degrees of freedom are restrained. Then, it was ensured in the static results that the loads reacting in this grid point were low (not affecting the results).

Although this approach has been observed to be valid (with a difference of only 0.16% with respect to analytical result and the finally chosen "Approach 2", see Table 4.4) for some single cases like the referred axial compression, other loading cases (specially combined loading ones) raised lots of issues which were hardly solvable. Therefore it was decided to look for another different approaches.

SIMPLY SUPPORTED AXIAL COMPRESSION with a/b=1				
Approach	Description	$\sigma_{cr}\ (MPa)$	Difference with analytical, %	**Difference App1-App2, %**
1	1 edge loaded in x, 1 edge restrained in x	6,3453	-0.44	**0,16**
2	2 edges loaded in x, no edges restrained in x	6,3351	-0.28	

Table 4.4. Comparison of the critical buckling load FEM results with first and second approach for simply supported edges axial compression with a/b=1 rectangular plate.

Then, the modeling of the loads and boundary conditions was approached by loading only one of the edges of the plate and constraining the other (for the case of axial compression), to get the reaction forces. Once got the reaction forces, the restraints were removed from the constrained edge and the previously obtained reaction force was applied. This is supposed to be equivalent. However, this approach did not work properly and the results obtained were far from the theoretical ones.

Later, it was considered the possibility to modelling the problem giving FEM the displacements (instead of the loads) to obtain then the loads. Recall from the section explaining Finite Element Method working that the method relates loads and displacements, and although the most common practice is to get the displacements from the loads, the problem can be also solver in the other way round. This option was discarded because it was more complicated than the finally selected approach ("Approach 2").

Approach 2 is based in applying directly all the loads involved at the problem, without using the reaction forces as applied loads. Therefore, no significant reaction forces are allowed to appear in this approach (this checking is one of the results validation procedures). The restrictions used for this case changed from previous approaches. The grid point which was usually restricted in all degrees of freedom and located at a corner, was moved to the plate center node and restricted in x and y translation and in plane rotation. The reason for this change was to let all the perimeter to be restricted only in out of plane translation for simply support case. The final configuration of the boundary conditions in Approach 2 for simply supported and clamped edges is illustrated in Fig.4.5.

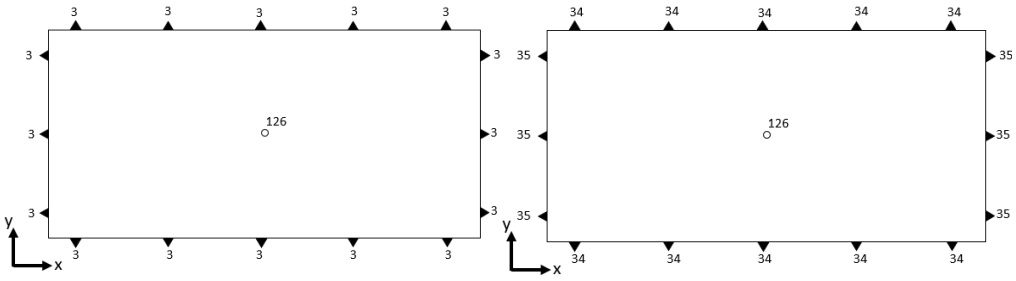

Figure 4.5. Rectangular plate boundary conditions configuration used for the cases of all edges simply supported (left) and all edges clamped (right). Notation for restrained degrees of freedom: 1 = x translation, 2 = y translation, 3 = z translation, 4 = x rotation, 5 = y rotation, 6 = z rotation.

This approach does not only give appropriate results, but is a general approach that can be used effectively for single loadings as well as for combined loadings. That is the reason why it has been finally chosen for this project.

Note that although this approach to model loads and boundary conditions can be applied in general to all cases, in cases such as those for plates with a/b=20 problems have appeared and one of the solutions considered implies changing slightly the reference boundary conditions (this case is to be explained in detail in a later section).

4.3.6 Analysis

In this project, the buckling problem has been solved performing buckling analyses in Nastran. The buckling solution in Nastran is preceded by default by a linear static analysis of the configuration under the applied loads. This static analysis is of interest, as it generates vital information to check the integrity and proper modeling technique for the plate of interest. This is accomplished by checking the FEM displacements, force and stress distribution in the plate

It is worth to mention that all the analysis have been carried out without using the AUTOSPC parameter, which automatically constrains degrees of freedom for which there is no associated stiffness. Although this may be useful in some cases and it is a common practice for some engineers, it risks adding unintended constraints that can result in an over-constrained model or a redistribution of the internal loads that does not correspond to the intended plate configuration.

The selection of the method to solve the eigenvalue problem had to be done. For that purpose Nastran offers three different eigenvalue extraction methods suitable for buckling analysis; inverse power method, enhanced inverse power method and Lanczos method.

Inverse power method looks for the lowest eigenvalue and eigenvector in a range, finding one root at a time, and the process to find each root is iterative. One drawback is that depending on the eigenvalue range selected, some critical eigenvalues may be lost.

Enhanced inverse power method improves the capabilities of previous method, because it uses a sequence to make sure that all the eigenvalues of the range are effectively found. This is a good choice when the model under analysis is quite large, and the range of interest of the eigenvalues is known. It works better when the eigenvalues of interest are the lowest modes.

Lanczos method is a combination of previous two methods. In the event that an eigenvalue cannot be extracted in the range specified, the software produces a message to warn the user. This method is especially appropriate for medium and large models, and it has the characteristic of improving the computational speed.

The choice of method has been done considering the size of the model, the number of desired eigenvalues, the available memory on the computer, and the capability of the user to accurately estimate the eigenvalues range. Lanczos method has been selected because many models and analysis are performed in this project, and the computational speed is a vital feature. Although enhanced inverse power method has been considered, it has been discarded because the range of interest of the eigenvalues is not well known in all cases. In addition, since the Lanczos method overcomes the limitations of the other two methods, it has been considered the most reliable one.

5 FEM results

Obtained FEM results are presented and discussed in this section. Additionally, the procedure employed to validate all the results is explained.

5.1 Results validation procedure

The validation of the results is a critical step to ensure that the information obtained from FEM is reliable. The validation process has been done concurrently with the modelling phase, resulting in model changes when the results obtained did not meet the validation criteria.

Validation of the results is performed for each single loading and loading combination for all the aspect ratios and boundary conditions. The checks carried out (based on reference 15 and 16 recommendations) are explained herein.

- ***Comparison with theoretical results***

When analyzing the results from NASTRAN, the resulting forces and stresses of the static solution have been compared with theoretically expected results.

Observe in Fig.5.1 that when applying a load uniformly along the edges, the load is uniformly distributed along plate elements (observe in the zoomed view that the load is similar in all the elements). The load being displayed in Fig.5.1 zoomed view is X membrane force, which is the compression force per unit length. In the case shown, a 300 N force is being applied to the plate, with has 100 mm length edges. Then, it is expected that X membrane forces are 3 N/mm. Consequently, it is observed that in this case, FEM result agree with theoretical results.

Note that in the corners different loads appear. This is because of boundary effects appearing at these regions.

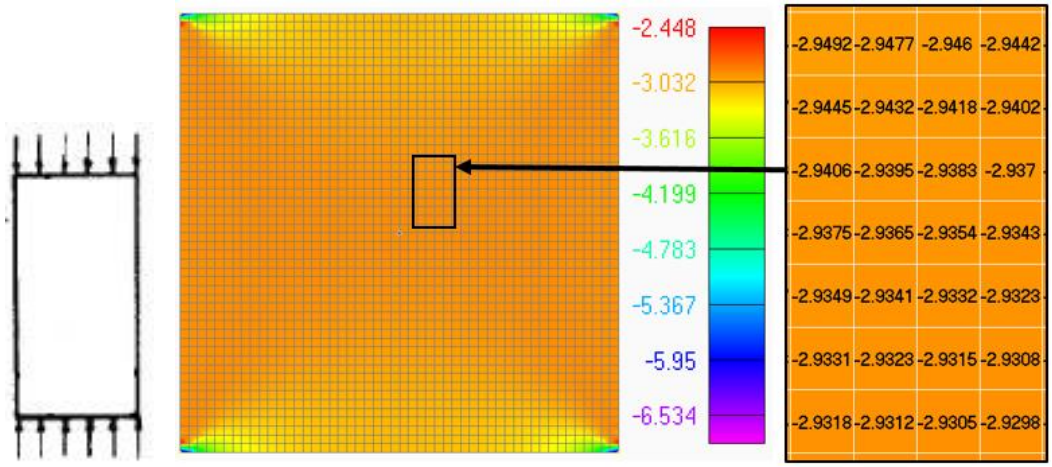

Figure 5.1. X membrane force distribution (left) and zoomed view (right). Case: Square plate (100 mm edge) under axial compression of 300 N at left-right edges.

For the loading cases with bending (Fig.5.2), since this work has only considered pure bending, unless plate is also subjected to axial compression, the neutral axis of the plate is expected to be found at the middle of it (observe in the zoomed view that membrane force changes of sign just the middle plate axis). Being the neutral axis in the middle, the loads appearing at upper and lower edges should be the same but in opposite senses.

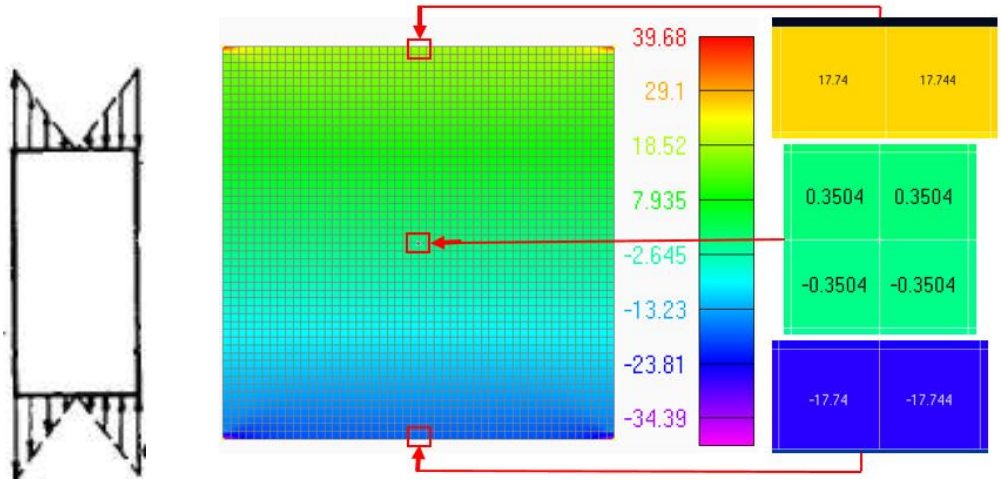

Figure 5.2. X membrane force distribution (left) and zoomed views (right). Case: square plate (100 mm edge) under 30000 N mm bending moment at left-right edges.

For the load combination of bending and axial compression, the neutral axis will not be in the middle of the plate (Fig.5.4). The resultant of the triangular distribution of forces representing bending and the axial compression will move neutral axis up or down from the middle plate axis (Fig 5.3).

Figure 5.3. Displacement of the neutral axis from the middle in a combination of bending and axial compression.

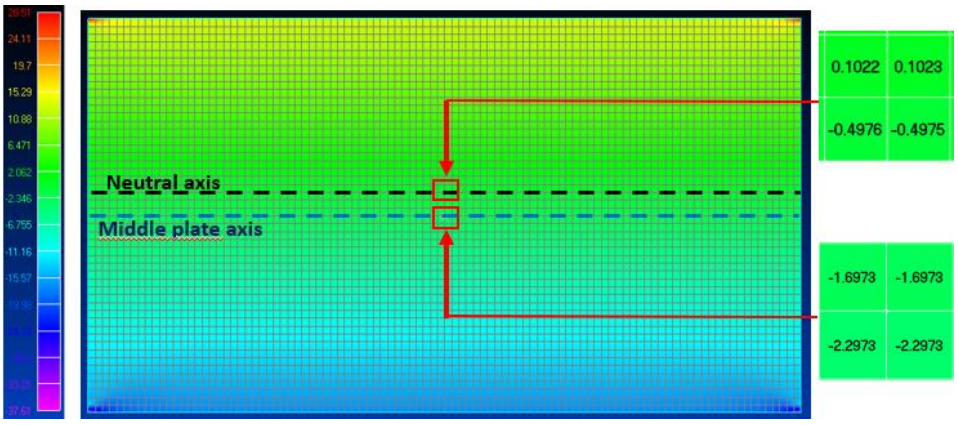

Figure 5.4. X membrane force distribution (left) and zoomed views (right). Case: square plate (100 mm edge) under a combination of bending and axial compression.

NASTRAN XY membrane force indicates the shear flow. Since from theory we know that shear flow (τ) is computed as eq.5.1 (where l is the edge length), for the sample case of a square plate subjected to a distributed 600 N force along its 100 mm edge, the shear flow at each element would be expected to be 6 N/mm.

$$\tau = \frac{F_{xy}}{l}\ (N/mm) \qquad (5.1)$$

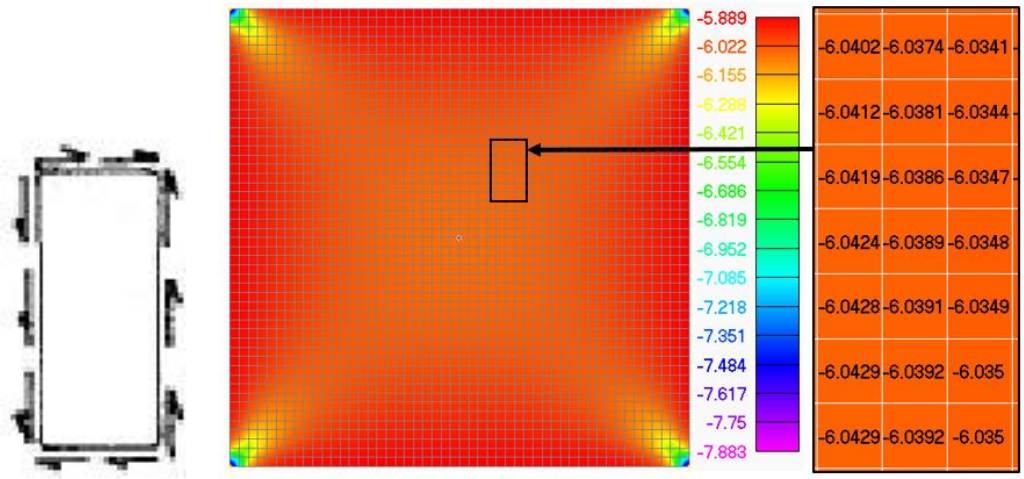

Figure 5.5. XY membrane force (left) with zoomed view (right). Case: square plate (100 mm edge) under a 600 N distributed force along its edge.

- ***FATAL and common errors***

When NASTRAN runs, , it provides among others an .f06 file, which provides feedback on the execution of the analysis, as well as any requested output results. This file lists warning and errors (both critical and non-critical ones) which are useful to determine what has actually occurred during execution when obtained output is not as expected.

When FATAL ERROR arises, the analysis stops and cannot continue. During this project, multiple errors of this type have been found (which were eventually solved). It is worth to outline the most common ones, such as fatal errors 9050 and 7340.

Fatal error 9050 states the analysis run was terminated due to excessive pivot ratios in matrix kernel. Together with this message, there is a warning message which are the nodes and degrees of freedom in which this is occurring. Practically speaking, this was solved by revising carefully the model to check if all the constraints are set (in the perimeter and the center of the plate).

Fatal error 7340 states the number of computed eigenvalues exceed allocated storage. This occurs because when solving an eigenvalue problem (like buckling problem in this work) there are too many eigenvalues for the software to be able to store them all. In practice, this issue is solved by setting in the analysis a smaller range of eigenvalues, such that the amount of eigenvalues in the range is smaller and the memory can handle them. Often this can be easily done by estimating the first mode eigenvalue (without considering rigid body modes eigenvalues) based on the theoretical results.

- ***Displacements and mode shapes***

Results related to displacements need to be analyzed critically. The user can realize if something in the model is wrong by observing if their order of magnitude is reasonable with the loads applied and the problem. Note that this is done in static analysis only, because in the buckling solution deformations are expressed by the eigenvector. This provides meaningless magnitudes; it shows only the displacements of the plate nodes in proportion one to the other, because the output eigenvector in NASTRAN is shown normalized to 1.

What is useful to check in buckling solution is that the obtained mode shapes are the expected. Observe in Fig.5.6 for example which mode shape was obtained when using not appropriate boundary conditions. Therefore, the plate deformed shape in buckling solution can also be an indicative of some errors occurring.

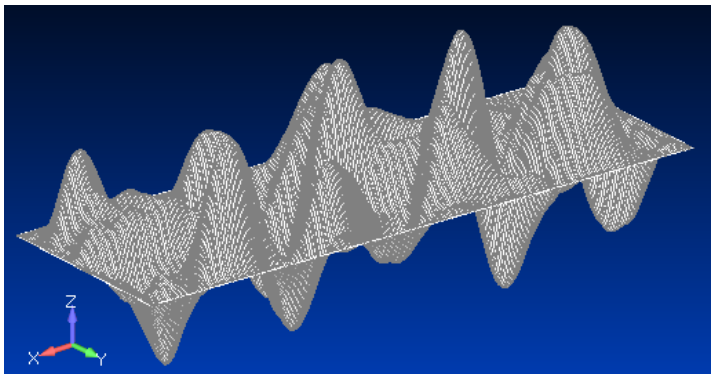

Figure 5.6. Resulted mode shape for a case in which boundary conditions were not set correctly.

- ***Reactions***

The static equilibrium of the structure can be checked in the .f06 file analyzing the resultants of the system loads. For all analysis equilibrium of loads is required, ensuring that no load resultant appears is vital.

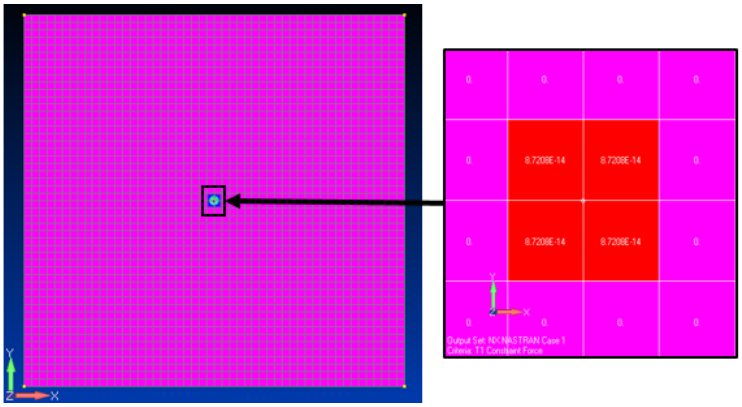

Figure 5.7. X Constraint force (left) with zoomed view (right). Case: square plate (100 mm edge) under a 300 N axial compression.

Additionally, since for all cases applied loads will be in equilibrium (recall from modelling section that it has been decided not to use reactions are to be used as applied loads), no significant reactions should appear anywhere in the plate. Remember that the boundary

conditions have been designed so that there is a node in the center where 3 degrees of freedom are restrained (the 2 in-plane translations, and the in-plane rotation). This implies that some reactions will appear at this node, but their values should be negligibly small (as it has been the case). Observe, for example, the constraint forces developed in a square plat loaded in axial compression (Fig.5.7), that are of the order of 10^{-14} .

- ***Epsilon***

Nastran gives an error measure index in terms of the term Epsilon. This is an error measure of the numerical accuracy of the software computation. This value shall be around 10^{-9} or lower to be considered acceptable. This requirement was satisfied by all the cases analyzed, with Epsilon values around 10^{-12} or lower.

5.2 Single loading

Before starting to simulate combined loading cases, single loading cases have been analyzed. Although this is not the core of the project, it is an important step for several reasons.

First of all, in order to later calculate the stress ratios (R_b, R_s, $R_{c(dir)}$…) it is necessary to previously compute the critical buckling loads of each loading when applied individually. Note that these ratios to be used with combined loadings will use the individual loadings critical loads obtained from FEM. Secondly, since the modeling phase is complex and many potential issues and errors might be faced, it is much better to tackle and understand these issues and errors with simple models. In this way, less issues are to be encountered in complex loading modeling phase, where understanding and solving them is harder and more tedious. Thirdly, it is valuable to compare buckling load predictions under single loading for the FEM with existing graphs and equations available from analytical and energy methods. Moreover, understanding the differences for single load cases can help to identify the source of the differences for the combined loadings.

As for the notation, the author will refer as "C" and "SS" to all edges clamped or all edges simply supported conditions respectively. Also note that an aspect ratio of a/b=20 has been used to model infinitely long plates. The validity of this assumption will be proven later when comparing FEM with analytical results. FEM results for single loading cases, which have been obtained with FEMAP (pre and post-processor) and NASTRAN (solver) are shown in Table 5.1.

SINGLE LOADING CRITICAL BUCKLING LOADS, σ_{crit} (MPa)								
a/b	Axial compression 		Transverse compression 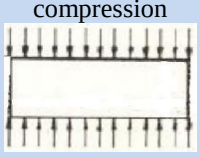		Longitudinal bending 		Shear 	
	SS	C	SS	C	SS	C	SS	C
1	6.3585	16.0306	6.3585	16.0306	40.7329	76.0300	14.7557	23.1014
1.2	6.5572	15.3163	-	-	38.7541	72.1035	12.6552	19.9722
1.5	6.9194	13.2655	-	-	38.5014	68.7021	11.4337	18.0948
2	6.3482	12.4690	2.4949	7.7392	38.0785	65.9334	10.3490	16.1928
3	6.3396	11.6340	1.9661	6.8671	38.2962	63.9761	9.2383	15.0733
4	6.3353	11.3932	1.7950	6.6178	37.9075	63.3092	8.8983	14.7006
20	6.3277	10.9794	1.5968	6.4030	37.8588	62.4400	8.5219	14.3574

Table 5.1. Critical buckling loads for single loadings. Legend: SS (all edges simply supported), C (all edges clamped).

Overall, it is observed (Table 5.1) that for all loadings the buckling load decreases as the aspect ratio increases. There is an exception in the case of axial compression for aspect ratios ranging between 1 and 2. There is an increase of the critical load from a/b=1 to 1.5 which occurs because the minimum energy state for low aspect ratio has fluctuations (observe in Fig.5.8 that curve in red of lower energy state has some peaks for low a/b). Additionally, critical loads for all clamped edges cases are well above for all simply supported edges cases.

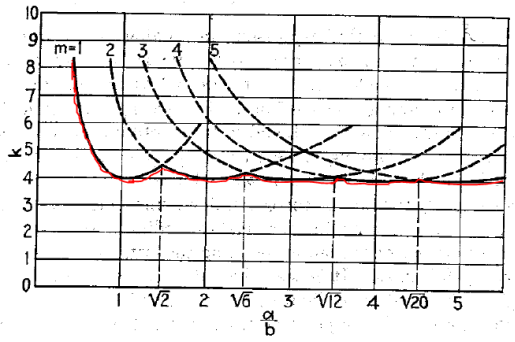

Figure 5.8. Buckling factor, k, for simply supported uniaxial compression (Ref.1).

Results obtained for axial compression are acceptable, with expected critical buckling load values and mode shapes. For a square plate the first mode shapes obtained (Fig.5.9) the number of buckle waves in longitudinal direction (m) increase with the mode shape and as the energy state increases (recall that first mode buckling happens at lower energy state).

Note that the first image represents a rigid body mode, which shall be discarded when analyzing buckling results. These modes appear in buckling analysis with a negligible small eigenvalue.

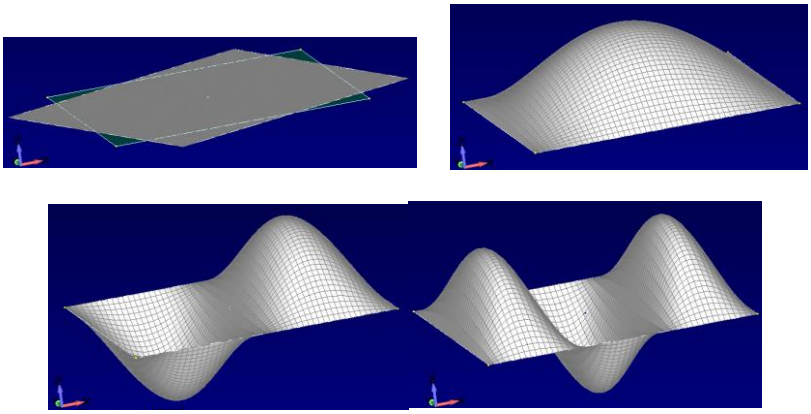

Figure 5.9. First 3 mode shapes for a square plate under axial compression. All edges simply supported. Rigid body mode in first image

The effect of the geometry in the deformed shape can be observed in Fig.5.10 for the case of axial compression. The number of buckle waves increases as the plate aspect ratio increases. Note that each mode shape takes place in a range on aspect ratios, and the mode shape changes when there is a change in the energy state of the plate. For the case of axial compression (Fig.5.10), observe that a/b=1 and 1.2 have the same mode shape (with $m = 1$). Recall from theoretical analysis (Fig.5.8) that the change to next energy state occurs when $a/b = \sqrt{2}$ (change from $m = 1\ to\ 2$).

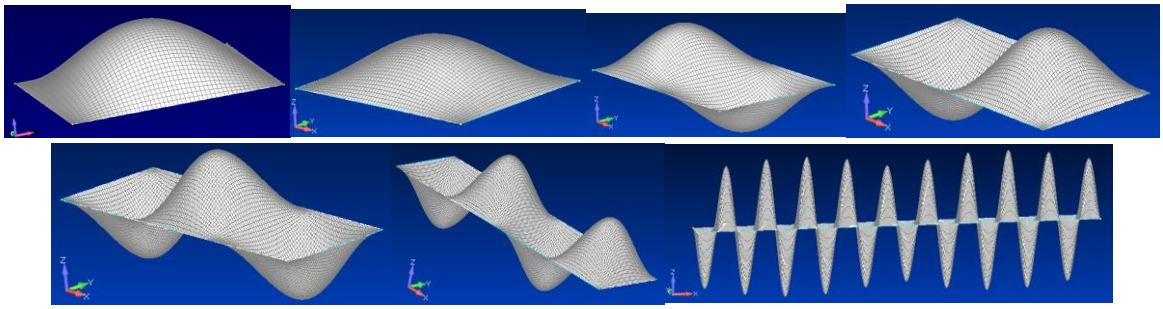

Figure 5.10. Mode shape for different geometries (a/b=1 ; 1.2 ; 1.5 ; 2 ; 3 ; 4 and 20)

As for mode shapes differences between simply supported and clamped edges cases, for the particular case of single axial compression, observe in Fig.5.10 that simply supported plates half-waves length are the same length as plate short edge for geometries a/b=1, 2, 3, 4… (when a/b is an integer number). This implies that for those cases, the number of half-waves will be a/b, and the wave will have square dimensions (same wave length in x and y directions). Observe Fig.5.11 for the case of a/b=20. When the aspect ratio is not an integer number (2nd and 3rd images in Fig.SL2 for a/b=1.2 and 1.5 respectively).

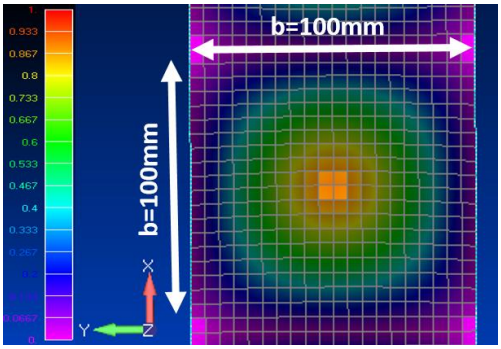

Figure 5.11. Contour plot of normalized z-traslation.

Additionally, in the mode shapes (for any geometry or loading) of clamped edges cases there is no rotation at the edges (Fig.5.13). On the other hand, cases with edges simply supported (Fig.5.12) present some rotation at the edges.

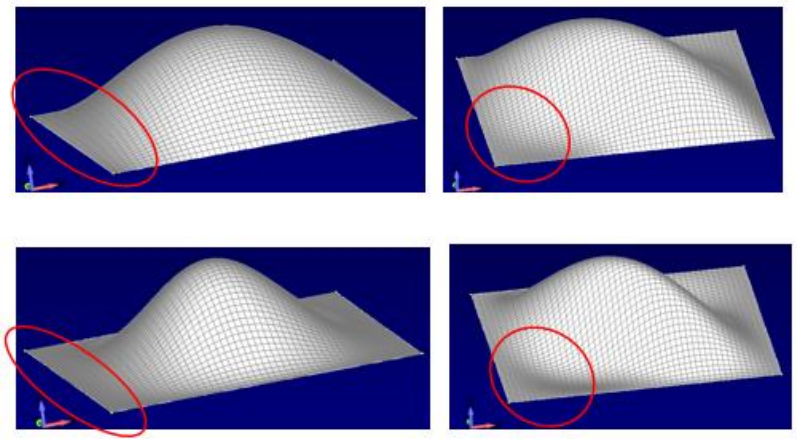

Figure 5.12 and 5.13. Mode shapes cases with all edges simply supported (above) and clamped (below)

For the particular case of single axial compression, observe in Fig.5.10 (above) that simply supported plates half-waves length are the same length as plate short edge for geometries a/b=1, 2, 3, 4… (when a/b is an integer number).

Mode shape resulted from shear buckling (Fig.5.14) has the buckle wave forming 45º with plate long and short edges. Note that the applied shear flow (white arrows) produce two resultant loads (red arrows) that are inclined 45º with respect to the edges. This produces a compression load in an axis at ±45º of longitudinal axis, which produces the buckle wave at this inclination. Note that when a shear load is applied, two critical loads will appear with the same magnitude but different signs. This is because buckling will occur for any of the two possible senses in which shear flow occurs; depending on the sense of the shear flow, one pattern or the opposite (see left and right images in Fig.5.13) will take place. This does not occur for axial or transverse compression, for which the applied load sense matters (a plate will not buckle under tension).

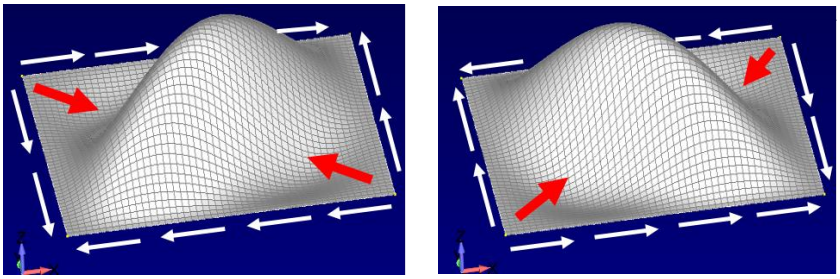

Figure 5.14. Shear buckling patterns.
Case of clamped edges square plate

Deformed buckling shapes for different geometries are presented in Fig.5.15. Similarly to axial compression case results, the number of half-waves increases with a/b.

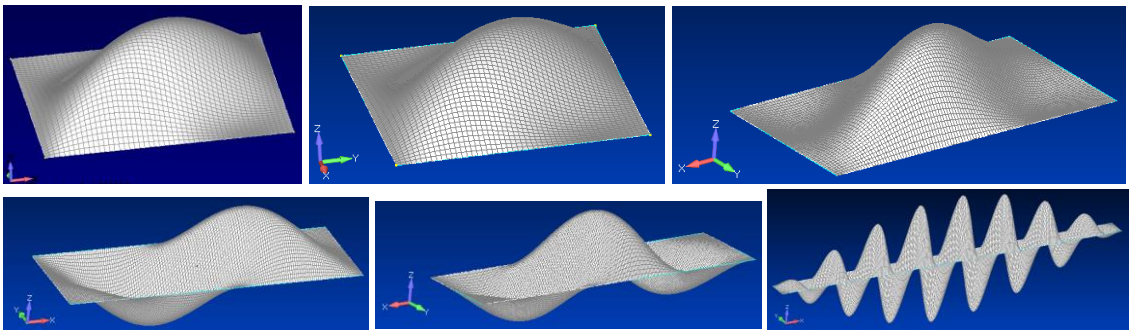

Figure 5.15. Mode shape for different geometries (a/b=1 ; 1.2 ; 2 ; 3 ; 4 and 20).
Case: Simply supported plates under shear load

Regarding the cases of plates under bending loads, similarly to the case of shear, two buckling loads of same magnitude and opposite sign (sense) appear (Fig.5.16). This is because buckling will occur independently of the sense in which the bending moment is applied. Buckling under bending occurs because the moments applied in the short edges produce two different load types in the same edge. The short edge is subjected partially to compression loads (red arrows), and partially to tension loads. The part under compression loads will buckle as if it was loaded under axial compression. On the contrary, the part under tension loads will remain flat.

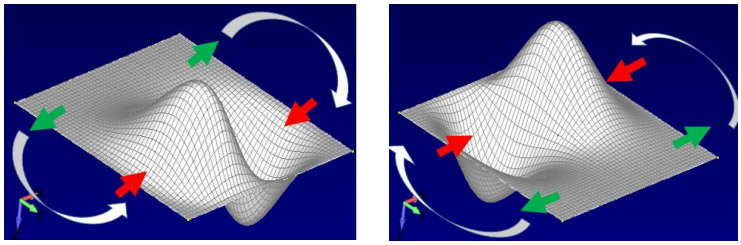

Figure 5.16. Bending buckling patterns.
Case of clamped edges square plate

Results for bending buckling produced mode shapes for different geometries are shown in Fig.5.17. For this case the number of buckle waves also increases with the aspect ratio. It can be observed that due to the plate part under tension loads, that the buckle wave is not symmetric with respect to its longitudinal axis. Image 7 of Fig.5.17 shows how the buckle wave is translated from the plate middle axis.

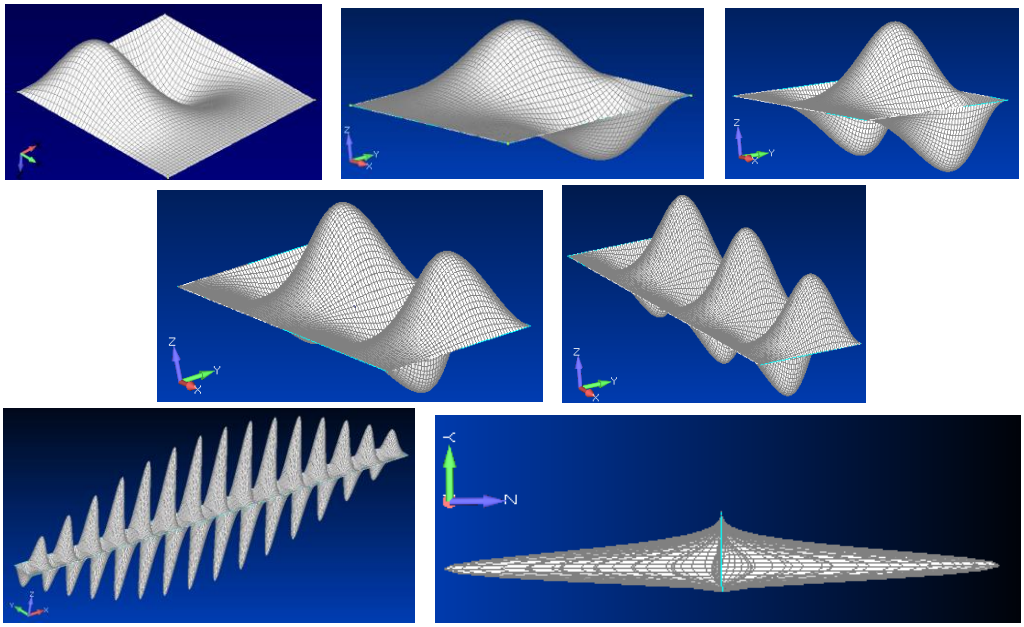

Figure 5.17. Mode shape for different geometries (a/b=1 ; 1.2 ; 2 ; 3 ; 4 and 20).
Image 7: YZ view of a/b=20 mode shape // Case: Simply supported plates under bending load

Transverse compression buckling results are similar to those of axial compression. The first 4 mode shapes of a/b=20 under transverse compression are shown in Fig.5.18. The number of waves increase with the mode shape order (1st, 2nd, 3rd…), indicating that the energy state is higher. This increase in wave amount also implies that the wave length decreases as the mode order goes up.

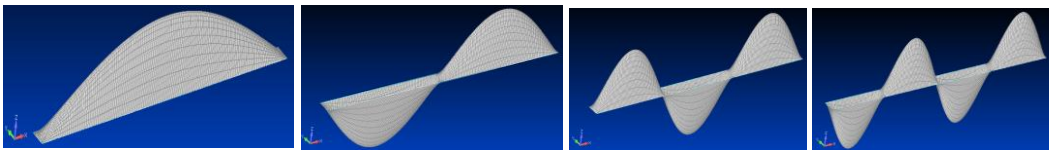

Figure 5.18. First 4 mode shapes for a/b=20 plate.
Case: Simply supported plates under transverse compression

5.3 Combined loading

In order to later compare FEM with analytical results (in the form of interaction curves and equations), curves and interaction equations have been generated with obtained FEM results. To obtain the curves and equations, around 10 and 20 particular load combinations have been analyzed for each combined load case and geometry. With the obtained results, a data fit has been performed in Excel software to fit all the results in an equation of the shape of eq.5.2 where p and q are the parameters to be obtained for each loading case and geometry. Then, the curves have been produced from the curve. Note that for the combination of bending and transverse compression, except for the case a/b=1 with simply supported edges, no satisfactory equation or curve has been obtained (because results do not fit in any equation). The errors of the equations-curves with respect to the FEM results are below 1% for most of the cases. All the equations are collected in Table 5.2.

$$R_1{}^p + R_2{}^q = 1 \qquad (5.2)$$

COMBINED LOADINGS – FEM INTERACTION EQUATIONS - $R_1{}^p + R_2{}^q = 1$												
a/b	Axial compression + Shear $R_X{}^p + R_S{}^q = 1$				Bending + Shear $R_B{}^p + R_S{}^q = 1$				Axial compression + Bending $R_X{}^p + R_B{}^q = 1$			
	SS		C		SS		C		SS		C	
	p	q	p	q	p	q	p	q	p	q	p	q
1	0.988	2.017	0.942	1.904	1.965	1.566	1.902	1.999	1.115	1.869	0.897	2.256
1.2	0.977	2.024	0.920	2.028	1.958	1.843	2.022	2.060	-	-	-	-
2	1.005	1.991	0.965	2.042	1.709	2.258	2.105	2.361	0.994	2.133	0.988	1.916
3	1.063	2.009	1.011	1.988	2.301	2.060	2.363	2.324	0.912	2.204	0.947	2.047
4	1.006	2.078	1.008	1.981	2.545	2.106	2.533	2.242	0.970	2.152	0.965	2.011
20	1.002	2.003	1.000	2.004	2.431	2.378	2.463	2.292	0.966	2.119	0.960	2.050

Table 5.2. Interaction equations produced from FEM results

For square plates under bending and transverse compression, eq.5.3 has been obtained fitting FEM results. The curve estimates FEM results with a mean error of 0.52%.

$$R_Y{}^{1.035} + R_B{}^{1.421} = 1 \qquad (5.3)$$

Following sections will present the interaction curves graphically. Note that as for the 4 load combinations studied small variations occur from a/b=3 to 4, and from a/b=1 to 1.2, only curves for a/b=1, 2, 3 and 20 will be shown.

- ***Axial compression and shear***

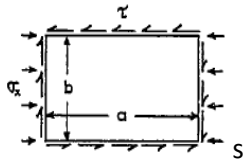

Figure 5.19. Combined axial compression and shear

Obtained FEM results for combination of axial compression and shear are shown in Fig.5.20. For the case of simply supported square plates, the deformed shapes and contour of the z-traslation are shown for 4 loadings.

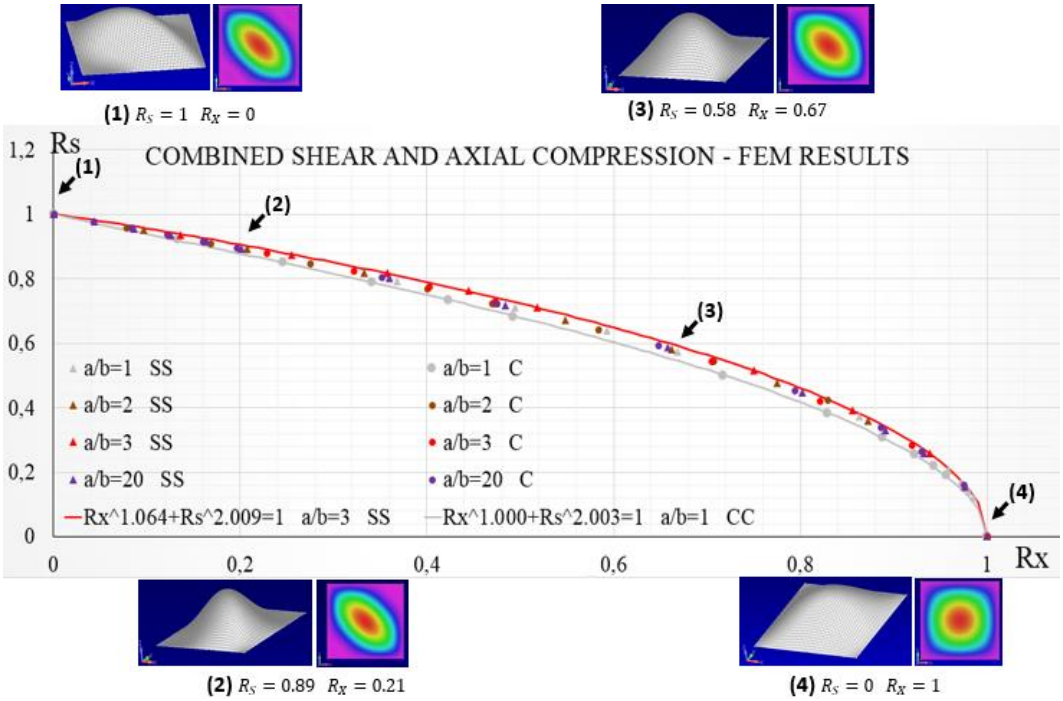

Figure 5.20. FEM results for combined shear and axial compression.

Overall, the results are very similar for different aspect ratios and rotational restraints. The maximum difference between the 12 cases studied (6 aspect ratios with 2 boundary condition types each) is found between cases of a/b=1.5 with all edges simply supported (red curve) and a/b=1 with edges clamped (grey curve). Note that for clarity, only the curves for those cases have been shown in the figure. The remaining curves appear in the middle of the two.

The error of the curve produced by data fit with respect to FEM results is for all cases below 0.5%, so the equations obtained for these cases is rather accurate for engineering purposes.

Images of the 4 particular loadings show the different deformed shapes along the curve. It is interesting to see the evolution of the mode shape along the curve. Note that as R_X increases, the buckle wave becomes square shaped (observe contour plot).

- ***Bending and shear***

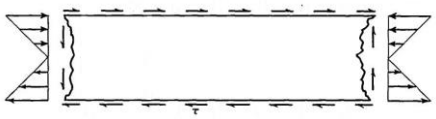

Figure 5.21. Combined axial compression and shear

FEM results for combined axial compression and shear (Fig.5.22 and 5.23) show that for both types of edges rotational restraints studied, the capacity to withstand load increases as the aspect ratio increases (observe that curves move up with increasing a/b).

In Fig.5.22, the case of a simply supported square plate is presented in (1). Observe in the contour plot that the shear load is notorious (wave extending along the diagonal) and the bending load is

appreciable because the maximum amplitude point of the wave (in red) is displaced down (in the image orientation) from the plate middle horizontal axis.

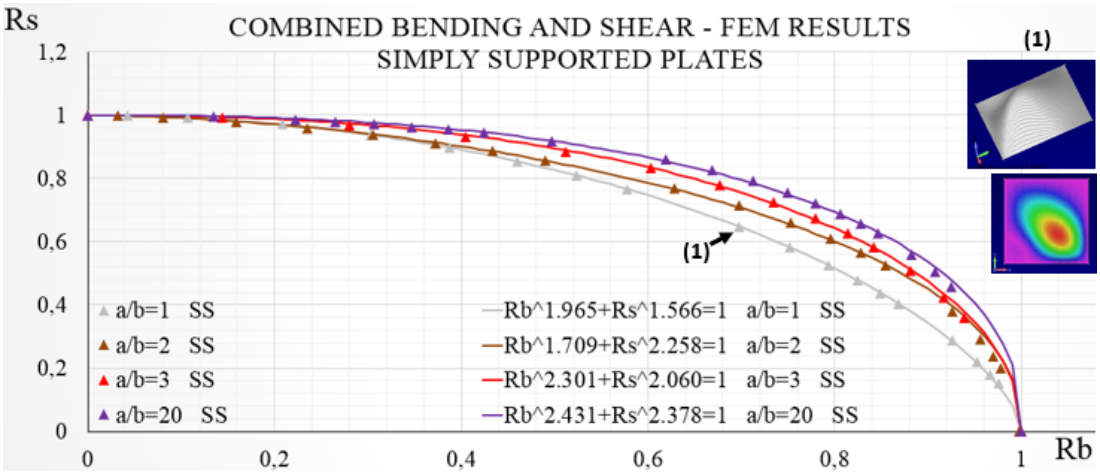

Figure 5.22. FEM results for simply supported plates under combined shear and bending

Clamped plates results show that for aspect ratios above 2 (brown curve), the curve does not change notoriously.

Additionally, the mode shapes of several points along a/b=1 curve are illustrated. It is clearly observed in the contour plots how the diagonally oriented wave turns gradually (cases (2) and (3)) and it ends up oriented parallel to the plate short edge in (4) (when no shear is present). It is also worth mentioning how a second wave is gradually created as the bending increases. Note that while in (1) only 1 wave appears (small negative displacements on the wave laterals may be caused by clamped boundary conditions), in (2) it is noticed that a second wave is starting to appear. Increasing further R_B this second wave increases, and eventually in (3) (with $R_B = 1$ and $R_B = 0$, both waves have the same magnitude.

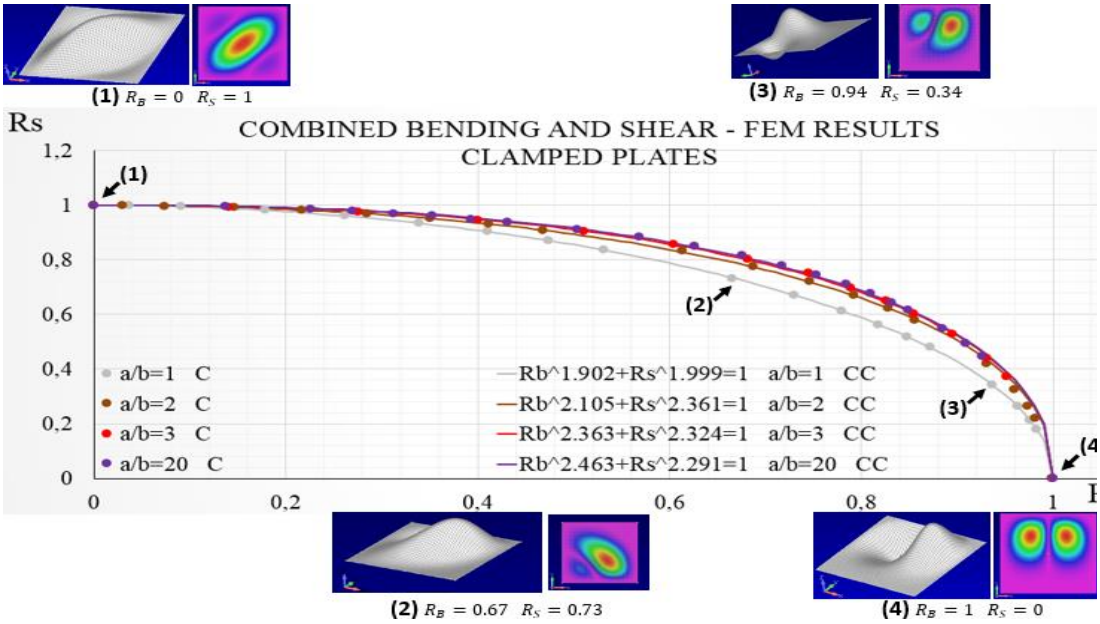

Figure 5.23. FEM results for clamped plates under combined shear and bending

If comparing obtained FEM results for simply supported and clamped edges, in Fig.5.24, 5.25, 5.26 and 5.27 it is clearly observed that clamped plates curves are above simply supported ones. It is also appreciated that as the aspect ratio increases, this difference decreases, having nearly the same curve for large aspect ratios (a/b=20). This may be because the effect of the boundary conditions decreases with the aspect ratio.

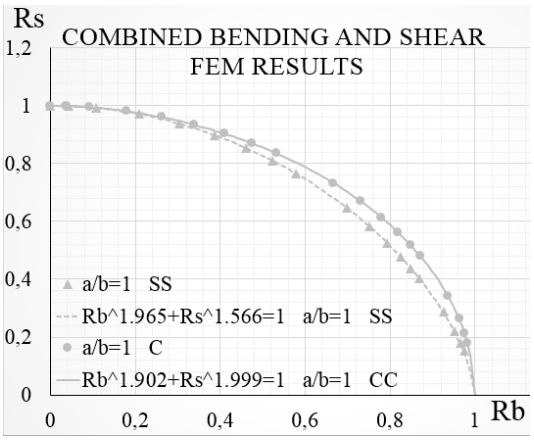

Figure 5.24. a/b=1 for Simply supported and Clamped edges cases

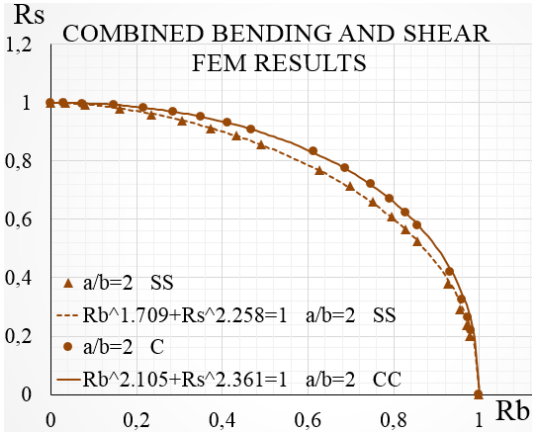

Figure 5.25. a/b=2 for Simply supported and Clamped edges cases

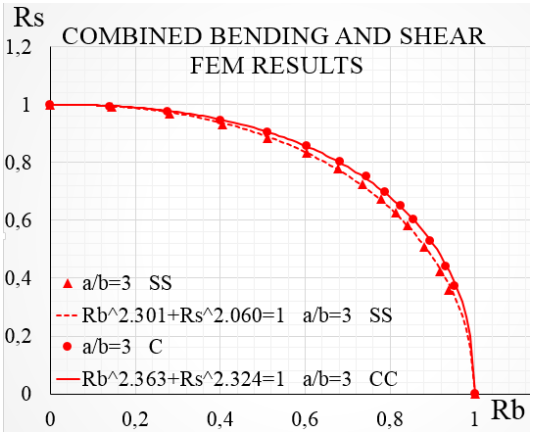

Figure 5.26. a/b=3 for Simply supported and Clamped edges cases

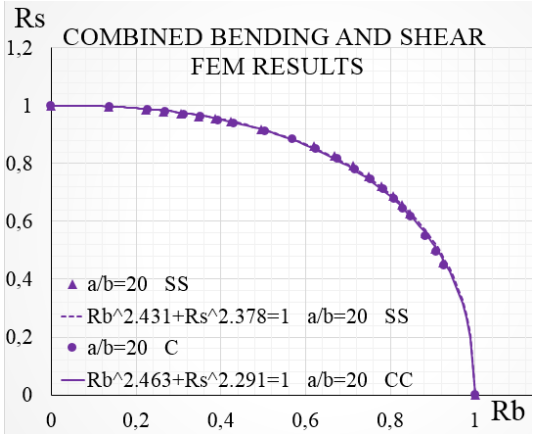

Figure 5.27. a/b=20 for Simply supported and Clamped edges cases

- ***Axial compression and bending***

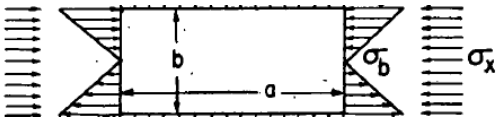

Figure 5.28. Combined axial compression and bending

The results obtained from FEM (Fig.5.29) are similar for all the geometries and boundary conditions cases analyzed. Note that the interaction curves for all the cases appear in a narrow region delimited by the interaction curves of a/b=2 simply supported plates (dashes curve) and a/b=2 with clamped edges (solid curve). As before, for clarity only the two most significant curves (the ones with highest and lowest R_B) are presented for clarity.

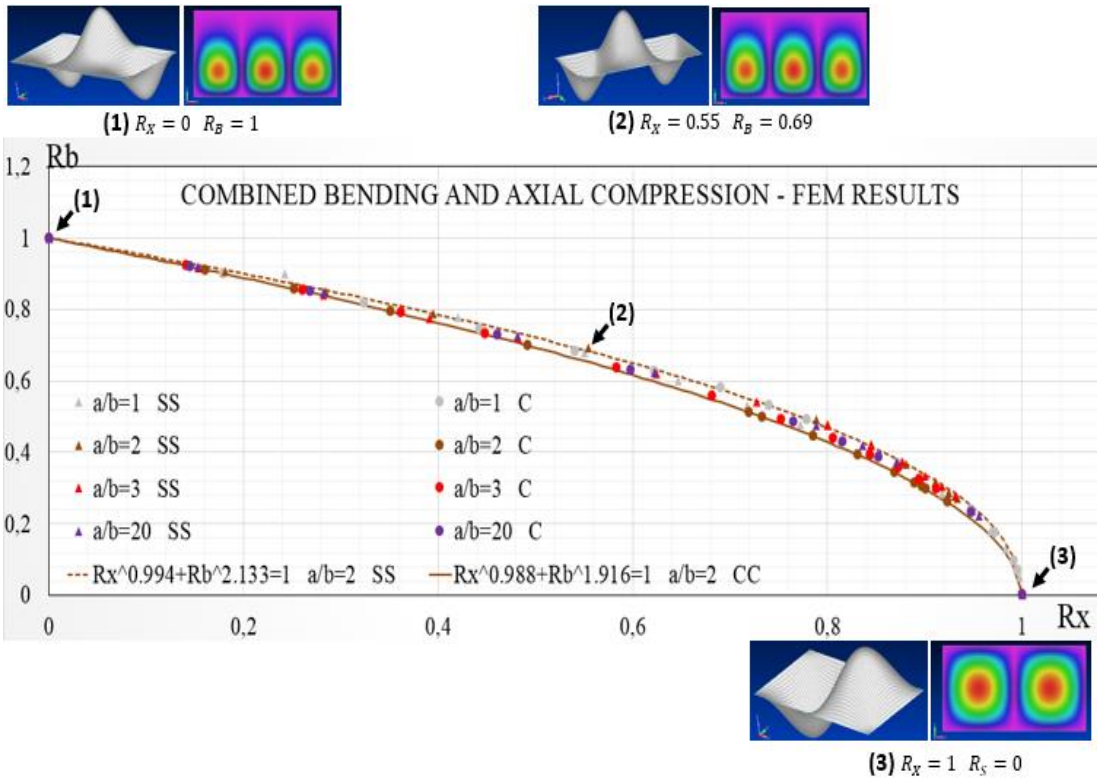

Figure 5.29. FEM results for combined shear and bending

Additionally, the mode shapes for 3 different points in the curve are presented (Fig.5.29) for the case of a/b=2 simply supported plates. In the case (2) translation contour plot, it is slightly appreciable that the buckle wave length in y direction (short edge or transverse direction) increases with R_X. This is due to the translation of the neutral axis caused by adding a compression load to the existing bending. Recall that when there is only a bending load (case (1)) the neutral axis is in the center, and the buckle wave extends (in transverse or y direction) from one long edge (in this case, the bottom one) to the neutral axis. When adding a compression load, the neutral axis moves away from the long edge (in this case, it moves up). In this way, as the gap between the long edge and the neutral axis increases, and consequently, the wave length in transverse direction increases. If the bending moment is reduced to 0, case (3) is reached, with a single axial compression, and without neutral axis (this would be up at the infinite from bottom edge in the image).

- ***Transverse compression and bending***

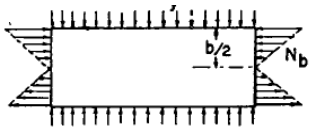

Figure 5.30. Combined transverse compression and bending

Unlike for the other 3 load combinations, results for combined transverse compression and bending (Fig.5.31 and 5.32) do not fit in an equation of $R_1{}^p + R_2{}^q = 1$ type. Other equation types have been tried but none of them is able to fit the results. The exception is the case of simply

supported square plate results, which fit with reasonable engineering accuracy eq.5.4 (observe grey curve in Fig.5.31.

$$R_Y{}^{1.035} + R_B{}^{1.421} = 1 \qquad (5.4)$$

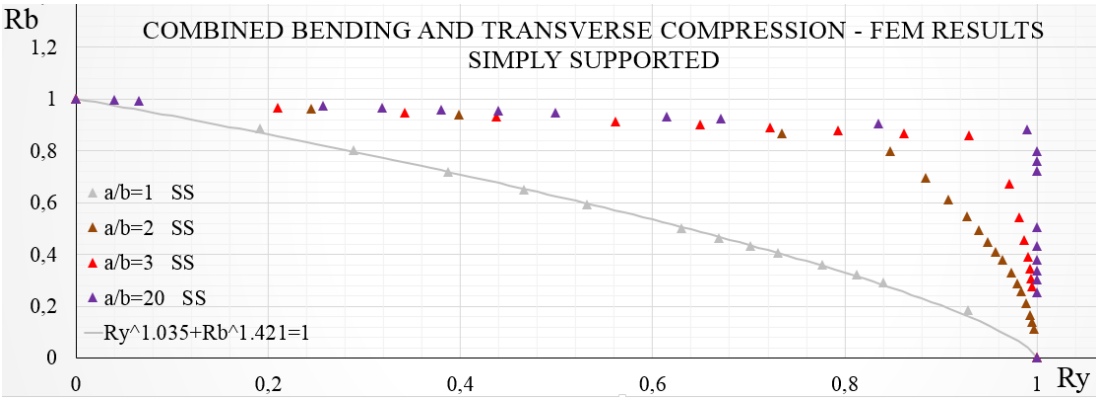

Figure 5.31. FEM Simply supported results for combined bending and transverse compression.

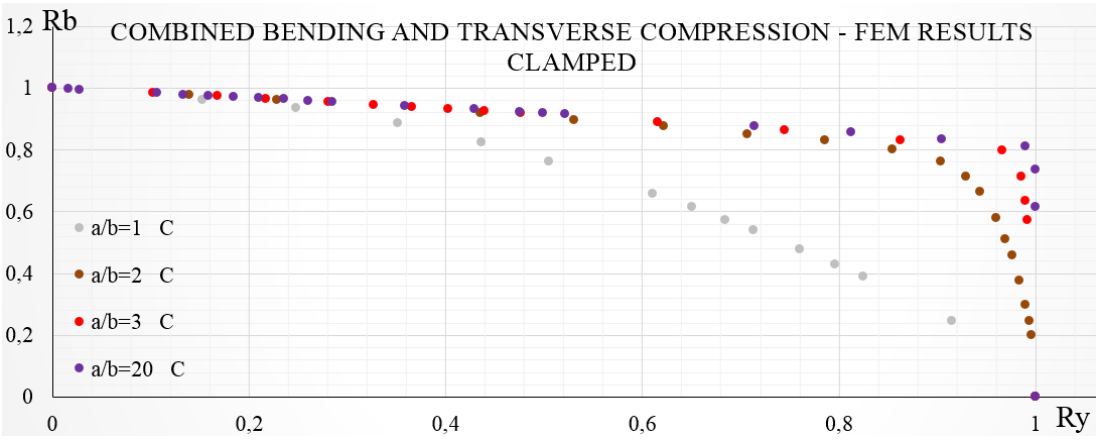

Figure 5.32. FEM Clamped plates results for combined bending and transverse compression.

It is worth explaining the physical meaning of a sudden change in the slope of the interaction curves. Note that in this load combination, for plates with a/b above 2, the curves have a relatively fast change in the slope (in the region $0.8 < R_Y < 1$ they change from around $\frac{\partial R_B}{\partial R_Y} = 0.85 \sim 0.9$ to $\frac{\partial R_B}{\partial R_Y} = -\infty$ (vertical line). This occurs for both clamped and simply supported plates. In Fig.5.33, FEM results for the case of simply supported a/b=2 plates are illustrated. Observe that the mode shapes of 4 different points along the curve are presented. Between cases (2) and (3) there is a sharp change in curve slope, which is associated to a transition from having 2 half-waves in the plate to have only one. Then, it is observed that for further increase of R_Y, the number of half-waves remains the same. This also occurs in the remaining curves with sharp changes in the slope.

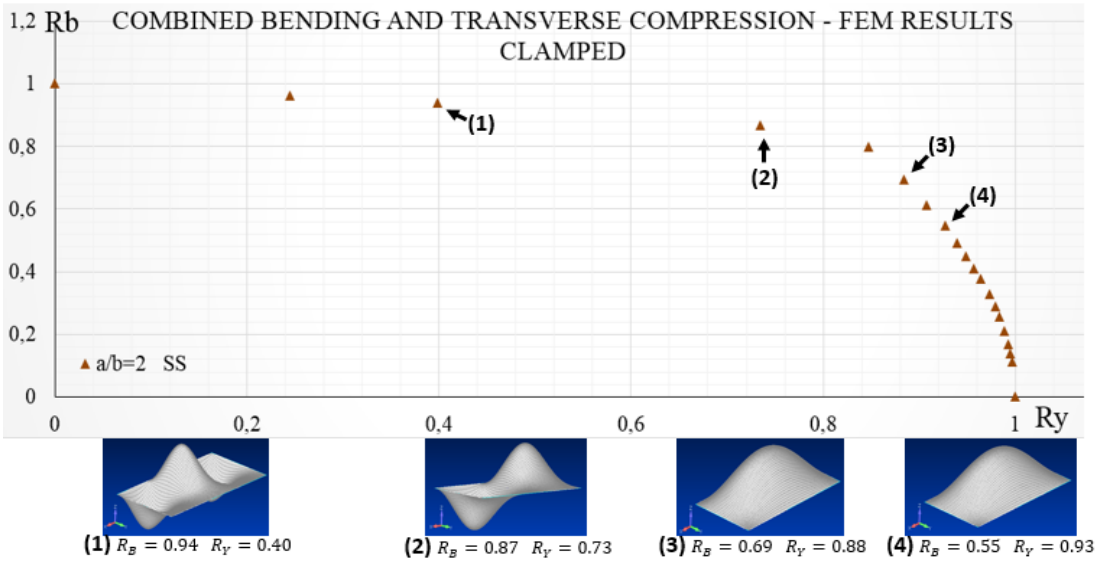

Figure 5.33. FEM Clamped plates results for combined bending and transverse compression.

In the case of simply supported plates, for the geometries a/b=2, 3 and 20, if only FEM results up to a certain R_Y are considered, result can fit accurately in straight lines. Observe for simply supported cases (Fig.5.33) that accurate equations are obtained if FEM data points up to around $R_Y = 0.95$ are considered for a/b=20 and 4, and up to $R_Y = 0.4$ for a/b=2.

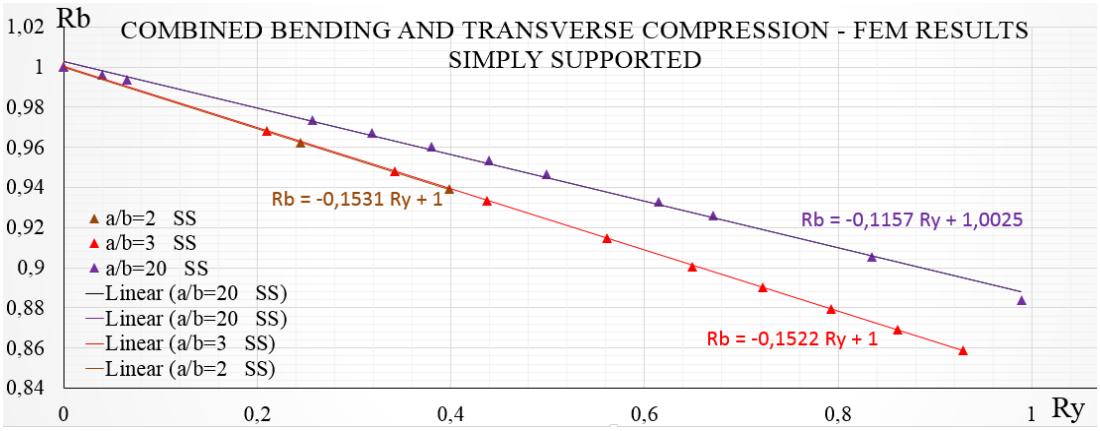

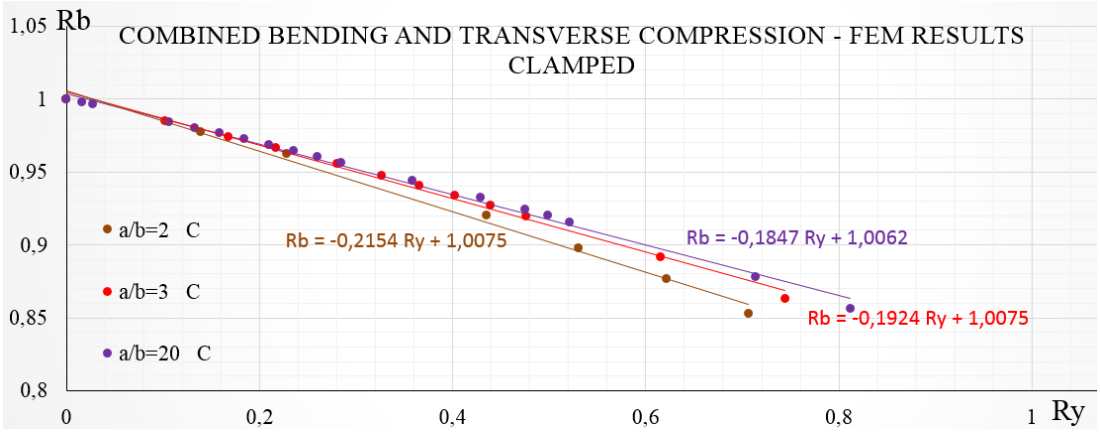

Figure 5.34 and 5.35. FEM data points results fitting in straight lines.
Clamped cases above. Simply supported below

Similarly, clamped plates cases can fit in straight lines (Fig.5.35) if FEM results up to around $R_Y = 0.75$. The resulting equations and their validity field are collected in Table 5.3. Note that for clamped square plates no equation has been found.

COMBINED BENDING AND TRANSVERSE COMPRESSION – FEM RESULTS - $R_B = mR_Y + n$								
a/b	CLAMPED				SIMPLY SUPPORTED			
	coefficients		Maximum error	validity	coefficients		Maximum error	validity
	m	n	(%)	$up\ to\ R_Y$	m	n	(%)	$up\ to\ R_Y$
2	-0.2154	1.0075	0.75	0.706	-0.1531	1	0.00	0.3981
3	-0.1924	1.0075	0.39	0.744	-0.1522	1	3.16	0.929
20	-0.1847	1.0062	0.56	0.812	-0.1157	1.0025	0.08	0.989

Table 5.3. Straight line equations produced from FEM results

6 Comparison FEM and theoretical results

This section presents a dissertation concerning a comparison between the results obtained by Finite Element Method and the results provided in the theory (by analytical methods, mainly the energy method).

Regarding the notation, when quantifying the difference between FEM and analytical results, a negative value will indicate that FEM predicted load is below the theory predicted one. In other words, a negative value will indicate that analytical prediction is not conservative. Also note that the method used with combined loadings to compute the differences is explained in detail in Annex A.

It is worth to mention that in general, for many engineering purposes, maximum differences and errors in buckling loads are acceptable up to 10%. The comparison will take this into account when analyzing the validity of the results. For curves-equations giving optimistic (not conservative) results, margins of safety are used (to remove the existing error that makes the result not conservative).

Overall, it is appreciated that FEM results fit reasonably well in theoretical interaction curves and plots. This trend varies slightly from one loading combination to the other, as well as from one aspect ratio to another, or when changing the boundary conditions. In general, when theoretical curves diverge from FEM results, theoretical buckling loads are optimistic.

6.1 Single loading

Differences between FEM and analytically obtained buckling loads are shown in Table 7.1, 7.2, 7.3 and 7.4. Note that in the absence in the references of available theoretical solutions for bending and transverse buckling loads with clamped edges, the differences have not been computed for these cases.

Overall, the differences are observed to be small in all cases (with differences around 1% or lower) except in transverse compression, where remarkably high values of $\Delta\sigma_{cr}$ (%) are appreciable. Therefore, being 1% a quite small error for engineering purposes, it can be considered that for axial compression, bending and shear loading cases, FEM and the energy method provide similar result.

$\Delta\sigma_{cr}$ (MPa) and $\Delta\sigma_{cr}$ (%) have been computed using eq.7.1 and eq.7.2 respectively, so if they are negative, this means that theoretically predicted buckling load is above FEM predicted one, giving a not conservative estimation. Note that terms $\Delta\sigma_{cr}|_{MIN}(\%)$ and $\Delta\sigma_{cr}|_{MAX}(\%)$ account for the potential error caused by k buckling coefficients extraction process (by a graph digitalizer) from the reference plots. It has been found that if this error source is taken into account, $\Delta\sigma_{cr}$ (%) value will be in the range determined by $\Delta\sigma_{cr}|_{MIN}(\%)$ and $\Delta\sigma_{cr}|_{MAX}(\%)$. See Annex B for the detailed explanation of this computation.

$$\Delta\sigma_{cr}\ (MPa) = \sigma_{cr-FEM} - \sigma_{cr-theory} \tag{7.1}$$

$$\Delta\sigma_{cr}(\%) = \frac{\Delta\sigma_{cr}\ (MPa)}{\sigma_{cr-theory}} \tag{7.2}$$

AXIAL COMPRESSION – DIFFERENCES FEM vs THEORY, σ_{crit} (MPa)				
a/b	Rotational restraint	$\Delta\sigma_{cr}$ (%)	$\Delta\sigma_{cr}\|_{MAX}$ (%)	$\Delta\sigma_{cr}\|_{MIN}$ (%)
1	SS	-0,07	0.92	-1.08
	C	0,40	1.38	-0.61
2	SS	-0,23	0.76	-1.25
	C	0,46	1.45	-0.55
3	SS	-0,76	0.24	-1.78
	C	-0,06	0.93	-1.07
4	SS	0,01	0.99	-1.01
	C	0,54	1.52	-0.47
20	SS	-0,12	0.88	-1.13
	C	-0,41	0.58	-1.43

Table 7.1. Differences in axial compression critical buckling load.

TRANSVERSE COMPRESSION – DIFFERENCES FEM vs THEORY, σ_{crit} (MPa)				
a/b	Rotational restraint	$\Delta\sigma_{cr}$ (%)	$\Delta\sigma_{cr}\|_{MAX}$ (%)	$\Delta\sigma_{cr}\|_{MIN}$ (%)
1	SS	-0,07	0.92	-1.08
2	SS	6.72	8.28	5.11
3	SS	3.93	5.54	2.27
4	SS	13.49	14.93	11.99
20	SS	0.95	2.61	-0.76

Table 7.2. Differences in transverse compression critical buckling load.

BENDING – DIFFERENCES FEM vs THEORY, σ_{crit} (MPa)				
a/b	Rotational restraint	$\Delta\sigma_{cr}$ (%)	$\Delta\sigma_{cr}\|_{MAX}$ (%)	$\Delta\sigma_{cr}\|_{MIN}$ (%)
1	SS	1,07	1.57	0.58
2	SS	0,10	0.60	-0.40
3	SS	0,05	0.55	-0.45
4	SS	-0,96	-0.96	-0.96
20	SS	0,15	0.15	0.15

Table 7.3. Differences in bending critical buckling load.

SHEAR – DIFFERENCES FEM vs THEORY, σ_{crit} (MPa)				
a/b	Rotational restraint	$\Delta\sigma_{cr}$ (%)	$\Delta\sigma_{cr}\|_{MAX}$ (%)	$\Delta\sigma_{cr}\|_{MIN}$ (%)
1	SS	1,17	2.35	-0.03
	C	0,50	1.09	-0.10
2	SS	1,04	1.63	0.44
	C	-0,79	-0.19	-1.40
3	SS	1,03	1.62	0.44
	C	-1,19	-0.59	-1.80
4	SS	0,48	1.07	-0.12
	C	-0,52	0.08	-1.12
20	SS	1,03	1.62	0.43
	C	1,04	1.63	0.44

Table 7.4. Differences in shear critical buckling load.

It is observed in the table that some cases have positive $\Delta\sigma_{cr}$ (%) values (meaning that theoretical results are conservative predictions). This does not agree with theoretical analysis, where it was explained that energy method predicted buckling load is equal or greater than exact method predicted one (giving optimistic estimates). It is reasonable to think that in single loading cases in which the displacement function can be estimated accurately (remember that this estimate is the key to obtain an accurate result in energy method), the predicted load shall be quite close to the exact one (and close to the FEM one, if assuming FEM result approaches rather accurately the exact solution).

In order to find the source of the positive $\Delta\sigma_{cr}$ (%) between FEM and theoretical results, two possibilities have been considered. Either FEM results are not accurate enough, or there is an error in the procedure to obtain $\sigma_{cr-theory}$.

Firstly, the procedure to obtain theoretical buckling load has been checked. It has been found that there is a potential source of error when obtaining k from the graphs. In Annex B the reader can find a preliminary study to quantify the maximum differences that can be caused due to this fact. In addition, this annex explains how the range of possible $\Delta\sigma_{cr}$ (%) (determined by $\Delta\sigma_{cr}|_{MIN}(\%)$ and $\Delta\sigma_{cr}|_{MAX}(\%)$) is computed. What this range means is that $\Delta\sigma_{cr}$ (%) is not a perfectly accurate value, so it could potentially be in the range.

If the error is considered, it is observed in the tables that the ranges delimited by $\Delta\sigma_{cr}|_{MIN}(\%)$ and $\Delta\sigma_{cr}|_{MAX}(\%)$ cover negative values for most of the cases.

For shear, there are several cases where $\Delta\sigma_{cr}|_{MIN}(\%)$ is around 0.44. For those cases the mesh has been refined, and $\Delta\sigma_{cr}|_{MIN}(\%)$ has decreased; for a/b=3 (SS) from +0.44% to +0.40%, for a/b=20 (SS) from +0.43% to -0.25%, and for a/b=20 (C) from +0.44% to -0.44%.

As for bending, when refining the mesh for cases a/b=1 (SS) and a/b=20 (SS), $\Delta\sigma_{cr}|_{MIN}(\%)$ becomes negative for both cases. For a/b=1 there is a decrease from +0.58% to -0.42%, and for a/b=20 from +0.15% to -0.06%. So, the range of potential $\Delta\sigma_{cr}$ (%) values covers for all cases.

In transverse compression, significant differences are observed. Even accounting for the potential error of the digitalizer, the errors cannot be explained. The mesh has been refined but $\Delta\sigma_{cr}|_{MIN}(\%)$ has only been reduced marginally. Ideally, an extremely fine mesh could remove the error. In addition, FEM model has been carefully checked but the obtained results, σ_{cr-FEM} seem to be correct.

One of the reasons that explains partially the high differences is that since transverse compression critical load values are quite low, small differences between FEM and analytical results create a large difference expressed in %. Additionally, it is worth mentioning that it also may occur that the theoretical graph employed to compute analytical result does not provide very accurate results. This could be investigated in future works.

In conclusion, although the error caused from k extraction from graphs can justify initially computed $\Delta\sigma_{cr}$ (%), there are a few cases (mainly in transverse compression loading) where estimated FEM load is still larger than energy method estimated load. This may indicate the presence of another error, some errors in FEM modelling (which has been carefully checked without detecting any error) or that for transverse compression case there are some small differences between FEM and exact solution.

6.2 Combined loading

- ***Combined shear and axial compression***

For combination of shear and axial compression, Fig.7.1 provides a general overview of all the cases, with different aspect ratios and edges rotational restraints (all edges simply supported or clamped). FEM results are to be compared with interaction equations $R_C + {R_S}^2 = 1$ (from reference 5) and $R_C + {R_S}^{1,75} = 1$ from references 9 and 10.

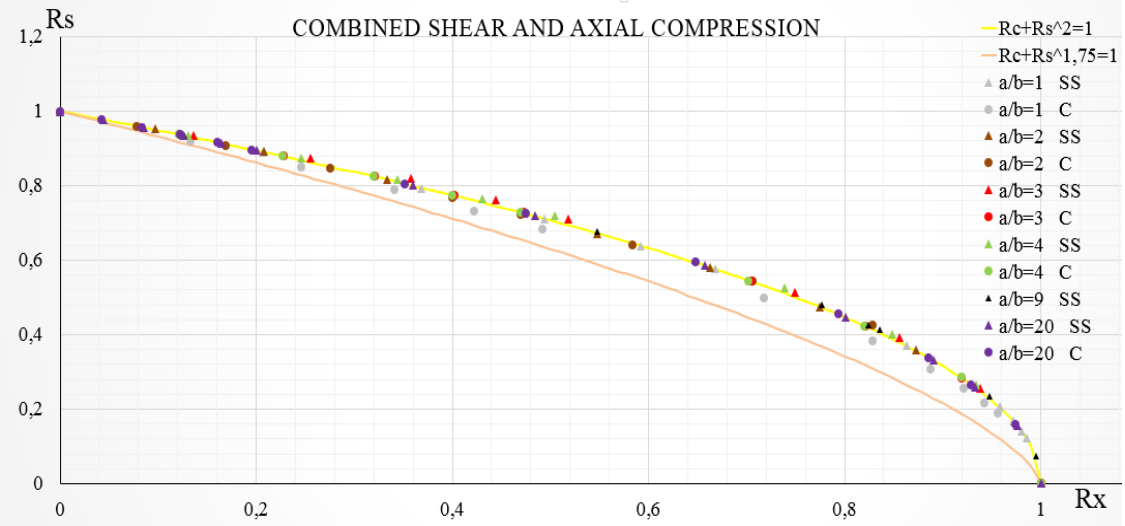

Figure 7.1. Shear and axial compression loading case for different all geometries and boundary conditions analyzed.

According to the theoretical analysis presented before, equation $R_C + {R_S}^2 = 1$ is only valid for all geometries if all edges are simply supported (Ref.6) or for infinitely long plates with any edges rotational restraint (Ref.5). These assumptions are to be checked using FEM results.

First of all, as for cases with all edges simply supported (recall that previous discussion was related to cases with all edges clamped), it is observed (Fig. 7.2) that all geometries fit reasonably well the interaction equation curve.

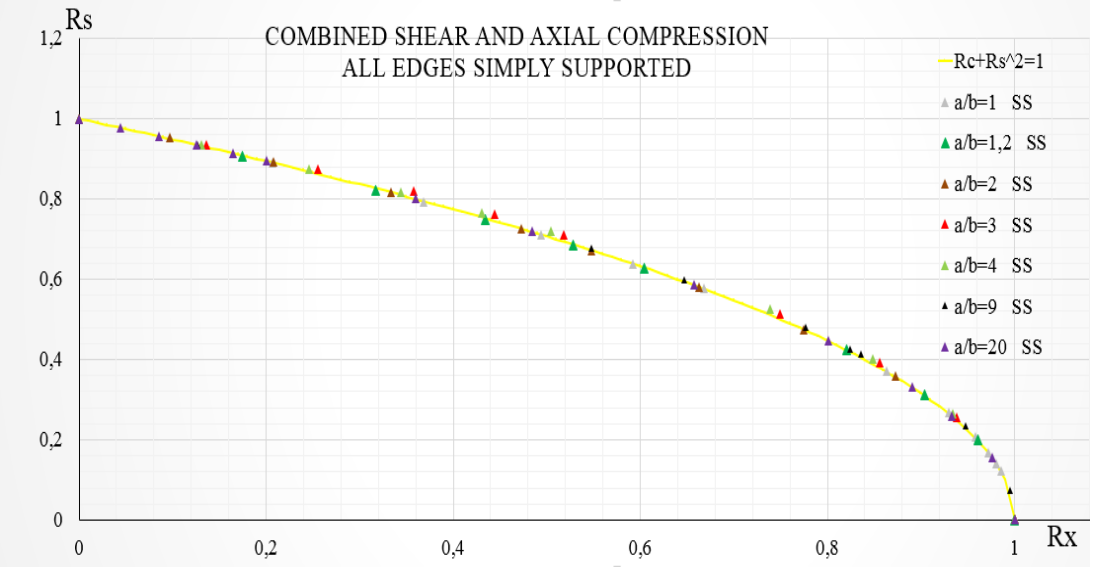

Figure 7.2. Shear and axial compression loading case for different aspect ratios for all edges simply supported.

Differences between FEM results and $R_C + {R_S}^2 = 1$ shown in Table 7.5 demonstrate that the difference is not related to the plate geometry. For all the aspect ratios analyzed with simply supported edges, the difference is extremely low, and interaction equation provided results are marginally conservative for all cases (except for a/b=1, where the difference is negligibly small). It is worth mentioning that for a/b=1 and 2, theoretical results are conservative or optimistic depending on R_C value; for a/b=1 using $R_C + {R_S}^2 = 1$ for $0.2 < R_C < 0.6$ is conservative, and for a/b=2, it is conservative for the range $0.47 < R_C < 0.66$.

In accordance with the small differences, FEM results equations are similar to $R_C + {R_S}^2 = 1$. Note that in the case of a/b=20 (where the mean difference is negligibly small) the equations coefficients are practically the same (1 / 1.002 and 2 / 2.003). No data fit has been done for the case a/b= 9 to obtain the equation.

DIFFERENCES FEM RESULTS AND $R_C + {R_S}^2 = 1$ COMBINED SHEAR AND AXIAL COMPRESSION - SIMPLY SUPPORTED			
a/b	Mean Difference, %	Maximum difference, %	FEM results equation
1	-0.07	-0.14	${R_C}^{0.987} + {R_S}^{2.017} = 1$
2	0.03	0.30	${R_C}^{1.005} + {R_S}^{1.991} = 1$
3	1.11	1.64	${R_C}^{1.064} + {R_S}^{2.009} = 1$
4	0.75	1.42	${R_C}^{1.006} + {R_S}^{2.078} = 1$
9	0.35	0.58	-
20	0.04	0.11	${R_C}^{1.002} + {R_S}^{2.003} = 1$

Table 7.5. Differences in between $R_C + {R_S}^2 = 1$ and FEM, for different aspect ratios with all edges simply supported.

Secondly, the differences for clamped plates are to be compared. Observe in Fig.7.3 FEM results for clamped edges

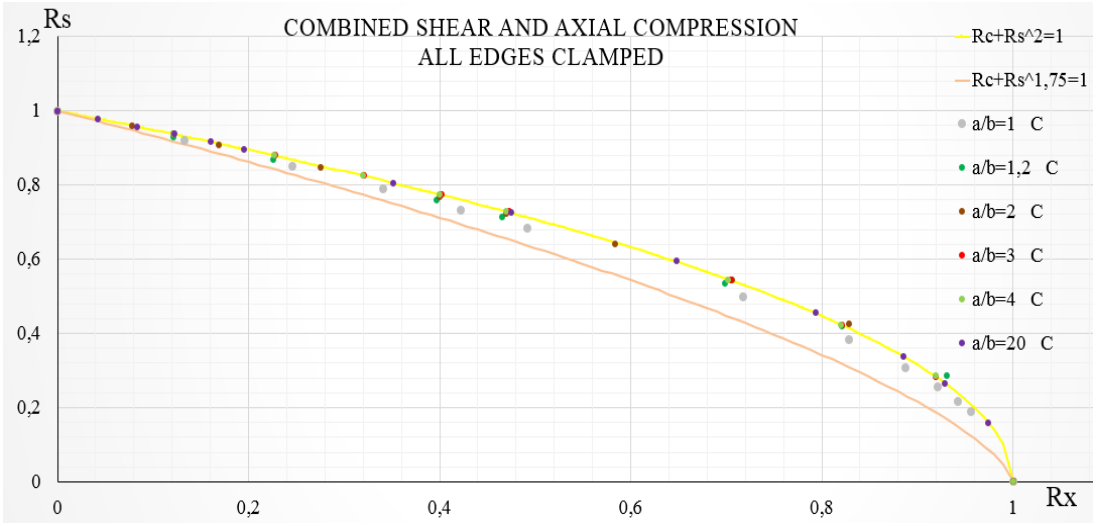

Figure 7.3. Shear and axial compression loading case for different aspect ratios for all edges clamped.

In clamped plates cases, the mean difference between the equation and the results obtained by FEM (Table 7.6) show that the largest difference is obtained for square plates (a/b=1). As the aspect ratio increases, the correlation between theoretical results and FEM improves, becoming essentially exact for aspect ratios above 3. For the small aspect ratios studied, theory provides optimistic predictions (but with little errors). As the aspect ratio decreases, the use of the theoretical equation becomes more optimistic. It is worth mentioning that in cases a/b=1.2 and 2, for some short ranges of R_C, conservative results are obtained. Note that equation $R_C + {R_S}^2 = 1$, although it is slightly optimistic, it can still be used for low aspect ratios using a margin of safety of around 2%.

DIFFERENCES FEM RESULTS AND $R_C + {R_S}^2 = 1$ COMBINED SHEAR AND AXIAL COMPRESSION - CLAMPED EDGES			
a/b	Mean Difference, %	Maximum difference, %	FEM results equation
1	-1.96	-2.87	${R_C}^{0.942} + {R_S}^{1.904} = 1$
1.2	-1.18	-1.77	${R_C}^{0.977} + {R_S}^{2.024} = 1$
2	-0.34	0.79	${R_C}^{0.965} + {R_S}^{2.042} = 1$
3	0.06	0.36	${R_C}^{1.011} + {R_S}^{1.988} = 1$
4	-0.06	-0.14	${R_C}^{1.008} + {R_S}^{1.981} = 1$
20	0.02	0.06	${R_C}^{1.000} + {R_S}^{2.003} = 1$

Table 7.6. Differences in between $R_C + {R_S}^2 = 1$ and FEM, for different aspect ratios with all edges clamped.

Therefore, the conclusion of reference 5 (stating that the equation $R_C + {R_S}^2 = 1$ is valid for combined shear and direct stress for infinitely long plates with equal restraints against rotation in all edges) may be corrected. That is, the equation is not only essentially exact for infinitely long plates, but also for medium-high aspect ratio plates (from a/b=3 in advance) for which the maximum differences are below 0.4%. Additionally, the equation also gives accurate results for the remaining aspect ratios.

The differences between the results provided by FEM and equation $R_C + {R_S}^{1,75} = 1$ are collected in Table 7.7 and 7.8 for simply supported and clamped edges respectively. Overall, it is reasonably accurate for engineering purposes, with all cases maximum errors well below 10%.

DIFFERENCES FEM RESULTS AND $R_C + {R_S}^{1.75} = 1$ COMBINED SHEAR AND AXIAL COMPRESSION - SIMPLY SUPPORTED			
a/b	Mean Difference, %	Maximum difference, %	FEM results equation
1	2.04	3.71	${R_C}^{0.987} + {R_S}^{2.017} = 1$
2	2.63	3.76	${R_C}^{1.005} + {R_S}^{1.991} = 1$
3	3.93	4.85	${R_C}^{1.064} + {R_S}^{2.009} = 1$
4	3.02	4.88	${R_C}^{1.006} + {R_S}^{2.078} = 1$
20	1.93	3.80	${R_C}^{1.002} + {R_S}^{2.003} = 1$

Table 7.7. Differences in between $R_C + {R_S}^{1.75} = 1$ and FEM, for different aspect ratios with all edges simply supported.

DIFFERENCES FEM RESULTS AND $R_C + {R_S}^{1.75} = 1$ COMBINED SHEAR AND AXIAL COMPRESSION - CLAMPED			
a/b	Mean Difference, %	Maximum difference, %	FEM results equation
1	0.71	1.38	${R_C}^{0.942} + {R_S}^{1.904} = 1$
2	2.15	4.35	${R_C}^{0.965} + {R_S}^{2.042} = 1$
3	2.65	3.78	${R_C}^{1.011} + {R_S}^{1.988} = 1$
4	2.57	3.63	${R_C}^{1.008} + {R_S}^{1.981} = 1$
20	2.71	3.72	${R_C}^{1.000} + {R_S}^{2.003} = 1$

Table 7.8. Differences in between $R_C + {R_S}^{1.75} = 1$ and FEM, for different aspect ratios with all edges clamped.

Observe that the differences are between 1.93% and 3.93% for simply supported cases, and between 0.71% and 2.71% for clamped cases. Note that in some cases the difference reaches nearly 5%. Correlation with this equation is seen to be worse than with $R_C + {R_S}^2 = 1$. However, unlike $R_C + {R_S}^2 = 1$, this equation is conservative for all cases.

It is also observed that lower differences are found when using the equation for clamped edges plates. Recall from theoretical analysis that reference 10 presents this equation for clamped plates. Then, it makes sense to find lower differences for these cases. Additionally, it is also reasonable to use the equation for simply supported plate cases, which is in agreement with reference 9, that presents the equation to be used with any edges rotational restraints.

Observing FEM results equation and $R_C + {R_S}^{1.75} = 1$, it is appreciable that if in the theoretical equation a term higher than 1.75 was used, the equation would approach better FEM results. Note that the lowest mean difference is found in case a/b=1 with clamped edges. The FEM equation for this case has the lowest coefficient for R_S (1.904) of all the equations shown, which makes the smallest difference between both equations R_S coefficients. Therefore, it is reasonable to think that if a coefficient 1.8 or 1.9 was used, more accurate results would be obtained while still getting conservative estimates for all cases (unlike equation $R_C + {R_S}^2 = 1$ which is not always conservative).

A study has been carried out to know the effect of using a R_S coefficient slightly larger than 1.75. It has been found that as the coefficient is further increased from 1.77, the accuracy is improved but for some clamped plates cases the estimations start to be optimistic. For simply supported cases conservative estimates are always obtained (only slightly optimistic results are obtained for square plates if coefficient 1.9 or above is used). If the equation $R_C + {R_S}^{\mathbf{1.8}} = 1$ is used, the estimations are optimistic for clamped square plates in the range $0.13 < R_C < 0.50$. For the remaining cases, the equation still gives conservative results. If the equation $R_C + {R_S}^{\mathbf{1.93}} = 1$ is used, all the clamped cases (except square plates) are still conservative. Above around coefficient

1.93, equation start to give optimistic results for plates of a/b=1.2 and 2. The obtained higher accuracy when using $R_C + {R_S}^{1.93} = 1$ instead of $R_C + {R_S}^{1.75} = 1$ can be observed in Tables 7.9 and 7.10, where the accuracy of the 3 equations studied in this section is analyzed. The advantage of this equation with respect to $R_C + {R_S}^2 = 1$ is that although it gives less accurate estimations, for all cases (except clamped square plates) the estimations are conservative.

DIFFERENCES FEM RESULTS AND INTERACTION EQUATIONS $R_C + {R_S}^{1.93} = 1$, $R_C + {R_S}^{1.75} = 1$, $R_C + {R_S}^2 = 1$ COMBINED SHEAR AND AXIAL COMPRESSION - SIMPLY SUPPORTED			
Mean Differences, %			
a/b	$R_C + {R_S}^{1.93} = 1$	$R_C + {R_S}^{1.75} = 1$	$R_C + {R_S}^2 = 1$
1	0.50	2.04	-0.07
2	0.69	2.63	0.03
3	1.72	3.93	1.11
4	1.24	3.02	0.75
20	0.54	1.93	0.04

Table 7.9. Mean differences between interaction equations and FEM results (simply supported plates)

DIFFERENCES FEM RESULTS AND INTERACTION EQUATIONS $R_C + {R_S}^{1.93} = 1$, $R_C + {R_S}^{1.75} = 1$, $R_C + {R_S}^2 = 1$ COMBINED SHEAR AND AXIAL COMPRESSION - CLAMPED			
Mean Differences, %			
a/b	$R_C + {R_S}^{1.93} = 1$	$R_C + {R_S}^{1.75} = 1$	$R_C + {R_S}^2 = 1$
1	-1.29	0.71	-1.96
2	0.13	2.15	-0.34
3	0.68	2.65	0.06
4	0.64	2.57	-0.06
20	0.74	2.71	0.02

Table 7.10. Mean differences between interaction equations and FEM results (clamped plates)

In conclusion, both interaction equations presented in the references provide accurate predictions for engineering purposes. For the case of $R_C + {R_S}^2 = 1$, the estimates are much more accurate (mean difference always below 1.96%). For clamped edges, it provides essentially exact results (with respect to FEM) for aspect ratios above 3. However, for small aspect ratios clamped plates, it gives slightly optimistic estimates. For simply supported edges, essentially exact results are obtained for infinitely long plates (a/b=20), and for plates with a/b>3, the difference is below 1%. As for equation $R_C + {R_S}^{1.75} = 1$, it gives less accurate estimates which are conservative in all cases. Depending on the case, mean differences range between 0.71% and 3.93%, with maximum differences reaching almost 5%. Although being apparently high differences, they can be affordable for many engineering applications. The accuracy of this equation can be improved by modifying coefficient 1.75, and using $R_C + {R_S}^{1.93} = 1$ (more accurate and conservative).

In order to prove that the difference between FEM and theoretical results is not due shortcomings in the FEM modeling, the mesh for the case a/b=1 (the one with the highest difference among those studied) has been refined. The case of a/b=1 with all edges clamped has been analyzed using FEM square elements (CQUAD4) of $2x2\ mm^2$ and$1x1\ mm^2$. The results obtained with the finer mesh ($1x1\ mm^2$) has not modified significantly the results (Fig.7.4). The difference obtained with a finer mesh is 2.17% (instead of 1.96% obtained with the initial mesh). The difference is rather small. This proves that the mesh density used initially (with 2 mm^2 elements) was accurate enough, and that the difference with respect to the interaction curve is not due to an incorrect mesh.

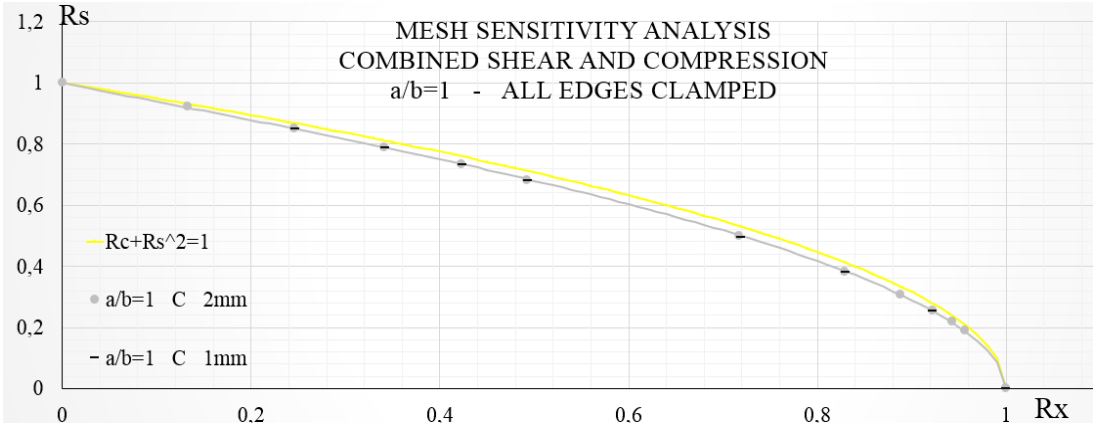

Figure 7.4. Mesh sensitivity analysis: (2 mm^2 and 1 mm^2 elements) for a/b=1 and clamped plates. Combined shear and axial compression

- ***Combined shear and longitudinal bending***

As for combination of shear and in longitudinal bending (Fig.7.5), the difference between FEM and analytical results is seen to depend on both the geometry and the edges rotational restraint. It is appreciated that apparently there is not a complete suitability for all cases for the interaction equation $R_B{}^2 + R_S{}^2 = 1$ (Ref.3) and NACA 2536 (Ref.11) interaction curve.

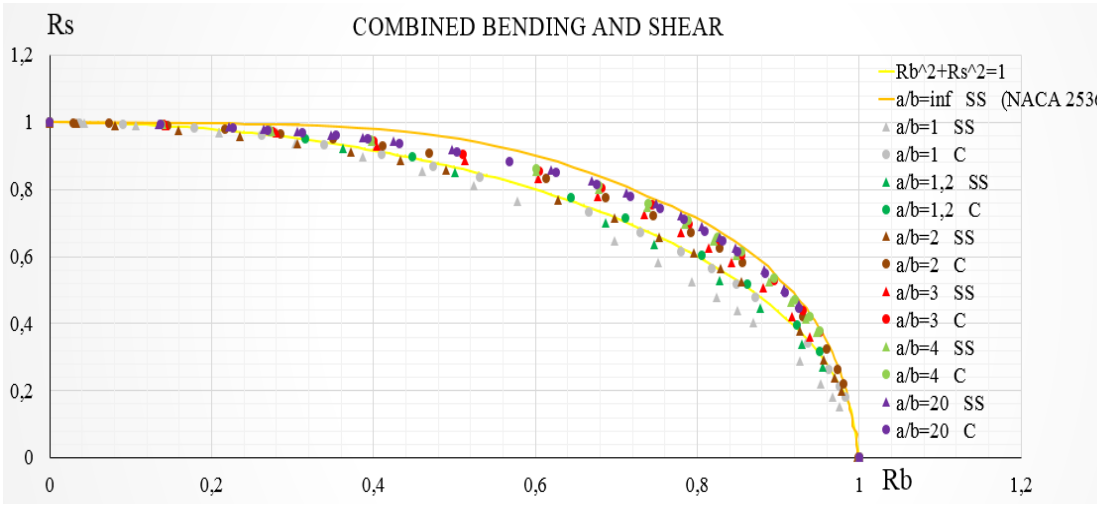

Figure 7.5. Combined shear and bending for different geometries and boundary conditions.

Note that interaction curve from equation $R_B{}^2 + R_S{}^2 = 1$ (Ref.3) and curve from NACA 1323 (Ref.12), explained in analytical results section, will be considered approximately the same, and therefore, discussion will only focus in the curve of the equation.

According to the reference 11, NACA 2536 interaction curve gives reasonably accurate predictions for simply supported infinitely long plates. The mean difference between this curve and FEM curve for a/b=20 case with edges simply supported (Fig.7.6) is found to be -1.40% (with maximum differences reaching -2.60%). This difference can be acceptable for engineering purposes, but it should be noted that the curve provides optimistic estimates.

In order to ensure the accuracy of the FEM result, and to remove a potential source of the difference stated, the FEM model mesh has been refined (using $2x2\ mm^2$ elements instead of the initially used $5x5\ mm^2$ elements). The results of this analysis (Table 7.11 and Fig.7.6), where values are seen to change only slightly, show that the difference is not due to the use of a mesh not accurate enough.

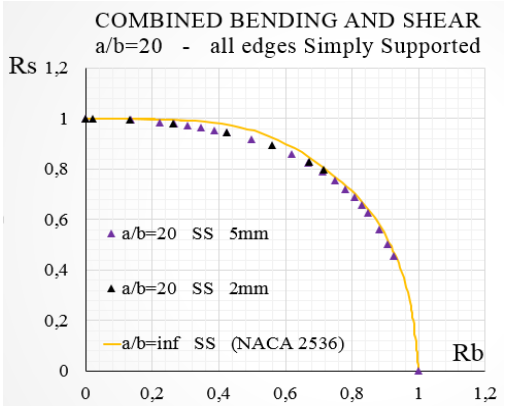

Figure 7.6. Mesh sensitivity analysis for two different mesh densities.

MESH SENSITIVITY ANALYSIS a/b=20 all edges SS		
Mesh element size	Mean Difference, %	Maximum difference, %
$5x5\ mm^2$	-1.40	-2.60
$2x2\ mm^2$	-1.48	-2.51

Table 7.11. Differences between NACA 2536 curve and FEM, with two different mesh densities.

The differences between NACA 2536 curve and FEM results for all the cases are shown in Tables 7.12 and 7.13. For both rotational restraint cases, the correlation between the curve and FEM results improve as the aspect ratio increases. The exception for this are the clamped plate cases of a/b=20 and 4, where the correlation is something better (0.42% more accurate) for a/b=4 plates. Since this difference is small, it can be assumed that for clamped plates with aspect ratios a/b≥4 the correlation is nearly the same for any geometry. Additionally, it is observed that independently of the rotational restraints, plates with a/b≥4 have their maximum differences below 5%. This is an acceptable value for engineering purposes, meaning that NACA 2536 could be used effectively for large aspect ratio plates with any edges rotational restraint for engineering applications. The user should know, however, that the equation gives optimistic estimates.

DIFFERENCES FEM RESULTS AND NACA 2536 CURVE COMBINED SHEAR AND BENDING - SIMPLY SUPPORTED			
a/b	Rotational restraint	Mean Difference, %	Maximum difference, %
20	SS	-1.40	-2.60
4	SS	-1.88	-3.92
3	SS	-3.55	-5.52
2	SS	-4.63	-9.32
1	SS	-7.95	-13.18

Table 7.12. Differences between NACA 2536 curve and FEM, for simply supported plates.

DIFFERENCES FEM RESULTS AND NACA 2536 CURVE COMBINED SHEAR AND BENDING - CLAMPED			
a/b	Rotational restraint	Mean Difference, %	Maximum difference, %
20	C	-1.97	-3.13
4	C	-1.55	-3.24
3	C	-1.98	-3.72
2	C	-2.33	-5.09
1	C	-4.98	-9.54

Table 7.13. Differences between NACA 2536 curve and FEM, for clamped plates.

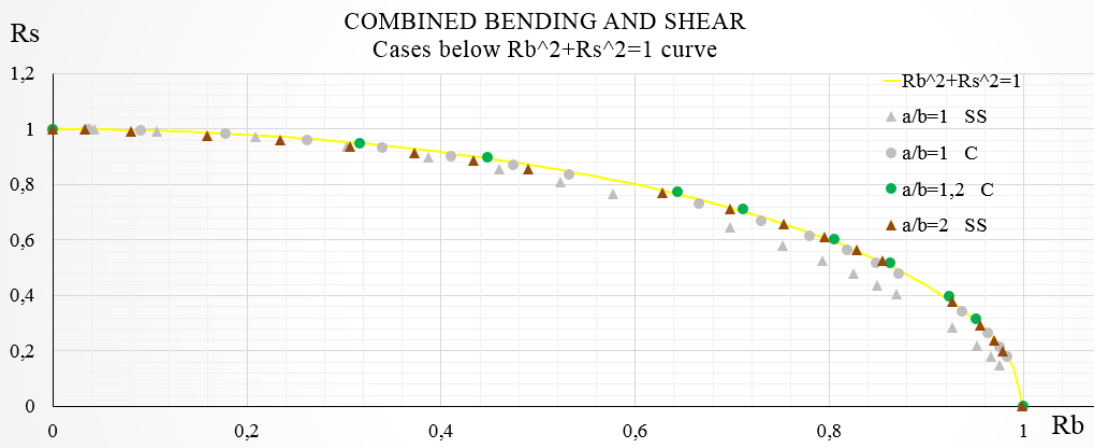

Figure 7.7. Combined bending and shear cases below equation Rb^2+Rs^2=1 curve

As for the curve given by $R_B{}^2 + R_S{}^2 = 1$, it is conservative for most of the cases (Fig.7.7). Table 7.14 shows that for low aspect ratios (a/b=1, 1.2 and 2) with simply supported edges, the curve is optimistic. It is appreciable (Fig.7.7) that the case of a square plate with clamped edges is slightly below the curve (with an optimistic mean difference of -0.51%). Observation of the case a/b=1.2 FEM results, which are above the curve (with a mean conservative difference of 0.41%), concludes that for clamped plates with aspect ratio something higher than 1 (between 1 and 1.2), the equation is already conservative (for a/b=1.2, FEM solution is already above the curve). The differences for simply supported and clamped plates are collected in Tables 7.14 and 7.15 respectively.

DIFFERENCES FEM RESULTS AND NACA 1323 CURVE ($R_B{}^2 + R_S{}^2 = 1$) COMBINED SHEAR AND BENDING - SIMPLY SUPPORTED			
a/b	Rotational restraint	Mean Difference, %	Maximum difference, %
20	SS	3.94	6.07
4	SS	2.91	4.84
3	SS	2.44	6.45
2	SS	-0.52	-1.47
1.2	SS	-1.32	-1.96
1	SS	-2.98	-5.17

Table 7.14. Differences between $R_B{}^2 + R_S{}^2 = 1$ (or NACA 1323 curve, which is similar) and FEM results. Simply supported plates.

DIFFERENCES FEM RESULTS AND NACA 1323 CURVE ($R_B{}^2 + R_S{}^2 = 1$) COMBINED SHEAR AND BENDING - CLAMPED			
a/b	Rotational restraint	Mean Difference, %	Maximum difference, %
20	C	3.92	5.65
4	C	3.71	5.64
3	C	3.69	5.55
2	C	1.32	3.75
1.2	C	0.41	0.73
1	C	-0.51	-0.96

Table 7.15. Differences between $R_B{}^2 + R_S{}^2 = 1$ (or NACA 1323 curve, which is similar) and FEM results. Clamped plates.

Therefore, the general trend for this loading combination is that ${R_B}^2 + {R_S}^2 = 1$ curve becomes more and more conservative for any edges rotational restraint as the aspect ratio increases. It gives the most accurate estimations (differences below 1% in absolute value) with respect to FEM for clamped plates with aspect ratios between 1 and 1.2. If all edges are simply supported the equation will become conservative for plates with aspect ratios above 2 (for a/b=2 FEM results are still below the curve with a mean difference of 1.03%).

All the previous demonstrates that both the curves provided by ${R_B}^2 + {R_S}^2 = 1$ and NACA 1323 (reference NACA 1323), are conservative for infinitely long plates with simply supported edges. For infinitely long plates the mean differences are almost 4% for both simply supported and clamped plates. This difference are however, acceptable for engineering purposes. The highest accuracy of equation ${R_B}^2 + {R_S}^2 = 1$ is obtained for small aspect ratio plates.

- ***Combined longitudinal bending and axial compression***

As for combination of bending and axial compression (Fig.7.8), FEM results are to be compared with a set of points for different aspect ratios simply supported plates from reference 4 and interaction equation ${R_B}^{1,75} + R_X = 1$ from reference 3.

Overall, the curve given by the equation gives conservative estimates if FEM results are taken as a reference. It is worthwhile to carry out an analysis quantifying the differences for the different cases. The resulted information from the analysis is depicted in Table 7.16 and 7.17.

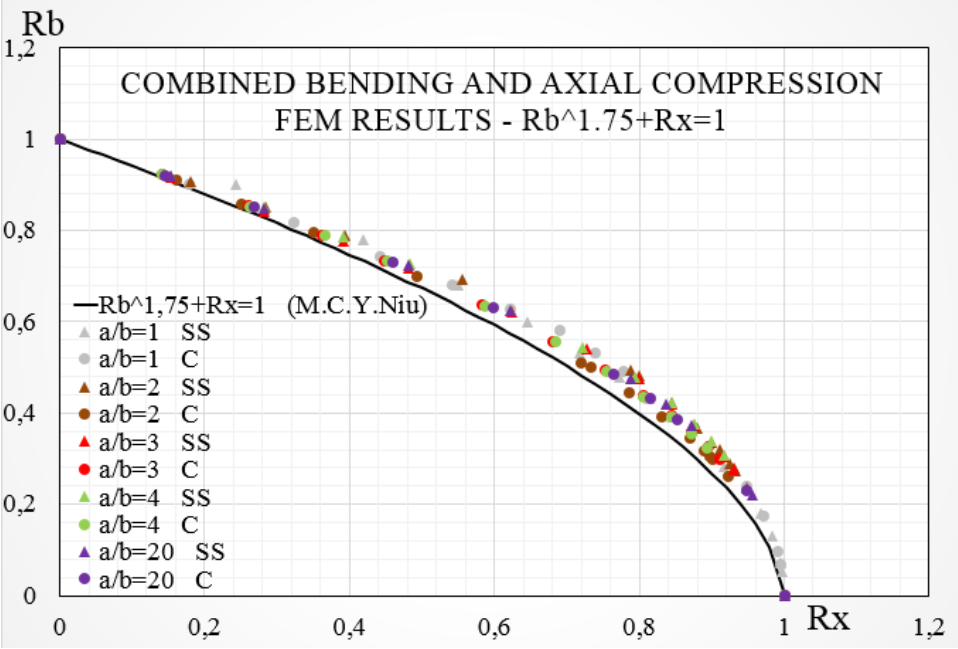

Figure 7.8. In plane bending and axial compression loading case for different geometries and boundary conditions. Comparison of FEM results with ${R_B}^{1,75} + R_X = 1$ from M.C.Y.Niu (Ref.3).

DIFFERENCES FEM RESULTS AND $R_B^{1,75} + R_X = 1$ COMBINED AXIAL COMPRESSION AND BENDING - SIMPLY SUPPORTED			
a/b	Rotational restraint	Mean Difference, %	Maximum difference, %
20	SS	3.49	4.73
4	SS	4.11	5.48
3	SS	3.74	5.86
2	SS	3.53	6.10
1	SS	3.39	4.36

Table 7.16. Differences between $R_B^2 + R_S^2 = 1$ and FEM results. Simply supported plates.

DIFFERENCES FEM RESULTS AND $R_B^{1,75} + R_X = 1$ COMBINED AXIAL COMPRESSION AND BENDING - CLAMPED			
a/b	Rotational restraint	Mean Difference, %	Maximum difference, %
20	C	2.46	3.76
4	C	2.80	3.35
3	C	2.87	3.53
2	C	2.01	2.36
1	C	2.68	5.66

Table 7.17. Differences between $R_B^{1,75} + R_X = 1$ and FEM results. Clamped plates.

Interaction equation $R_B^{1,75} + R_X = 1$ gives conservative estimation for all cases analyzed. It is appreciable that the correlation with clamped cases is remarkably better (with mean differences of 2-3% and maximum differences between 3-6%). Simply supported plates show higher differences (about 3-4% mean differences and 4-6% maximum differences). The accuracy does not seem to depend on the geometry.

Another source of comparison come from the set of points provided by Robert G. Noel at reference 4 for different aspect ratios. The reference gives 10 points for each geometry. A data fit has been performed to fit these points in an equation of shape $R_1^p + R_2^q = 1$. These curves (together with FEM results) are illustrated in Fig.7.9 to 7.12 (one for each curve for clarity). The differences are collected in Tables 7.18 and 7.19 below.

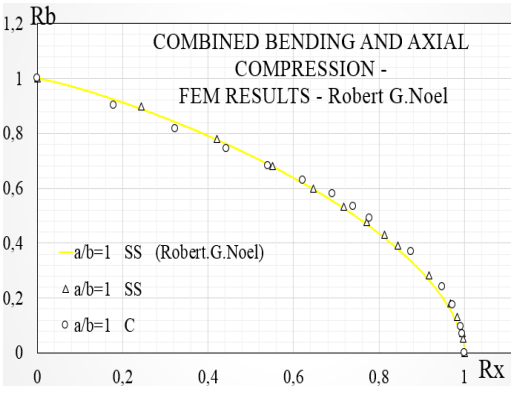

Figure 7.9. Combined bending and axial compression for a/b=1 plates (Ref.4).

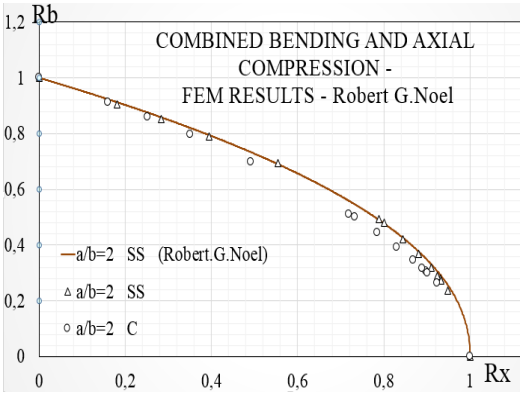

Figure 7.10. Combined bending and axial compression for a/b=2 plates (Ref.4).

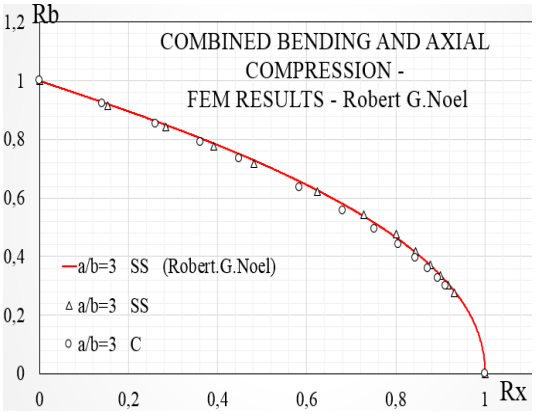

Figure 7.11. Combined bending and axial compression for a/b=3 plates (Ref.4).

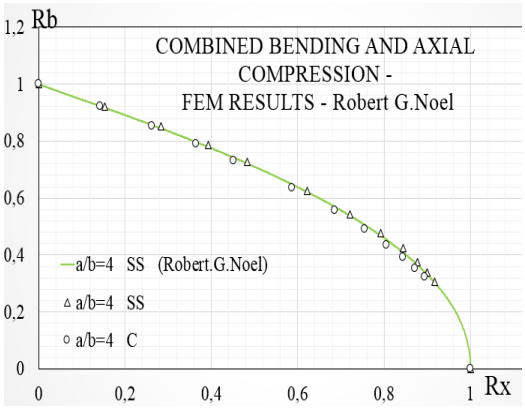

Figure 7.12. Combined bending and axial compression for a/b=4 and infinitely long plates

DIFFERENCES FEM RESULTS AND Robert G.Noel COMBINED AXIAL COMPRESSION AND BENDING - SIMPLY SUPPORTED				
a/b	Rotational restraint	Mean Difference, %	Maximum difference, %	Robert G.Noel equation
20	SS	0.64	0.92	$R_X^{0.947} + R_B^{2.134} = 1$
4	SS	0.94	1.71	$R_X^{0.947} + R_B^{2.134} = 1$
3	SS	-0.40	-0.97	$R_X^{0.967} + R_B^{2.144} = 1$
2	SS	-0.58	-0.81	$R_X^{1.000} + R_B^{2.182} = 1$
1	SS	0.55	1.04	$R_X^{1.186} + R_B^{1.753} = 1$

Table 7.18. Differences between FEM results and Robert G. Noel theoretical results. Simply supported.

DIFFERENCES FEM RESULTS AND Robert G.Noel COMBINED AXIAL COMPRESSION AND BENDING - CLAMPED				
a/b	Rotational restraint	Mean Difference, %	Maximum difference, %	Robert G.Noel equation
20	CC	-0.17	-0.25	$R_X^{0.947} + R_B^{2.134} = 1$
4	CC	-0.55	-0.66	$R_X^{0.947} + R_B^{2.134} = 1$
3	CC	-1.30	-1.92	$R_X^{0.967} + R_B^{2.144} = 1$
2	CC	-2.66	-4.04	$R_X^{1.000} + R_B^{2.182} = 1$
1	CC	-1.62	-2.40	$R_X^{1.186} + R_B^{1.753} = 1$

Table 7.19. Differences between FEM results and Robert G. Noel theoretical results. Clamped.

Individual observation of these plots shows that unlike equation $R_B{}^{1,75} + R_X = 1$, Robert G. Noel curves do not always give conservative estimations. In particular, all clamped cases provide results slightly conservative (with between -2.66 and -0.55% mean differences). It is worth mentioning that for clamped square plate case, the curve gives conservative estimates for around $R_X = 0.6$ in advance. For simply supported cases, the curves give conservative estimates for square and a/b=4 plates. Therefore, note that Robert G. Noel curves are, in general, slightly optimistic.

The correlation between Robert G. Noel curves and obtained FEM results is relatively accurate. Simply supported cases present a higher degree of accuracy with mean differences always below 1% (absolute value) with really accurate estimations. Curves for clamped edges plates show also accurate predictions, always below 2.66% (absolute value). It is worth to note that for some cases

(in particular a/b=2) the maximum difference reaches 4%. However, this is still considered an acceptable difference for engineering purposes.

Finally, it is worth to analyze the correlation between Robert G. Noel curve for a/b=4 and FEM results for infinitely long plates (a/b=20). It is interesting to observe that the correlation is quite accurate, with mean differences of only 0.64% and -0.17% for simply supported and clamped plates respectively. Consequently, this indicated that curve for a/b=4 can be effectively used for infinitely long plates with any edges rotational restraint (although note that for clamped edges the curve will give marginal optimistic estimates).

- ***Combined longitudinal bending and transverse compression***

As for combination of longitudinal bending and transverse compression, this section will compare FEM results with those provided in the references 13, 11, 4 and 9.

Firstly, recall the disagreement existing between equation $R_B{}^{1,75} + R_Y = 1$ from reference 9 and the remaining references. This equation has been tested with FEM results for different aspect ratios from 1 to 20 (Fig.7.13). It is clear that the equation curve remains far of all cases, with exception of the case of square plates. For square plates with either simply supported or clamped edges, the difference FEM-equation is smaller, but still considerable (for clamped case, the equation prediction can reach differences of 9.37% (with a mean difference of 4.92%), and for simply supported case, maximum difference reaches 6.10% (3.78% mean difference). Although correlation for simply supported square plates is not that bad, the fact of being optimistic and that differences can reach 6% in some regions makes its use not desirable. Consequently, the use of the interaction equation is not recommended for any combined bending and transverse compression loading case.

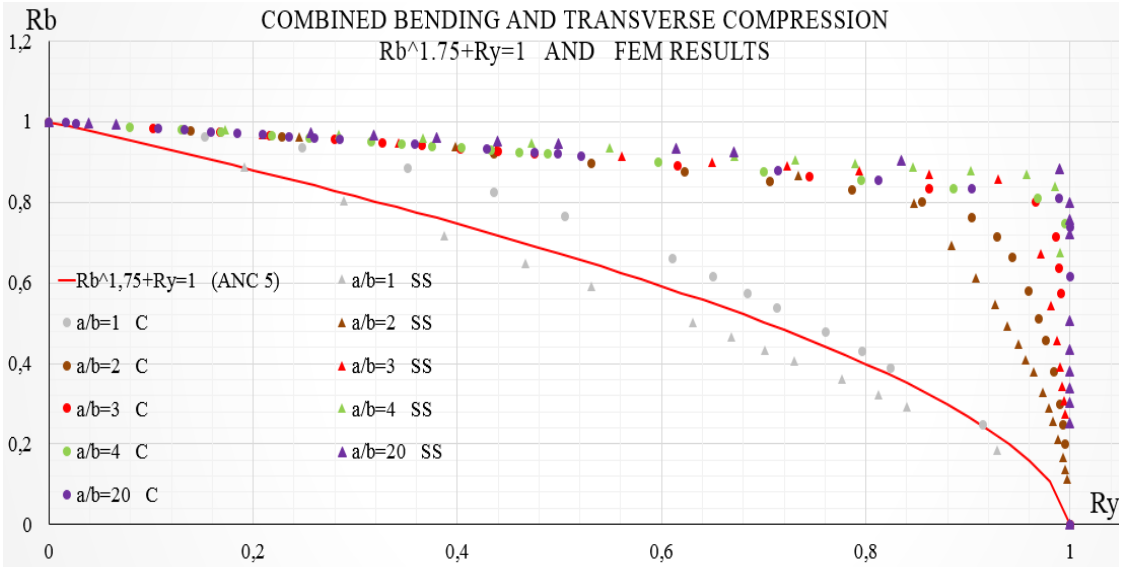

Figure 7.13. Combined bending and transverse compression. FEM results and $R_B{}^{1,75} + R_Y = 1$ (Ref.9). FEM results for different aspect ratios and edges rotational restraints.

Then, it is worth to focus the discussion in the comparison between FEM results and remaining references presented interaction curves (Fig.7.14, 7.15, 7.16 and 7.17). Recall that all the three references computed these curves from the energy method, so the curves will be so referred.

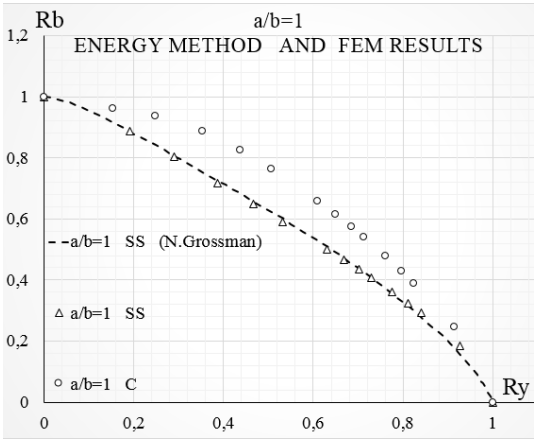

Figure 7.14. Comparison energy method and FEM results for a/b=1 with different elastic restraints.

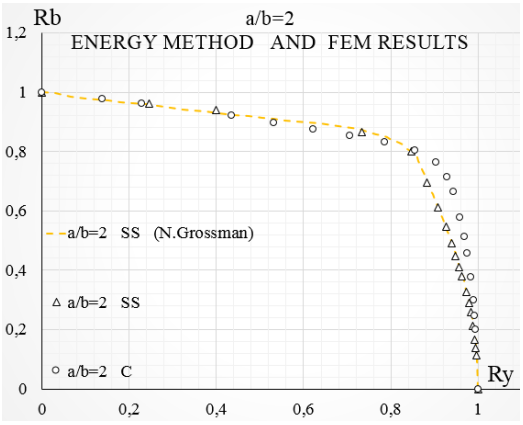

Figure 7.15. Comparison energy method and FEM results for a/b=2 with different elastic restraints.

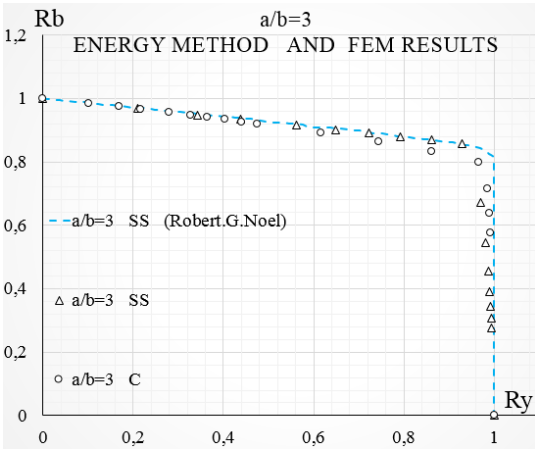

Figure 7.16. Comparison energy method and FEM results for a/b=3 with different elastic restraints.

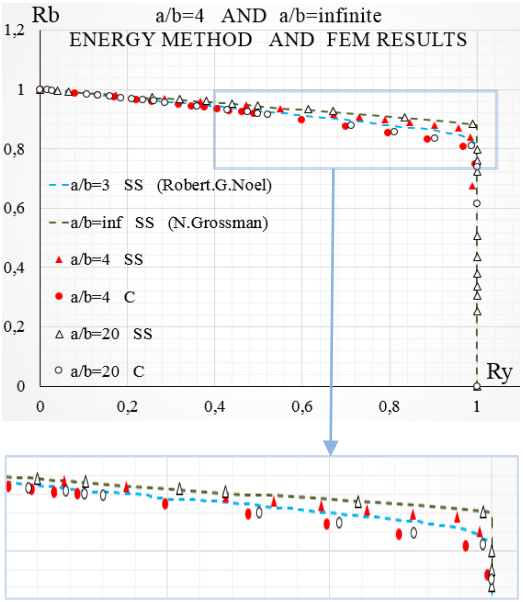

Figure 7.17. Comparison energy method and FEM results with different elastic restraints. Energy method curves for a/b=infinite and 3. FEM results for a/b=infinite and 4.

Overall, it is observed (Fig.7.14, 7.15, 7.16 and 7.17) that energy method provides results with engineering accuracy (if taken FEM as reference). The curves are especially valid for simply supported edges plates (as expected from the theoretical analysis), for which the maximum differences do not exceed 2% (optimistic differences). However, their use for clamed plates should not be discarded; they provide maximum differences (optimistic) of around 6% which is acceptable for engineering purposes. Additionally, interaction curves for all the 4 geometries studied provide optimistic estimates.

Fig.7.17 also shows that for simply supported plates under the combination of bending and transverse compression, plates with a/b =4 will already behave as infinite plates (because FEM results for a/b=4 have a mean difference of only 0.36% with energy method a/b=infinite curve). Therefore, for this load combination simply supported plates can be effectively assumed to be infinitely long plates

It has been observed that as the aspect ratio increases, the curves (and the FEM results) become less smooth, forming a/b=1 results a smooth curve from ($R_y = 0,\ R_b = 1$) to($R_y = 1,\ R_b = 0$). On the other hand, in a/b=2 the curve starts to become square shaped, and in a/b=3 the corner that makes a sharp transition in the results close to $R_y = 1$ is obvious. Physically speaking, the sharp transition implies that the deformed plate wave length changes rapidly from finite to infinite length. This has been checked observing the deformed shapes in FEM. See in Fig.7.18 and 7.19, how the wave length changes (in a small range of R_y) from being finite to infinite. This, which is shown only for the case of a/b=4, occurs whenever sharp transitions take place in interaction curves.

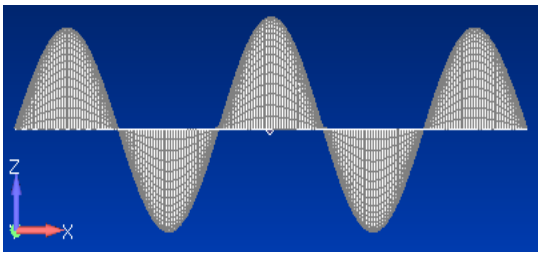

Figure 7.18. Mode shape of a/b=4 simply supported plate with

$R_y = 0.957, R_b = 0.870$

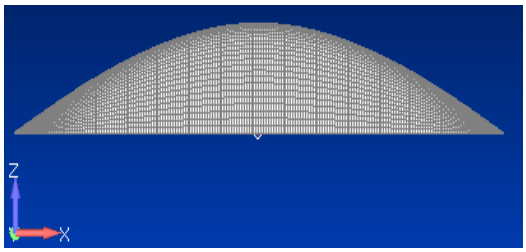

Figure 7.19. Mode shape of a/b=4 simply supported plate with

$R_y = 0.985\ ,\ R_b = 0.839$

It is worth to put special attention in Fig.7.17, as it reveals interesting features. Observe that being theoretical curves of a/b=3 and infinite so close one from the other, in the absence of a curve for a/b=4 in the references, in order to make engineering estimations it shall be useful to know that the results for a/b=4 will appear in that enclosed area. Being the area that narrow, effective estimations can be performed.

Reference 13 also presents for the relation between plate aspect ratio and k_y with the deformed shape of the plate. Based on the deformed shapes obtained with FEM, it is worthwhile to analyze the validity of Fig.7.20 presented by reference 13. Note in this figure that, in the curves for $k_y = 1$ and $k_y = 1.25$, two regions (I and II) have been specified. Each of these regions has a particular deformed shape, depending on its buckling mode. The reference states that for the regions **I** of both curves, the deformed shape will have 1 half wave, while for the region **II** (the region on the right once the cusp is overcome) 2 half waves will appear. It has been checked that for both curves, $k_y = 1$ and $k_y = 1.25$ this statement is valid, as it can be seen in Fig. 7.21 and 7.22 for $k_y = 1$ and $k_y = 1.25$ respectively).

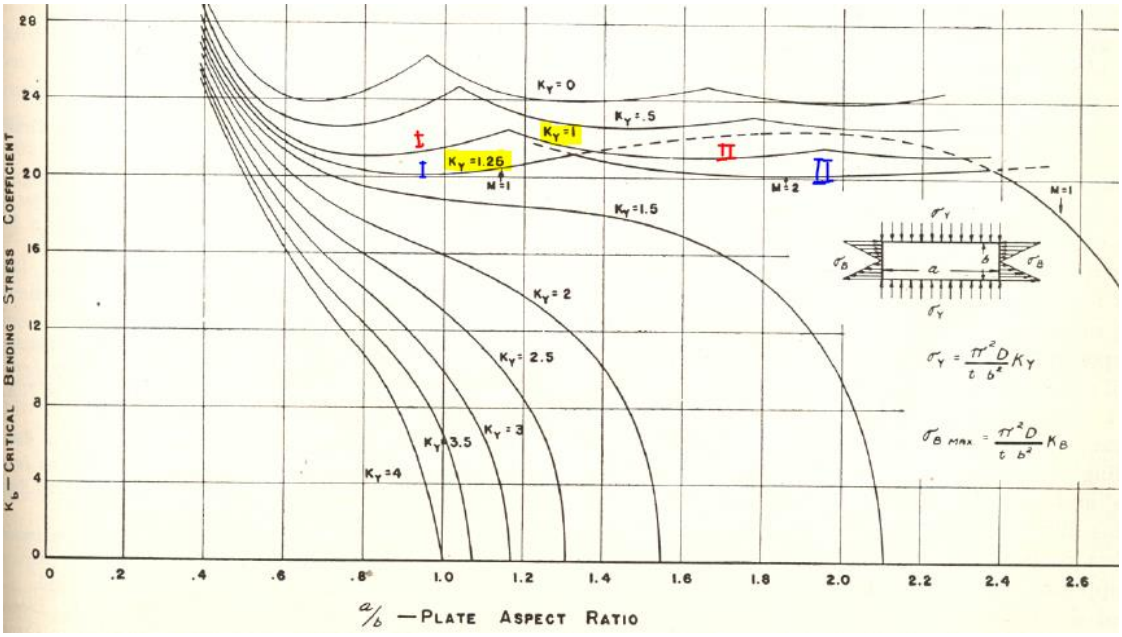

Figure 7.20. Instability coefficients for simply supported plates on combined bending and transverse compression. The cusps denote the change in the amount of half waves (M) in the plate. Indexes **I**, **II**, **I** and **II** refer to different regions. Source: Ref.13

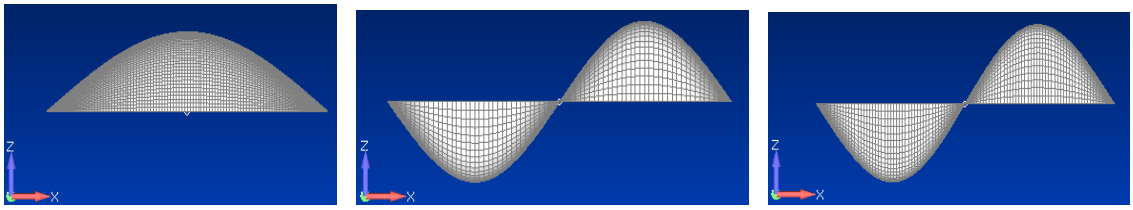

Figure 7.21. Deformed shapes of the plates upon buckling with $k_y = 1$ for different geometries: a/b=1 (left), a/b=1.5 (middle) and a/b=2 (right).

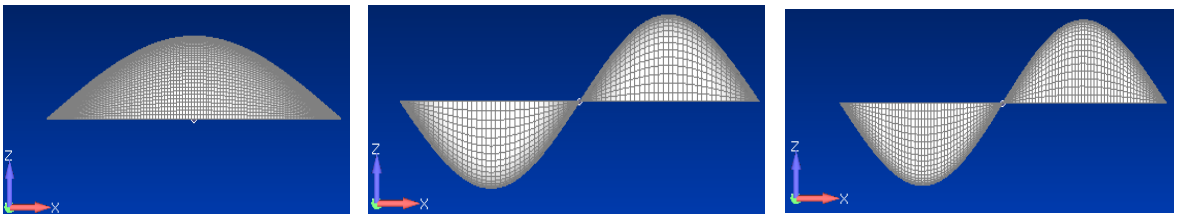

Figure 7.22. Deformed shapes of the plates upon buckling with $k_y = 1.25$ for different geometries: a/b=1 (left), a/b=1.5 (middle) and a/b=2 (right).

Additionally, the results from the comparison of 6 particular loading combinations of curves $k_y = 1$ and $k_y = 1.25$ are illustrated in Table 7.20. The errors, which are in generally below 1% (with the exception among the cases studied for the case of a/b=1.5 and $k_y = 1$) are considered to be acceptable for engineering purposes.

CRITICAL COMBINED LOADING DIFFERENCES Fig.7.20 AND FEM COMBINED BENDING AND TRANSVERSE COMPRESSION			
Case			Difference %
a/b	k_y	k_b	
1	1	21.51	0.82
1	1.25	20.13	0.79
1.5	1	21.06	1.28
1.5	1.25	20.47	0.61
2	1	21.46	0.81
2	1.25	20.18	0.39

Table 7.20. Differences between Fig.7.20 (Ref.13) and FEM results for simply supported plates.

Referring to table I of reference 11, where the results half-wave-length ratios (λ/b) for infinitely long simply supported plates are shown (based on the energy method), a comparison has been carried out with ratios obtained in FEM. The results of this analysis are summarized in Table 7.21. Note that in this case, the difference, percentage value is not that relevant, because being for b=100mm for the FEM models, a difference of only 1mm (for instance) in the half-wave length will build an error of the order of 1-2%. As initially the results obtained had little accuracy, the mesh was refined (from $5x5\ mm^2$ to $2x2\ mm^2$) and the results became more reliable (presented in Table 7.21).

λ/b DIFFERENCES NACA 2536 AND FEM COMBINED BENDING AND TRANSVERSE COMPRESSION				
Case		NACA 2536	FEM	Difference, %
k_b	k_y			
22.66	0.5	0.70	0.68	2.94
21.82	0.8	0.70	0,70	0.00
21.22	1	0.90	0,88	1.02

Table 7.21. λ/b Differences between Ref. 11 results and FEM for infinitely long simply supported plates.

In addition, as done with reference 13, the difference of reference 11 with respect to FEM in the buckling load predictions has been studied. The results are shown in Table 7.22.

CRITICAL COMBINED LOADING DIFFERENCES NACA 2536 AND FEM COMBINED BENDING AND TRANSVERSE COMPRESSION			
Case			Difference %
a/b	k_y	k_b	
infinite	0.5	22.66	0.05
infinite	0.8	21.82	-0.05
infinite	1	21.22	-0.28

Table 7.22. Differences between NACA 2536 (Ref.11) results and FEM. Infinitely long simply supported plates.

Now, if the differences of FEM with results of reference 13 (Table 7.20) and 11 (Table 7.22) are observed, it is appreciable that the differences are remarkably lower for the second case. This may be either due to the different method used by the references to solve the problem, or because the differences (FEM-reference results) are lower for infinitely long plates. Since both references use the energy method with proved reliability and accuracy in both cases, this reason should be discarded. Therefore, it may be more sensible to argue that for infinitely long plates lower differences will be found between FEM and energy method solution.

7 Conclusions

Comparison of flat plates buckling under combined loadings given by analytical solutions available and by the results obtained from FEM conclude the following points:

Comparison of single loading FEM and analytical results has shown that the energy method prediction approaches FEM results for axial compression, bending and shear loadings with high accuracy. As expected from theoretical analysis, the energy method results give optimistic estimates.

Based on FEM results for load combinations, several $R_1{}^p + R_2{}^q = 1$ shaped interaction equations have been proposed (Table 8.1), which approach obtained FEM results with high accuracy and can be used effectively for engineering purposes. For combined transverse compression and bending cases, results for some of the geometries have been fitted with straight lines equations (Table 8.2).

COMBINED LOADINGS – FEM INTERACTION EQUATIONS - $R_1{}^p + R_2{}^q = 1$												
a/b	Axial compression + Shear $R_X{}^p + R_S{}^q = 1$				Bending + Shear $R_B{}^p + R_S{}^q = 1$				Axial compression + Bending $R_X{}^p + R_B{}^q = 1$			
	SS		C		SS		C		SS		C	
	p	q	p	q	p	q	p	q	p	q	p	q
1	0.988	2.017	0.942	1.904	1.965	1.566	1.902	1.99	1.115	1.869	0.897	2.256
1.2	0.977	2.024	0.920	2.028	1.958	1.843	2.022	2.060	-	-	-	-
2	1.005	1.991	0.965	2.042	1.709	2.258	2.105	2.361	0.994	2.133	0.988	1.916
3	1.063	2.009	1.011	1.988	2.301	2.060	2.363	2.324	0.912	2.204	0.947	2.047
4	1.006	2.078	1.008	1.981	2.545	2.106	2.533	2.242	0.970	2.152	0.965	2.011
20	1.002	2.003	1.000	2.004	2.431	2.378	2.463	2.292	0.966	2.119	0.960	2.050

Table 8.1. Interaction equations produced from FEM results.
SS-All edges Simply Supported C-All edges Clamped

COMBINED BENDING AND TRANSVERSE COMPRESSION – FEM RESULTS - $R_B = mR_Y + n$								
a/b	CLAMPED				SIMPLY SUPPORTED			
	coefficients		Maximum error	validity	coefficients		Maximum error	validity
	m	n	(%)	$up\ to\ R_Y$	m	n	(%)	$up\ to\ R_Y$
2	-0.2154	1.0075	0.75	0.706	-0.1531	1	0.00	0.3981
3	-0.1924	1.0075	0.39	0.744	-0.1522	1	3.16	0.929
20	-0.1847	1.0062	0.56	0.812	-0.1157	1.0025	0.08	0.989

Table 8.2. Straight line equations for combined bending and transverse compression solutions from FEM

For combination of shear and axial compression, $R_X + R_S{}^2 = 1$ estimates acceptable results for all cases. It gives essentially exact predictions for large aspect ratio clamped plates (a/b≥3) and very accurate predictions (slightly optimistic) for small aspect ratio plates (maximum differences below 3%). The mean difference in clamped plates decreases as the aspect ratio increases. For simply supported plates, the equation generally gives conservative and accurate estimates with mean differences below 1.2%. For infinitely long simply supported plates, the equation gives essentially exact solutions.

Additionally, equation $R_X + {R_S}^{1,75} = 1$ gives estimates with mean differences ranging between 0.7% and 4% with respect to FEM results. It is conservative results and relatively accurate for all cases. To improve the accuracy of this equation, a new equation ($R_X + {R_S}^{1,93} = 1$) has been introduced, which gives estimates with mean differences ranging between 0.1% and 1.7%. The estimates are conservative for all cases except for clamped square plates.

The three equations ($R_X + {R_S}^2 = 1$, $R_X + {R_S}^{1,75} = 1$ and $R_X + {R_S}^{1,93} = 1$) for combined shear and axial compression are considered accurate for engineering purposes.

For combined bending and shear, NACA 2536 curve for infinitely long plates gives relatively accurate correlation with FEM results for a/b=20 (-1.40% and -1.97% differences for simply supported and clamped edges respectively). This interaction curve loses accuracy and becomes more optimistic if lower aspect ratios are analyzed, not being accurate enough for engineering purposes for a/b≤2 (where there are maximum differences above 5%).

Interaction equation ${R_B}^2 + {R_S}^2 = 1$ and NACA 1323 give good correlations for clamped plates with a/b around 2. For lower a/b it gives optimistic estimates, and for larger ones it provides conservative estimates (3.94% for infinitely long plates). In the case of clamped plates, the best correlation is obtained for nearly square plates (between 1 and 1.2). For higher aspect ratios, the difference increases giving conservative estimates, reaching almost 4% mean difference for infinitely long plates.

The equation ${R_B}^{1,75} + R_X = 1$ for combined bending and axial compression has been proven to give conservative predictions and more accurate estimates for clamped plates than for simply supported ones. For clamped edges, the mean differences range between 2-3%, and for simply supported edges between 3-4%. The differences are not seen to depend on the geometry. For both elastic restraints analyzed, maximum differences can reach almost 6% for some cases.

Interaction curves provided by Robert G. Noel provide optimistic estimations for all clamped plates analyzed, and for some simply supported cases. Additionally, it has been found that they provide really accurate estimations for simply supported plates (mean below 1% for all cases) and acceptable estimations for clamped plates (below 2.7% for all cases). Finally it has been demonstrated that Robert G. Noel curves for a/b=4 can be used with high accuracy for infinitely long plates with any elastic restraint.

As for combined bending and transverse compression, it has been proved that equation ${R_B}^{1,75} + R_Y = 1$ is not valid for engineering purposes, with optimistic and very inaccurate estimations. For this load combination, interaction curves for a/b=1, 2, 3 and 4 provided in the references (Noel, Grossman and NACA 2536) provide really accurate predictions (slightly optimistic) for simply supported cases, essentially exact for some regions and with maximum differences in the worst cases below 2%. For clamped plates the use of these equations is not recommended because they give inaccurate and optimistic estimates. Additionally, it has been demonstrated that curves for a/b=4 can be effectively used for simply supported infinite plates. Finally, it has been found that the energy method solutions (from the references) provide slightly better correlation with FEM results for lower aspect ratios.

CONCLUSIONS: INTERACTION CURVES AND EQUATIONS					
Equation / curve	Loads	Ref.	MAX. Differences	Conservative?	Observations
$R_X + {R_S}^2 = 1$	CO+SH	5	SS: 1.64% CC: small a/b ->3% CC: large a/b exact	YES, except square plates	RECOMMENDED SS: exact for a/b=infin. CC: exact for a/b≥3
$R_X + {R_S}^{1.75} = 1$	CO+SH	9, 10	4.88	YES	RECOMMENDED
$R_X + {R_S}^{1.93} = 1$	CO+SH	PRESENT WORK	2.32	YES, except a/b=1 clamped	RECOMMENDED
NACA 2536	BE+SH	11	a/b≥4 -> around4% small a/b ->around10%	NO	RECOMMNENDED only for high a/b
${R_B}^2 + {R_S}^2 = 1$ NACA 1323	BE+SH	3	around 6%	High a/b=YES Low a/b=NO	RECOMMNENDED
${R_B}^{1.75} + R_X = 1$	BE+CO	3	SS: 6.10% CC: a/b=1 ->5.66% CC: a/b≥2 ->3.76%	YES	RECOMMNENDED
Robert. G. Noel	BE+CO	4	SS: 1.71% CC: 4.04%	C: YES S: some cases	RECOMMNENDED C: exact for a/b=infin.
${R_B}^{1.75} + R_Y = 1$	BE+CO(tra)	9	All >10% a/b=1 , C: 9.37% a/b=1 , SS: 6.10%	NO	NOT recommended
N. Grossman Robert. G. Noel NACA 2536	BE+CO(tra)	13, 4, 11	SS: ≤2% C: 6% Not valid for square pl.	NO	RECOMMENDED up to Ry=0.85-0.95 -a/b=4 curve valid for infinite plates

Table 8.3. Concluded evaluation of interaction equations and curves

8 Future work

In this work several relevant load combinations have been studied, but some other such as simultaneous combination of shear, bending and transverse compression (common in aircraft shear webs) were not studied. It may be interesting to study this loading combination.

Additionally, future work could focus on the comparison of FEM and theoretical results comparison for different boundary conditions than the studied in this work. In particular, FEM results may be obtained for edges rotational restraints between clamped or pinned, such as those with different ϵ (degree of rotational restraint).

Future work may also study with FEM the effect of the additional transverse stress on the longitudinal buckling stress. Theoretical work available in references 2 and 17 could be compared to FEM results.

A comparison between FEM and theoretical solution of the 2nd buckling mode (2nd lower energy state) could be carried out as well.

It may also be interesting to study the minimum mesh size requirements for optimal FEM predictions. Ideally, FEM solution shall approach exact solution for extremely fine mesh.

9 References

1. Timoshenko, S., *Theory of Elastic Stability*; McGraw-Hill Book Company, New York, 1963, 2nd edition
2. George Gerard and Herbert Becker, *Handbook of Structural Stability Part I – Buckling of Flat Plates*, N.A.C.A. T.N. No. 3781, July 1957
3. Michael C. Y. Niu, *Airframe stress analysis and sizing*, March 2001, 2nd edition
4. Robert G. Noel, *Elastic Stability of Simply Supported Flat Rectangular Plates Under Critical C*ombinations of Longitudinal Bending, Longitudinal Compression, and Lateral Compression, Journal of aeronautical sciences, vol.19. no.12, December 1952
5. Elbridge Z. Stowell and Edward B.Schwartz, *Critical stress for an infinitely long flat plate with elastically restrained edges under combined shear and direct stress*, N.A.C.A. Wartime Report, L-340, 3K13, November 1943
6. Batdorf, S. B., and Stein, M., *Critical Combinations of Shear and Direct Stress for Simply Supported Rectangular Flat Plates*, N.A.C.A. T.N. No1223, March, 1947
7. Batdorf, S. B., and Houbolt, John C., *Critical Combinations of Shear and Transverse Direct Stress for an Infinitely Long Flat Plate with Edges Elastically Restrained Against Rotation*, N.A.C.A T.R. No.847, 1946
8. Batdorf, S. B., and Houbolt, John C., *Critical Combinations of Shear and Transverse Direct Stress for an Infinitely Long Flat Plate with Edges Elastically Restrained Against Rotation*, N.A.C.A. Wartime Report, L-4L14, 1945
9. Department of Defense United States of America, *Elements Strength of Metal Aircraft Elements*, ANC-5, June 1951
10. Hopkins, H. G., and Rao, B. V. S. C., *The Initial Buckling of Flat Rectangular Panels under Combined Shear and Compression*, R. & M. No. 1965, British A.R.C., 1943
11. Johnson, Aldie E., Jr., and Buchert, Kenneth P., *Critical Combinations of Bending, Shear, and Transverse Compressive Stresses for Buckling of Infinitely Long Flat Plates*, N.A.C.A. T.N. No 2536, 1951
12. Schuette, Evan H., and McCulloch, James C., *Charts for the Minimum Weight Design of Multiweb Wings in Bending*, N.A.C.A. T.N. No1323, 1947
13. Grossman, Norman, Elastic Stability of Simply Supported Flat Rectangular Plates Under Critical Combinations of Transverse Compression and Longitudinal Bending, Journal of aeronautical sciences, vol.16, no.5, May 1949
14. V. Piscopo, *Refined buckling analysis of plates under shear and uniaxial compression*, Sustainable Maritime Transportation and Exploitation of Sea Resources, pg.297-304, 2012
15. UGS Corp, *NX Nastran Getting Started Tutorials*, 2007
16. George Campbell, Wen Ting and Peyman Aghssa, Claus C.Hoff, *Buckling and geometric nonlinear analysis of a tie rod in MSC/NASTRAN version 68*
17. S. B. Batdorf, Manuel Stein, and Charles Libove, *Critical Combinations of Longitudinal and Transverse Direct Stress for an infinitely long flat plate with edges elastically restrained against rotation*, N.A.C.A. Wartime Report L6A05, March 1946

10 Bibliography

- Timoshenko, S., *Theory of Elastic Stability*; McGraw-Hill Book Company, New York, 1963, 2nd edition
- P. S. Bulson, *The Stability of Flat Plates*, Chatto & Windus, 1970
- E. F. Bruhn, *Analysis & Design of Flight Vehicle Structures*, 1973
- Michael C. Y. Niu, *Airframe stress analysis and sizing*, March 2001, 2nd edition
- Robert Millard Jones, *Buckling of bars, plates and shells*, 2006
- UGS Corp, Nastran Quick Reference Guide, 2007
- UGS Corp, Nastran Theoretical Manual, 2007
- UGS Corp, Nastran User Guide, 2007
- UGS Corp, Nastran Element Library Reference, 2007
- UGS Corp, *NX Nastran Getting Started Tutorials*, 2007
- UGS Corp, Nastran Glossary, 2007
- UGS Corp, Nastran Numerical Methods User Guide, 2007

Annex

Annex A: Method to compute differences between FEM-interaction curves.

It is worth to explain how the method used to compute the differences. This method has been used to compute the % differences between FEM and theoretical curves and equations predicted results. The method is based on the concept of margin of safety for interaction curves.

Let say that there are, for example, two loads A and B, and the difference between the FEM results (which are known) and the interaction curve needs to be obtained. Observe FigA1, where green cross represents FEM data point for which the difference is to be calculated, and red curve represent the theoretical interaction curve. The difference will be determined by doing X'-x, where X' is the radial distance from the center to the theoretical point, and x is the distance from the center to the FEM point. To compute the % difference, it is as simple as doing: (x-X')/X'.

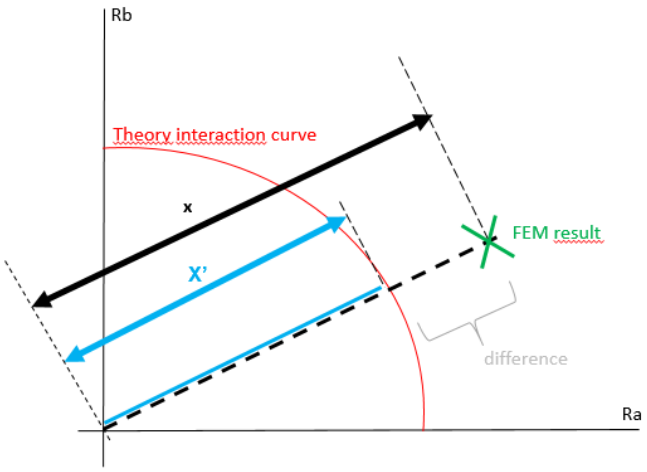

Figure A1. Graphical explanation of the method to compute differences FEM-theoretical curves

One of the issues here is to determine the point of the interaction curve that needs to be compared with the FEM point. It is the point that the FEM radial line (dashed line in Fig.A1) crosses in the interaction curve (red curve). The characteristic that these 2 points have in common is that they have the same proportion of loads. That is, the ratio $\frac{R_A}{R_B}$ for FEM point will be equal to the $\frac{R_A}{R_B}$ of the corresponding theoretical curve point. Having the theoretical interaction equation, as many points with their corresponding ratios $\frac{R_A}{R_B}$ can be calculated. Then, multiple ratios have been extracted from the curve. Later, with Excel software INDEX and MATCH commands the theoretical ratio $\frac{R_A}{R_B}$ which was closest to FEM ratio has been selected among all the theoretical ratios. Once having found the theoretical ratio similar to the FEM one, the point of the curve belonging to this ratio has been obtained. Knowing the point, the radial distance from the center is got (X' in Fig.A1). Finally, as x is known, the % difference can be easily obtained doing (x-X')/X'.

Sometimes, it may happen that the theoretical curve is obtained from a digitalized image and the equation is not known. In those cases, a data fit has been performed to obtain the equation. In the event the data fit does not succeed providing an accurate equation, this method cannot be used.

Two important points need to be considered when using this methodology. Firstly, although the example explained was done with a FEM point above the interaction curve (a conservative case), the method can be also applied if FEM point is below the curve. In such case, the obtained difference value would be negative (recall that negative values mean that the theoretical estimation is not conservative). Secondly, note that for this method multiple ratios $\frac{R_A}{R_B}$ need to be calculated for interaction curve points. Since Excel tool will look for the more similar theoretical ratio to the FEM ratio (and it will not warn you if the most similar one is very different), the more ratios that are extracted, the less error that will have the method. Ideally, with infinite theoretical ratios, Excel will find a ratio identical to the FEM one, meaning that no error is being done.

Annex B: Analysis graphs digitalizing procedure accuracy

A graph digitalizer tool (*GetData Graph Digitizer 2.26*) has been used in this work for:

- Obtaining *k* buckling coefficients from the theoretical graphs in the references for the cases of axial compression, shear, bending and transverse compression.
- Converting to excel format (for computation of differences with FEM results) available combined loadings theoretical interaction curves from the references.

In order to know the order of magnitude of the errors caused by the digitalizing process, a preliminary analysis has been carried out. This analysis determines the maximum errors caused by the digitalizing process. The error sources are mainly; the width of the curves (digitalizer does not always take the middle point) and the errors due to interpolation (note that when digitalizing, an infinite points curve is transformed in a finite number of points curve).

The analysis has concluded that:

- For axial compression *k* coefficient graph (Fig.3.3):
  Maximum difference is **1%**.
- For shear *k* coefficient graph (Fig.3.4):
  Maximum difference is **0.6%**. For a/b<1.7 it is **1.2%.**

- For bending k coefficient graph (Fig.3.5):
  Maximum difference is **0.5%.** For a/b≥3.2 it is **0%** (no digitalizing is needed).
- For transverse compression (Fig.3.5):
  Maximum difference is **4%.** For a/b≥0.8 it is **1.7%**
- Digitalized interaction curves errors are for all cases below **1%**

Based on these results (denoted as $MAX\ dig.error$), the error for the comparison between FEM and theoretical results for single loading have been computed. $\Delta\sigma_{cr}|_{MAX}$ and $\Delta\sigma_{cr}|_{MIN}$ are obtained from eq.SL103 and eq.SL104, which have been derived using eq.A1 and accounting for the error in $\sigma_{cr-theory}$ using eq.A2.

$$\Delta\sigma_{cr} = \frac{\Delta\sigma_{cr}\,(MPa)}{\sigma_{cr-theory}} \quad (A1)$$

$$\sigma_{cr-theory}(considering\ error) = \sigma_{cr-theory} \pm e_{dig} = (1 \pm MAX\ dig.error)\sigma_{cr-theory} \quad (A2)$$

$$e_{dig} = \sigma_{cr-theory}.MAX\ dig.error \quad (A3)$$

$$\Delta\sigma_{cr}|_{MAX}(\%) = \frac{\Delta\sigma_{cr}\,(MPa)+e_{digitalizer}}{\sigma_{cr-theory}+e_{digitalizer}} \quad (A4)$$

$$\Delta\sigma_{cr}|_{MIN}(\%) = \frac{\Delta\sigma_{cr}\,(MPa)-e_{digitalizer}}{\sigma_{cr-theory}-e_{digitalizer}} \quad (A5)$$

The obtained results for all the previous terms are shown in tables below.

AXIAL COMPRESSION – DIFFERENCES FEM vs THEORY, $\sigma_{crit}\ (MPa)$							
a/b	Rotational restraint	σ_{cr-FEM} (MPa)	$\sigma_{cr-theory} \pm e_{dig}$ (MPa)	$\Delta\sigma_{cr} \pm e_{dig}$ (MPa)	$\Delta\sigma_{cr}$ (%)	$\Delta\sigma_{cr}\|_{MIN}$ (%)	$\Delta\sigma_{cr}\|_{MAX}$ (%)
1	SS	6,3585	6,3632 ± 0.0636	-0,0047 ± 0.0636	-0,07	-1,08	0,92
	C	16,0306	15,9670 ± 0.1597	0,0636 ± 0.1597	0,40	-0,61	1,38
2	SS	6,3482	6,3630 ± 0.0636	-0,0148 ± 0.0636	-0,23	-1,25	0,76
	C	12,4690	12,4119 ± 0.1241	0,0571 ± 0.1241	0,46	-0,55	1,45
3	SS	6,3396	6,3882 ± 0.0639	-0,0486 ± 0.0639	-0,76	-1,78	0,24
	C	11,6340	11,6410 ± 0.1164	-0,0070 ± 0.1164	-0,06	-1,07	0,93
4	SS	6,3353	6,3350 ± 0.0634	0,0003 ± 0.0634	0,01	-1,01	0,99
	C	11,3932	11,3325 ± 0.1133	0,0607 ± 0.1133	0,54	-0,47	1,52
20	SS	6,3277	6,3350 ± 0.0633	-0,0073 ± 0.0633	-0,1	-1,13	0,88
	C	10,9794	11,0250 ± 0.1103	-0,0456 ± 0.1103	-0,41	-1,43	0,58

Table A1. Differences in axial compression critical buckling load.

TRANSVERSE COMPRESSION – DIFFERENCES FEM vs THEORY, $\sigma_{crit}\ (MPa)$							
a/b	Rotational restraint	σ_{cr-FEM} (MPa)	$\sigma_{cr-theory} \pm e_{dig}$ (MPa)	$\Delta\sigma_{cr} \pm e_{dig}$ (MPa)	$\Delta\sigma_{cr}$ (%)	$\Delta\sigma_{cr}\|_{MIN}$ (%)	$\Delta\sigma_{cr}\|_{MAX}$ (%)
1	SS	6,3585	6,3632 ± 0.0636	-0,0047 ± 0.0636	-0,07	1,60	-1,80
2	SS	2.4949	2,3377 ± 0.0397	0.1572 ± 0.0397	6,72	8,28	5,11
3	SS	1.9661	1,8917 ± 0.0322	0.0744 ± 0.0322	3.93	5,54	2,27
4	SS	1.7950	1,5817 ± 0.0269	0.2133 ± 0.0269	13.5	14,93	11,99
20	SS	1,5968	1,5817 ± 0.0269	0,0151 ± 0.0269	0,96	2,61	-0,76

Table A2. Differences in transverse compression critical buckling load.

BENDING – DIFFERENCES FEM vs THEORY, $\sigma_{crit}\ (MPa)$							
a/b	Rotational restraint	σ_{cr-FEM} (MPa)	$\sigma_{cr-theory} \pm e_{dig}$ (MPa)	$\Delta\sigma_{cr} \pm e_{dig}$ (MPa)	$\Delta\sigma_{cr}$ (%)	$\Delta\sigma_{cr}\|_{MIN}$ (%)	$\Delta\sigma_{cr}\|_{MAX}$ (%)
1	SS	41,1370	40,6997 ± 0.2035	0,437 ± 0.2035	1,07	1,57	0,58

2	SS	38,0785	38,0393 ± 0.1902	0,039 ± 0.1902	0,10	0,60	-0,40
3	SS	38,2962	38,2765 ± 0.1914	0,020 ± 0.1914	0,05	0,55	-0,45
4	SS	37,9075	38,2765 ± 0.0000	-0,369 ± 0.0000	-0,96	-0,96	-0,96
20	SS	37,8588	37,8020 ± 0.0000	0,057 ± 0.0000	0,15	0,15	0,15

Table A3. Differences in bending critical buckling load.

SHEAR – DIFFERENCES FEM vs THEORY, σ_{crit} (MPa)							
a/b	Rotational restraint	σ_{cr-FEM} (MPa)	$\sigma_{cr-theory} \pm e_{dig}$ (MPa)	$\Delta\sigma_{cr} \pm e_{dig}$ (MPa)	$\Delta\sigma_{cr}$ (%)	$\Delta\sigma_{cr}\|_{MIN}$ (%)	$\Delta\sigma_{cr}\|_{MAX}$ (%)
1	SS	14,7557	14,5845 ± 0.1750	0,1712 ± 0.1750	1,17	2.35	-0.03
	C	23,1014	22,9863 ± 0.2758	0,1151 ± 0.2758	0,50	1.09	-0.10
2	SS	10,3490	10,2428 ± 0.0615	0,1062 ± 0.0615	1,04	1.63	0.44
	C	16,1928	16,3223 ± 0.0979	-0,1294 ± 0.0979	-0,79	-0.19	-1.40
3	SS	9,2383	9,1438 ± 0.0549	0,0946 ± 0.0549	1,03	1.62	0.44
	C	15,0733	15,2548 ± 0.0915	-0,1814 ± 0.0915	-1,19	-0.59	-1.80
4	SS	8,8983	8,8559 ± 0.0531	0,0424 ± 0.0531	0,48	1.07	-0.12
	C	14,7006	14,7770 ± 0.0887	-0,0764 ± 0.0887	-0,52	0.08	-1.12
20	SS	8,5219	8,4350 ± 0.0506	0,0869 ± 0.0506	1,03	1.62	0.43
	C	14,3574	14,2100 ± 0.0853	0,1474 ± 0.0853	1,04	1.63	0.44

Table A4. Differences in shear critical buckling load.